

University of Alberta

QUANTUM MOLECULAR DYNAMICS: PRACTICAL SEMICLASSICAL APPROACHES

by

Bilkiss Banoo Issack



A thesis submitted to the Faculty of Graduate Studies and Research in partial fulfillment of the requirements for the degree of **Doctor of Philosophy**.

Department of Chemistry

Edmonton, Alberta
Fall 2007



Library and
Archives Canada

Bibliothèque et
Archives Canada

Published Heritage
Branch

Direction du
Patrimoine de l'édition

395 Wellington Street
Ottawa ON K1A 0N4
Canada

395, rue Wellington
Ottawa ON K1A 0N4
Canada

Your file *Votre référence*
ISBN: 978-0-494-32982-5
Our file *Notre référence*
ISBN: 978-0-494-32982-5

NOTICE:

The author has granted a non-exclusive license allowing Library and Archives Canada to reproduce, publish, archive, preserve, conserve, communicate to the public by telecommunication or on the Internet, loan, distribute and sell theses worldwide, for commercial or non-commercial purposes, in microform, paper, electronic and/or any other formats.

The author retains copyright ownership and moral rights in this thesis. Neither the thesis nor substantial extracts from it may be printed or otherwise reproduced without the author's permission.

AVIS:

L'auteur a accordé une licence non exclusive permettant à la Bibliothèque et Archives Canada de reproduire, publier, archiver, sauvegarder, conserver, transmettre au public par télécommunication ou par l'Internet, prêter, distribuer et vendre des thèses partout dans le monde, à des fins commerciales ou autres, sur support microforme, papier, électronique et/ou autres formats.

L'auteur conserve la propriété du droit d'auteur et des droits moraux qui protègent cette thèse. Ni la thèse ni des extraits substantiels de celle-ci ne doivent être imprimés ou autrement reproduits sans son autorisation.

In compliance with the Canadian Privacy Act some supporting forms may have been removed from this thesis.

Conformément à la loi canadienne sur la protection de la vie privée, quelques formulaires secondaires ont été enlevés de cette thèse.

While these forms may be included in the document page count, their removal does not represent any loss of content from the thesis.

Bien que ces formulaires aient inclus dans la pagination, il n'y aura aucun contenu manquant.


Canada

Abstract

This thesis presents practical methods for the quantum mechanical treatment of large complex molecular systems in classical molecular dynamics simulations. The proposed approach is based on the inclusion of constraints in semiclassical initial value representation (SC-IVR). The latter has proved itself as an effective means of including quantum effects, such as tunneling and interference, at least qualitatively, in classical simulations. Prior to the present work, however, no provision was made in SC-IVR, for a general and practical treatment of large geometrically constrained molecules which are ubiquitous in large-scale classical simulations. The work presented in this thesis therefore, represents our endeavour to extend the applicability of SC-IVR to a wider class of molecular systems, with a focus on large molecular systems.

The approach is first implemented and tested on atomic systems, on a series of van der Waals clusters in particular. Bound state energies are determined and compared to the corresponding exact quantum mechanical quantities. Quantitative accuracy is observed both for the zero-point energy and excited state energies. The method is then extended to treat molecular systems and successfully applied to the calculation of the intermolecular vibrational bound states of a dimer of rigid water molecules. An alternative approach is also developed by using a recently proposed version of SC-IVR, which makes use of a time-averaging procedure, with potentially improved applicability to large systems. The combination of the constraint SC-IVR with the time-averaged technique is able to capture quantum effects for a molecular system

through the reproduction of the zero-point energy. Both methods bear promise for an accurate quantum mechanical treatment of dynamical systems of high complexity and dimensionality.

Acknowledgements

Words fail to express my extreme gratitude to my supervisor Prof. Pierre-Nicholas Roy for welcoming me in his group and introducing me to the world of molecular dynamics. His generous guidance, unparalleled enthusiasm and dedication have helped make my Ph. D. research an enjoyable experience. Throughout my thesis-writing, he showed exceptional patience and offered useful suggestions. Without his support and encouragement, completion of this thesis would not have been possible! A former student once said that it would be hard to find a better supervisor. I couldn't agree more!

I am also indebted to Dr. Nicholas Blinov for many helpful discussions and valuable advice. His unconditional willingness to help, in particular, is deeply acknowledged. I wish to thank Nicole Oro and Prof. Alexander Brown who have collaborated on research related to the water hexamer and protonated methane, respectively. It is a pleasure to acknowledge the time and effort of Yoonie Huh, Stephanie Wong, Meena Dowlut, Nicolas Bouffard and Dr. M. Iqbal Issack who have read parts of my thesis and offered constructive input. I am also grateful to my Ph. D. committee members, some of whom have provided very pertinent comments. As this is an article-based thesis, it is only right that I acknowledge the anonymous reviewers to whom The Journal of Chemical Physics sent the original manuscripts and who have provided useful comments.

I am much obliged to the past and current members of the Roy group: (in alphabetical order) Dr. Norberto Castillo, Javier Cuervo, Dr. Robert Ganzynkiewicz, Kyle Greene, Ben Harland, Yoonjung (Yoonie) Huh, Dr. Yong Dong (Lucy) Liu, Yuan Ma, Paul Moffat, Nicole Oro, Mikyung Seo, Xiao Geng (James) Song, Yalina Tritzant and Stephanie Wong for providing a stimulating and fun environment to work in as well as for their wonderful company outside the office.

I wish to thank Dr. Dhanjay Jhurry and Dr. Ahmad Khodabocus, my undergraduate professors at the University of Mauritius, for instilling in me the interest for quantum chemistry and for graduate studies, respectively. I would like to thank in addition, Dr. Robert Choong Kwet Yive for his encouragement and kind assistance writing letters and with various applications over the years.

I am particularly grateful to Dr. Anna Jordan and Dr. Norberto Castillo for helping me get through difficult times in my final year.

I would like to thank all my friends who have provided encouragement and mo-

tivation and helped make my stay in Edmonton a pleasurable one. Thanks go to Zahira and Nicolas, in particular, for all the emotional support, entertainment and caring they provided.

Last but not least, I would like to thank my family *Jolimie*, *Mota* and *Lelou* for their faith in me as well as their lifelong encouragement and support of my studies, and everything they have done for me over the years.

Table of Contents

1	Introduction	1
1.1	Context	1
1.2	Definitions	2
1.3	Born-Oppenheimer Approximation	4
1.4	Classical Molecular Dynamics	6
1.5	Quantum Dynamics	8
1.6	Approximate Quantum Dynamics	13
1.7	Semiclassical Dynamics	15
1.7.1	Derivation of the propagator	15
1.7.2	Features of SC-IVR	18
1.7.3	Applications of SC-IVR	21
1.7.4	The void in SC-IVR	24
1.7.5	Original contributions to knowledge and overview	25
2	Ground state	33
2.1	Introduction	33
2.2	Theoretical approach	35
2.2.1	Representation of the wave function	37
2.2.2	Inclusion of constraints	38
2.3	Numerical example: Rare-gas trimers	40
2.3.1	Sampling of initial conditions	41
2.3.2	Dynamics	42
2.3.3	Reduction in zero point energy	43
2.4	Conclusion and Outlook	45
3	Excited states	51
3.1	Introduction	51
3.2	Theoretical approach	54
3.3	Numerical example: Small Argon clusters	57
3.3.1	Sampling of initial conditions	58
3.3.2	Dynamics	60
3.3.3	Bound state energies	61

3.4	Conclusion and Outlook	66
4	Extension to hydrogen bonded molecular systems: water dimer dynamics	70
4.1	Introduction	70
4.2	Theory and Methods	73
4.3	Calculations for the water dimer	77
	4.3.1 Calculation of the survival amplitude	78
	4.3.2 Bound state energies	80
4.4	Conclusions	82
5	Quantum molecular dynamics from a single trajectory	91
5.1	Introduction	91
5.2	Theory	93
5.3	Methods and Results	96
5.4	Conclusions	98
6	Conclusions	102
6.1	Complementary discussion of the results	104
	6.1.1 van der Waals clusters	105
	6.1.2 Water clusters	106
	6.1.3 Software development	107
6.2	Future Directions	108
	6.2.1 Larger water clusters: the hexamer	108
	6.2.2 CH_5^+	110
A	WKB approximation	114
B	Van Vleck's Propagator	118
C	Manual	121

List of Tables

2.1	Masses and parameters for the Lennard-Jones potential for argon and neon.	41
2.2	Zero-Point Energies (in kJ mol^{-1}). Results of exact quantum mechanical, and SC-IVR treatment based on the exact log-derivative HK (SCIVR^E) and the approximate (SCIVR^A) prefactors. The result from the harmonic approximation (HA) is included for reference. The difference, δ , between the various approximations and the exact results is also given. The energies are given with respect to the bottom of the total potential.	44
2.3	The difference in dissociation energies between the argon and neon trimers per number of vibrational degree of freedom d	45
3.1	Comparison of exact quantum mechanical bound state energies and the corresponding SC-IVR results for argon clusters. Energies are given with reference to the minimum of the potential in kJ mol^{-1} . Calculations are performed using the full approximate HK prefactor (SCIVR^A) as well as the absolute value (SCIVR^{abs}) approximation. The percentage difference, δ , between the exact and SC-IVR calculations is also provided	62
4.1	SC-IVR bound state energies (in kJ mol^{-1}) for $(\text{H}_2\text{O})_2$ and $(\text{D}_2\text{O})_2$ calculated with reference to the minimum of the potential ($D_e = -27.36 \text{ kJ mol}^{-1}$).	80
4.2	Comparison of zero point energies (kJ mol^{-1}) of the water dimer using the TIP3P and TIP4P potentials. Energies are given with reference to the minimum of the potential.	81
4.3	Comparison of SC-IVR and harmonic zero point energies (kJ mol^{-1}) of $(\text{H}_2\text{O})_2$ and $(\text{D}_2\text{O})_2$. Energies are given with reference to the minimum of the potential.	82
6.1	Comparison of the predictions of our method using the Lennard-Jones potential with experimentally determined vibrational spacings for the argon dimer in kJ mol^{-1}	106

6.2 Comparison of SC-IVR ZPEs of $(\text{H}_2\text{O})_2$ and $(\text{D}_2\text{O})_2$. Energies are given in kJ mol^{-1} with reference to the minimum of the potential. . . 107

List of Figures

1.1	Schematic representation of SC-IVR calculation	19
2.1	Distribution of atomic distances for $\text{Ar}_2^{\text{rigid}} + \text{Ar}$ (top) and $\text{Ne}_2^{\text{rigid}} + \text{Ne}$ (bottom). The circles and the triangles represent the unconstrained interatomic distances. The solid line indicates the distribution of distances along the constrained direction. A sample size of 10000 configurations is used.	47
2.2	Power spectra for the argon (top panel) and neon (lower panel) trimers. The solid line corresponds to the results for the regular trimer and the broken line shows results for the constrained trimer. The results are obtained based on the exact log-derivation expression for the HK prefactor. The exact results (dotted vertical lines) are also included.	48
3.1	Sampling distribution of atom pair distances, d , for the three model systems. (a) Ar_2 dimer: the arrow indicates the position of the potential minimum. (b) Ar_3 trimer: the filled triangles, circles, and squares represent the pair distance between the three possible atom pairs. (c) $\text{Ar}_2^{\text{rigid}}\text{Ar}$ complex: the solid line corresponds to the constrained distance while the filled triangle and squares correspond the remaining two unconstrained distances.	60
3.2	Real part of the survival amplitude (a), and associated power spectrum (b) for the Ar_2 dimer.	63
3.3	Real part of the survival amplitude (a), and associated power spectrum (b), for the Ar_3 trimer.	64
3.4	Real part of the survival amplitude (a), and associated power spectrum (b), for the $\text{Ar}_2^{\text{rigid}}\text{Ar}$ complex.	65
4.1	Distribution of atomic distances for $(\text{H}_2\text{O})_2$ for the pairs (a) XH1, (b) XH2, and (c) YO1, where $X=\text{O1, H1 or H2, H3, O2 and H4}$ and $Y=\text{H1 and H2, H3, O2 and H4}$ in this order, from left to right. Atomic labels on each of the two water monomers are H1, H2, and O1 and H3, H4, and O2, respectively. Distributions of intramolecular pair distances are truncated along the vertical axis for clarity.	84

4.2	Three-dimensional atomic densities generated from sampled positions of the water dimer wave function.	85
4.3	(a) Real and (b) imaginary parts of the survival amplitude for $(\text{H}_2\text{O})_2$	86
4.4	Power spectrum showing the bound state energies of $(\text{H}_2\text{O})_2$	87
4.5	Power spectrum showing the bound state energies of $(\text{D}_2\text{O})_2$	88
5.1	Zero-point energy determination from the power spectrum in kJ mol^{-1} for $T=0$ (i.e., no time-averaging).	98
5.2	Three-dimensional atomic densities generated from the dynamical sampling of positions along the trajectory.	99
5.3	Convergence of ZPE in kJ mol^{-1} with time-averaging length T . The horizontal line represents the ZPE obtained from the full SC-IVR calculation of Ref. [10].	100
6.1	The cyclic, book and boat conformations of the water hexamer, courtesy of N. Oro, unpublished (2005).	109
6.2	The delocalisation of the hydrogen atoms in CH_5^+	111

List of Abbreviations

BO	<i>Born-Oppenheimer</i>
CMD	<i>Centroid Molecular Dynamics</i>
DVR	<i>Discrete Variable Representation</i>
FBIVR	<i>Forward-Backward Initial Value Representation</i>
HK	<i>Herman-Kluk</i>
IR	<i>Infra Red</i>
IVR	<i>Initial Value Representation</i>
MCTDH	<i>Multi-Configuration Time Dependent Hartree</i>
MD	<i>Molecular Dynamics</i>
MMTK	<i>Molecular Modelling Toolkit</i>
PES	<i>Potential Energy Surface</i>
PIMC	<i>Path Integral Monte Carlo</i>
PIMD	<i>Path Integral Molecular Dynamics</i>
QM/MM	<i>Quantum Mechanics/Molecular Mechanics</i>
RBDMC	<i>Rigid Body Diffusion Monte Carlo</i>
RPMD	<i>Ring Polymer Molecular Dynamics</i>
SC-IVR	<i>Semiclassical Initial Value Representation</i>
SPA	<i>Stationary Phase Approximation</i>
SPC/E	<i>Simple Point Charge/Extended</i>
TA	<i>Time Averaged</i>
TIP3P	<i>Transferable Intermolecular Potential 3 Point</i>
TIP4P	<i>Transferable Intermolecular Potential 4 Point</i>
WKB	<i>Wentzel-Kramers-Brillouin</i>

Chapter 1

Introduction

1.1 Context

In 1929, Paul Dirac declared that *“The underlying physical laws necessary for the mathematical theory of a large part of physics and the whole of chemistry are thus completely known, and the difficulty is only that the exact application of these laws leads to equations much too complicated to be soluble. It therefore becomes desirable that approximate practical methods of applying quantum mechanics should be developed, which can lead to an explanation of the main features of complex atomic systems without too much computation”* [1]. Nearly 80 years later, applications of quantum mechanics have come a long way due to technological advances in computer power and the development of efficient algorithms. However, save a few exceptions, exact (real-time) quantum dynamical calculations remain limited to small molecular systems. Thus, Dirac’s comment remains a hard reality even today! The development of *“approximate practical methods”* is precisely the goal of this thesis.

While there are many approximate techniques to obtain dynamical information from a quantum system, each technique has its own merits and drawbacks. semiclassical initial value representation (SC-IVR) allows us to probe quantum mechanical properties of systems within classical molecular dynamics (MD) simulations. Based on semiclassical theory, the method holds great promise for the treatment of systems of high complexity and dimensionality. MD simulations of such systems are often performed in Cartesian coordinates by imposing geometric constraints on mo-

tions of “lower importance” (to the problem of interest). However, prior to this work, a general and practical technique for applications to constrained systems was quasi-non-existent in SC-IVR. We have developed an approach to study constrained molecular systems in Cartesian coordinates with SC-IVR and thereby contributed to the extension of the applicability of SC-IVR to more complex systems. Following the development, the method was first successfully tested on model constrained atomic clusters and subsequently applied to a molecular system.

The introduction is organised as follows. We start in Sec. 1.2 with a lexical definition with the purpose of establishing a common terminology. The following section, Sec. 1.3, offers a description of the Born-Oppenheimer approximation, a fundamental approximation in modern day quantum mechanical treatment of atoms and molecules. Subsequent sections survey some of the existing methods of studying dynamical systems at the classical (Sec.1.4), quantum (Sec.1.5) and hybrid (Sec.1.6) levels of theory. Finally, in Sec.1.7, we conclude the chapter with a concise discussion of semiclassical methods, with particular emphasis on SC-IVR.

This is an article-based thesis, i.e., Chapters 2, 3 and 4 have appeared as articles in the literature, and Chapter 5 has been submitted for publication. Thus, the reader will encounter an introduction and a description of the theoretical method at the beginning of each forthcoming chapter.

1.2 Definitions

Effective communication calls for a common terminology (or language) and common semantics (or meaning). In theoretical and computational chemistry specifically, definitions can be somewhat arbitrary and subjective. Thus, a description of the various predictive tools of research employed in the field is particularly useful in dispelling any possible ambiguities. In this section, basic terms such as theory, computation and modelling are defined and put into context using examples encountered in the rest of the thesis. Cambridge Dictionary defines theory as *a formal statement of the rules on which a subject of study is based or of ideas which are suggested to explain*

a fact or event or, more generally, an opinion or explanation [2]. In scientific usage, these rules can often be formulated mathematically. For example, quantum theory describes the dynamics of a particle of mass m by the Schrödinger equation

$$i\hbar\frac{\partial\Psi}{\partial t} = -\frac{\hbar^2}{2m}\frac{\partial^2\Psi}{\partial\mathbf{r}^2} + V(\mathbf{r})\Psi(\mathbf{r}, t) , \quad (1.1)$$

where i is the imaginary unit, Ψ is the time-dependent wave function, t is the time and $\hbar = h/2\pi$, h being Planck's constant. V represents the potential energy as a function of the coordinates of the particle, \mathbf{r} . All theories aspire to generality. In reality, however, most theories have limitations. The actual range of validity of a theory needs to be determined through experimental testing. For instance, Newtonian mechanics is experimentally observed to break down for small microscopic systems. Despite its limited applicability, the high practicality resulting from the simplicity of classical mechanics has shaped it into a theory so robust that it has earned itself the title of a *law* [3]. And so, classical equations of motion are also referred to as Newton's laws. The second law, for example, states that the rate of change of momentum of a body is proportional to the resultant force acting on the body and is in the same direction, and is mathematically given by

$$\mathbf{F} = \frac{d\mathbf{p}}{dt} = m\mathbf{a} , \quad (1.2)$$

where \mathbf{F} is the force and \mathbf{p} and \mathbf{a} are the momentum and the acceleration, respectively [4].

The main objective in the development of theories is to achieve general formulations, irrespective of practical consequences. Thus, while Eq. (1.1) governs the dynamical evolution of a quantum system, it is intractable for the large majority of systems in nature. It becomes therefore, necessary to introduce approximations in such theories, via the creation of models, in order to achieve a practical implementation. Models offer a simplified and more practical version of the theory, often at the expense of generality. A substantial portion of efforts in the development of models is devoted to parametrization, the process by which constants in a model are determined. This can be achieved empirically by fitting to experimentally determined

values or through a fit to data obtained from more accurate calculations. Models are ubiquitous in the theoretical/computational field. In a broad sense, classical molecular dynamics, which employs classical mechanics to describe the motion of atoms and molecules, can be seen as a form of modeling. Another example encountered in Chapter 4 is the popular empirical TIP3P water model which describes the interaction between water monomers.

The transition from theory to practice is achieved through methods. Back of the envelope calculations can be performed to determine physical quantities of interest either through the direct application of a theory or a model. However, in many cases, solutions cannot be determined analytically. In such cases, one needs to resort to numerical methods which require a digital computer for efficiency of the computations. Methodological development proceeds in several stages. Once a practical means of applying the theory is devised (*creation*), *implementation* ensues, often through the development and use of efficient computer algorithms. The next step involves the rigorous *testing* of the developed method for a series of model systems to determine its applicability and limitations before it can be applied for its ultimate predictive goal (*application*). It is in the final stage that the connection is made with experiments via the reproducibility and prediction of experimental physical measurements. Although formally a part of methodological development, *application* is often regarded as an independent subject. Research work presented in this thesis focuses on *creation*, *implementation* and *testing* aspects; applications of the method are discussed in the closing chapter.

1.3 Born-Oppenheimer Approximation

In 1963, Richard Feynman noted that “*everything that living things do can be understood in terms of the jiggings and wiggings of atoms*” [5]. This jiggling and wiggling of atoms can be described by the time-dependent Schrödinger equation

$$i\hbar \frac{\partial \Phi(\mathbf{R}, \mathbf{r}, t)}{\partial t} = \hat{H} \Phi(\mathbf{R}, \mathbf{r}, t), \quad (1.3)$$

where \mathbf{R} and \mathbf{r} are vectors representing the nuclear and electronic coordinates, respectively, $\Phi(\mathbf{R}, \mathbf{r}, t)$ is the wave function and \hat{H} is the Hamiltonian. For a closed, isolated system, \hat{H} is time independent and is given by

$$\hat{H} = - \sum_A \frac{\hbar^2}{2m_A} \nabla_A^2 - \frac{\hbar^2}{2m_e} \sum_i \nabla_i^2 - \frac{e}{4\pi\epsilon_0} \sum_{i,A} \frac{Z_A}{|r_i - R_A|} + \frac{e^2}{4\pi\epsilon_0} \sum_{i < j} \frac{1}{|r_j - r_i|} + \frac{1}{4\pi\epsilon_0} \sum_{A < B} \frac{Z_A Z_B}{|R_B - R_A|}. \quad (1.4)$$

The indices A and B refer to nuclei and i and j refer to electrons. The first term is the kinetic energy operator for each nucleus of mass m_A . The second term is the kinetic contribution of the electrons to the energy with m_e designating the electronic mass. The third term represents the attractive Coulombic interaction between electrons and nuclei bearing charges e and Z , respectively. The last two terms correspond to the repulsion resulting from the electron-electron interaction and the nuclear-nuclear interaction [6]. Note that the spin-orbit coupling and hyperfine interactions are neglected in the above Hamiltonian.

Alternatively, the above equation can be re-written in a more compact fashion as

$$\hat{H} = \hat{T}_N(\mathbf{R}) + \hat{T}_e(\mathbf{r}) + \hat{V}_{eN}(\mathbf{r}, \mathbf{R}) + \hat{V}_{ee}(\mathbf{r}) + \hat{V}_{NN}(\mathbf{R}), \quad (1.5)$$

where \hat{T} is the kinetic energy operator and \hat{V} is the corresponding operator for the potential energy [7]. The term $\hat{V}_{eN}(\mathbf{r}, \mathbf{R})$ prevents us from separating \hat{H} into nuclear and electronic parts. Consequently, the wave function cannot be expressed as a product of the nuclear and electronic terms.

The Schrödinger equation with such a non-separable Hamiltonian can be solved analytically only for atoms containing a single electron. For the remaining vast majority of multi-electron systems which form the core of chemistry, solutions make use of the Born-Oppenheimer (BO) approximation. Born and Oppenheimer [8] showed that the motion of the nuclei can be decoupled from electronic motion as a result of the very different timescales of the two motions. The justification lies in the observation that the electron is much lighter than the nucleus and hence the electron charge density is able to quickly rearrange in response to the slower nuclear motion. Conversely, the nucleus can be regarded as being fixed with respect to electronic motion.

The mathematical significance of the BO approximation is that it makes the Hamiltonian separable through a parametric dependence on the nuclear coordinates so that the total wave function is given as $\Psi(\mathbf{r}; \mathbf{R})\chi(\mathbf{R})$. In practice, the Schrödinger equation is solved for a fixed geometry and the corresponding electronic energy is calculated by diagonalizing the Hamiltonian. If this procedure is repeated at varying geometries, one eventually obtains the energy over a range of coordinates of the nuclei. This electronic potential energy is the desired potential energy surface (PES) for nuclear motion and it can be used to investigate the dynamics of the nuclei.

The BO ansatz assumes that no excitation of electrons occurs upon nuclear motion. In other words, the nuclei evolve on a single adiabatic PES (i.e., associated with a single electronic quantum state). The BO approximation can be safely applied to a large number of physical situations. However, processes such as charge transfer and photochemistry are inherently nonadiabatic and characterised by a coupling of the electronic and nuclear motions. In such cases, the BO approximation is said to break down. For the systems studied in this thesis, the BO separation is always a reasonable approximation.

1.4 Classical Molecular Dynamics

Molecular dynamics literally refers to the simultaneous motion of a number of atomic nuclei and electrons constituting molecular entities. In this section, we describe an approximate, yet powerful, method which tracks the classical motion of atoms (nuclei only) on a PES (by invoking the BO approximation). The PES, also called the force-field, is often an empirically determined function describing the interactions between atoms in a system through a sum of bonded forces corresponding to chemical bonds, bond angles and dihedral angles, and non-bonded interactions associated with van der Waals forces and electrostatic charge.

Classical molecular dynamics (MD) describes the time-evolution of a system approximately, according to classical mechanics. The initial state of a system is specified by its phase space variables: its momentum \mathbf{p}_i and its position \mathbf{q}_i . The dynamical

problem consists of finding solutions to Newton’s equation of motion $\mathbf{F} = m \mathbf{a}$ (see Eq. (1.2)) where the force \mathbf{F} on each atom is obtained from the gradient of the PES. Solutions are determined for a given initial condition at regular time intervals known as the *time step*, each time generating new momenta and positions $(\mathbf{p}_t, \mathbf{q}_t)$. Equations of motions are generally integrated numerically through the implementation of robust algorithms such as the Verlet integrator [9]. The end result of the dynamics is a trajectory, a series of momenta and positions as a function of time, guided by the forcefield given an initial point in the phase space.

MD can be combined with “on-the-fly” quantum mechanical calculations of the electronic potential energy through *ab initio* methods. *Ab initio* MD allows the study of bond breaking and bond formation, which typically cannot be treated via empirical classical potential functions. However, the benefit of generating accurate potential energies and their gradients comes at a price: the intensive computation involved in the calculation of the electronic wavefunction makes *ab initio* methods computationally expensive. A popular “on-the-fly” technique is Car-Parrinello [10] MD.

An important criterion in assessing the practicality of an MD simulation is its cost, where the term “cost” is equated with the total length of computer simulation time in the jargon. By definition, simulations carried out in the microcanonical ensemble (i.e., with fixed number of particles N , volume V and total energy E) require that the total energy be conserved throughout the simulations [11]. However, the numerical nature of the integration procedure can give rise to instabilities, hence leading to a violation of the energy conservation condition. This can be prevented by employing small time steps during the trajectory calculation. The computational bottleneck of MD simulations, however, is the force calculation required at every time step. Consequently, decreasing the time step or increasing the total length of the simulation can significantly add to the computational cost. To keep simulations affordable, an optimum time step, corresponding to the largest possible time step that will satisfy the energy conservation criterion, needs to be found. Typical time steps employed in simulations of molecular systems are about 10 times shorter than the fastest characteristic timescale of the motion of interest.

The loss of accuracy incurred by the introduction of an approximation, namely a classical description of the nuclear dynamics, is accompanied by a huge practical benefit: it significantly reduces the computational effort of the simulations, thereby opening applications of the technique to a wider pool of candidates. MD has been successfully applied to a number of problems, within chemistry and in other related fields. It has become the tool of choice for simulating high-dimensional complex systems, such as biological molecules [12] and nanostructures [13, 14]. The interdisciplinary nature of applications of the technique in particular is well illustrated in the review of Entel *et al.* on “Molecular Dynamics Simulations in Biology, Chemistry and Physics” [15].

1.5 Quantum Dynamics

While the approximate classical treatment of nuclear motion afforded by MD can be adequate for some systems, other problems require the use of a higher level of theory for a reliable description of their dynamic nature. An inherent limitation of MD is its inability to describe classically forbidden processes such as tunneling, zero-point motion, coherence and interference. Such phenomena are especially relevant when light atoms (such as hydrogen) are involved and have important implications in chemistry and biology.

Spectroscopy, one of the most widely used characterization tool used in chemistry, is another classical example. Spectroscopic techniques take advantage of the interaction between matter and radiation to probe the structure of compounds at the molecular or atomic scale. Spectroscopy is a broad subject, which can be subdivided into numerous categories depending on the nature of the method and the interactions involved. The essence of the techniques relies on the quantization of energy levels, a concept that can only be described using quantum mechanics. The accurate prediction and interpretation of any spectrum in general therefore benefits from a quantum mechanical treatment of the dynamics.

Quantum dynamical studies of molecular systems endeavour to numerically solve

the many-particle time-dependent Schrödinger equation given by Eq. (1.3). If the Hamiltonian is time-independent, the propagated wave function may be expanded into a set of eigenstates of \hat{H} ,

$$\Psi(t) = \sum_j a_j e^{-iE_j t/\hbar} \varphi_j, \quad (1.6)$$

where

$$\hat{H}\varphi_j = E_j\varphi_j \quad \text{and} \quad a_j = \langle \varphi_j | \Psi(0) \rangle. \quad (1.7)$$

According to the expansion in Eq. (1.6), a knowledge of the wave function $\Psi(t)$ for all times is equivalent to the knowledge of all eigenstates φ_j and energies E_j . Consequently, the choice of following quantal motion by the time-dependent or time-independent approach is a matter of taste or practicality (i.e., numerical efficiency). The remainder of this section and the next section are devoted to a discussion of the various quantum mechanical methods available to study nuclear motion within the accuracy of the BO approximation.

Although formally equivalent, the time-independent approach appears simpler because the time variable has disappeared from the equation. In this case, the Schrödinger equation is reduced to an eigenvalue problem where energy levels and wave functions are determined from the eigenvalues and eigenvectors of the Hamiltonian, respectively. The time-dependent solution to the Schrödinger equation is an initial value problem that is sometimes more attractive than its time-independent counterpart. For example, processes involving continuum states, such as scattering, can be better studied using the time-dependent picture. Additionally, methods involving an approximation of the wave function are more accurate in the time-dependent version since the time-dependent wave packet tends to be more localized in phase space than the eigenstates. Finally, only the time-dependent approach provides a correct description if the Hamiltonian itself varies with time.

The standard technique of solving the Schrödinger equation in either picture involves constructing a matrix representation of the Hamiltonian from a set of basis functions. In principle any complete set of basis functions can be chosen to expand

the wave function. In practice, however, one would like to select an efficient basis set such that accurate results can be obtained with the use of the minimum number of basis functions. The discrete variable representation (DVR) is a popular method which offers a general prescription of generating basis functions in a localized (in coordinate space) but discrete representation [16, 17]. Numerical solutions to the Schrödinger equation involves the diagonalization of the Hamiltonian. The computational effort involved in the diagonalization routine grows exponentially with the number of atoms present in the system. Consequently, exact basis set calculations are limited in terms of the treatable system size. Currently such methods can be applied to study systems of up to six atoms [18]. An additional drawback is the lack of generality: most calculations are performed in internal coordinates which demands a re-definition of the coordinates for every new system.

An alternative method that has been successful in accurately describing polyatomic systems is the multi-configuration time dependent Hartree (MCTDH) algorithm [19, 20]. The approximation involves expanding the Hamiltonian as a sum of products of one-particle operators. The wave function is then determined by variationally solving the time-dependent Schrödinger equation. MCTDH requires that all possible configurations be built from the set of possible single-particle functions. As a result, like standard methods, the technique also suffers from exponential scaling. However, the product form of the Hamiltonian leads to a reduction in the numerical cost of the calculation compared to standard approaches [21]. Therefore, MCTDH can be applied to larger systems. For instance, the method has been applied to the calculate the absorption spectrum of vibronically coupled systems such as pyrazine, by treating all 24 vibrational modes [22]. The main limitation of the method lies in the non-trivial generation of the initial MCTDH wave function, more specifically in the difficulty of tailoring a set of single-particle functions in Cartesian coordinates. It should be noted that MCTDH results are numerically exact when converged with respect to the number of configurations.

Broadly speaking, time-dependent quantum mechanical approaches can be divided into real-time and imaginary-time approaches. The techniques mentioned so

far, propagate the wave function in real time. Despite the encouragingly successful applications of MCTDH to larger system sizes, systems with hundreds of degrees of freedom still lie outside the scope of real-time full quantum calculations due the exponential scaling of numerical effort with the number of degrees of freedom. An attractive approach for the exact quantum mechanical treatment of larger polyatomic systems is offered by Feynman's path integral formalism [23, 24]. Path integral methods show a more favourable scaling since the bottleneck now lies in the evaluation of an integral whose dimensions grow linearly with the number of degrees of freedom. Following is a brief review of the underlying theory of path integral methods. We start by looking at the matrix element of the time evolution propagator in the position representation, i.e., the transition amplitude between the initial position state $|\mathbf{x}_i\rangle$ and the final position state $\langle\mathbf{x}_f|$

$$K(\mathbf{x}_i, \mathbf{x}_f, t) = \langle\mathbf{x}_f|e^{-i\hat{H}t/\hbar}|\mathbf{x}_i\rangle . \quad (1.8)$$

The Hamiltonian is given in Cartesian coordinates as

$$\hat{H} = \hat{T} + \hat{V} = \sum_{j=1}^F \frac{\hat{p}_j^2}{2m_j} + V(\hat{q}_1, \dots, \hat{q}_F) , \quad (1.9)$$

where \hat{p}_j and m_j are the momentum operator and mass associated with the j^{th} degree of freedom respectively and $\hat{q}_1, \dots, \hat{q}_f$ are the position operators. If the propagator is split into many small time slices $\Delta t = t/N$, we can rewrite Eq. (1.8) as

$$K(\mathbf{x}_i, \mathbf{x}_f, t) = \lim_{\Delta t \rightarrow 0} \int d\mathbf{x}_1 \dots \int d\mathbf{x}_{N-1} \prod_{k=1}^N \langle\mathbf{x}_k|e^{-i\hat{H}\Delta t/\hbar}|\mathbf{x}_{k-1}\rangle . \quad (1.10)$$

Since the operators for the potential and kinetic energies do not commute, the short time propagator is approximated as a Trotter product

$$e^{-i\hat{H}\Delta t/\hbar} = e^{-i\hat{T}\Delta t/\hbar}e^{-i\hat{V}\Delta t/\hbar} + O((\Delta t)^2) . \quad (1.11)$$

This leads to the following expression for the matrix element of the short time prop-

agator:

$$\begin{aligned} \langle \mathbf{x}_k | e^{-i\hat{H}\Delta t/\hbar} | \mathbf{x}_{k-1} \rangle &= \prod_{j=1}^F \left[\left(\frac{m_j}{2\pi i \hbar \Delta t} \right)^{1/2} \right. \\ &\times \left. \exp \left[\frac{i}{\hbar} \left(\sum_{j=1}^F \frac{m_j}{2\Delta t} |q_{j,k} - q_{j,k-1}|^2 - \Delta t V(\mathbf{x}_k) \right) \right] \right]. \end{aligned} \quad (1.12)$$

The oscillatory nature of the time-evolution propagator makes the real-time study of dynamical systems impractical through path integral techniques. As a result, dynamical quantities are calculated in imaginary time instead. Replacing the real time variable, t , with $t \rightarrow -i\tau\hbar$, and substituting the short time propagator in Eq. (1.10) give rise to an expression for the evolution of a system of quantum particles which is analogous to the evolution of an ensemble of classical ring polymers. In this picture, nearest neighbours (beads) on a ring polymer are connected with springs while $V(\mathbf{x})$ is the external potential. The multidimensional integral, representing an integral over all possible paths connecting \mathbf{x}_i to \mathbf{x}_f in an imaginary time $n \times \tau$, is traditionally evaluated by Monte Carlo techniques [25] (PIMC). Path integral theory has also been successfully combined with molecular dynamics techniques in path integral molecular dynamics (PIMD) [26, 27, 28, 29]. The results are exact in the limit of infinite time slices (number of beads). In practice, a finite number of time slices is sufficient to achieve converged results. Path integral techniques offer a powerful means of calculating time-independent *equilibrium* (i.e., imaginary-time) properties for molecular systems with hundreds of atoms. There have been numerous applications ranging from electron transfer in myoglobin [30] to proton transfer through hydrogen bonds [31] to the study of quantum effects in liquid water [32, 33, 34, 35] and helium [36]. Recent condensed phase studies have focused on investigations of superfluidity in helium and hydrogen clusters with a variety of dopants including carbonyl sulfide [37, 38], nitrous oxide [39, 40] and cyanoacetylene [41].

In order to compare calculated quantities with experimental *non-equilibrium* (i.e., dynamical) observables, a conversion from imaginary time to real time is necessary. In principle, real-time behaviour can be inferred via numerical analytic continuation. In reality, the transformation is far from being trivial. Although there have been reports

of successful implementations [42] which provide useful short real time information for the calculation of rate constants [43, 44], path integral methods are essentially restricted to the study of equilibrium properties.

Despite considerable progress in the field of quantum dynamics via the development of methods and algorithms as well as technological improvements, sadly, the real-time dynamics of large complex molecular systems remain largely intractable with currently available exact quantum mechanical methods.

1.6 Approximate Quantum Dynamics

Motivated by the need to overcome the limitations of exact real time quantum dynamics, increasing efforts are geared towards the development of approximate methods for treating complex molecular systems. Some hybrid approaches, which combine classical and quantum mechanics to different levels, are rapidly gaining in popularity without superseding exact techniques nonetheless. For small quantum systems, real time exact techniques remain unparalleled in performance and provide useful benchmarks for methodological developments. The current section briefly surveys a few of the available methods to provide a reader with a flavour for the variety of approaches that have been developed to study complex systems as well as to put the current work into context.

A common approach is to treat “light” particles such as electrons (in non-adiabatic systems) or hydrogen atoms quantum mechanically and to use classical mechanics to describe the motion associated with the “heavier” particles. The quantum particles are evolved in real-time via the time-dependent Schrödinger equation while the classical propagation is given by Newtonian mechanics. The difficulty in this technique lies in the coupling of the quantum and classical subsystems: *How do we permit each of the subsystems to influence and be influenced by the other subsystem?* [45]. Several forms of quantum-classical dynamics exist, depending on the models used to describe the coupling. Popular examples include mean-field [46] and trajectory surface hopping [47] approaches. The latter scheme has been successfully applied by Billeter *et al.*

to the simulation of proton transfer reactions in large biomolecules such as enzyme liver alcohol dehydrogenase in an aqueous environment [48] (~ 75000 atoms). The authors report good agreement of their calculated kinetic isotope effect for the overall rate with experimental measurements. A main limitation of this type of dynamics is that it is applicable only to systems where quantum degrees of freedom can be singled out. When the distinction becomes ambiguous, one needs to resort to alternative methods.

Approaches stemming from path integral theory and its exploitation of the isomorphism of a quantum particle with a classical ring polymer, as mentioned in Sec. 1.5, present attractive alternatives for describing quantum effects in high-dimensional systems. The two methods described here are centroid molecular dynamics (CMD) [49, 50, 51] and ring polymer molecular dynamics (RPMD) [52]. Just as conventional MD traces the trajectory of classical particles, CMD and RPMD follow the classical evolution of beads on classical ring polymers. The two techniques differ essentially in the way dynamical quantities are calculated from the trajectory variables in real time. RPMD employs average bead positions and momenta to determine quantities at every time step. In CMD on the other hand, time-dependent quantities are calculated from the phase space variables of *centroids* which represent the centres of mass of the classical ring polymers. Typically these path-integral derived techniques can provide a good description of processes occurring on short timescales. Applications of CMD include the calculation of rate constants [53, 54] and transport properties such as diffusion coefficients of liquid water [55] and liquid hydrogen [56, 57]. Similar processes have been investigated using RPMD by Manolopoulos *et al.* [58, 59, 60]. In principle, there is a high potential for applications to complex systems since the techniques present a favourable scaling with system size. Yet, to date, systems of appreciably high complexity and dimensionality remain unexplored by such methods.

The last but certainly not the least of methods to be discussed is based on semiclassical theory. Since the work presented in this thesis aims at extending the applicability of a semiclassical approach, it is only natural that its discussion be more thorough than the techniques mentioned so far. A description of the underlying theory as well

as a discussion of the method in general are presented in the Sec. 1.7.

1.7 Semiclassical Dynamics

Semiclassical approaches are characterised by their ability to obtain quantum dynamical information from classical trajectories. This feature offers the promise of combining the best of two worlds: the power to capture quantum effects while retaining the intuitive nature of classical mechanics as well as a favourable scaling with dimensionality.

Historically, semiclassical theory became popular with the formulation of the Wentzel-Kramers-Brillouin (WKB) approximation in the 1920's. The standard WKB approach was mainly developed for treating one dimensional problems and has enjoyed great success in systems with separable Hamiltonians. It provides a solution to the Schrödinger equation following a semiclassical expansion of an exponential wave function. Appendix A takes the reader through the derivation of the WKB wave function.

The most popular semiclassical technique, in terms of applications, is undoubtedly the Semiclassical initial value representation (SC-IVR). The propagator used in SC-IVR is derived from an older expression for the propagator which was proposed by van Vleck in 1928 [61]. A derivation of van Vleck's (coordinate) propagator is presented in Appendix B. In the current section, the SC-IVR propagator is derived from van Vleck's propagator. A description of the SC-IVR propagator itself, however, is omitted since it can be found in the theory sections of the subsequent chapters.

1.7.1 Derivation of the propagator

The transition amplitude or matrix element of the time-evolution operator (propagator) between an initial wave packet Ψ_i and a final wave packet Ψ_f can be written as

$$K_{fi}(t) = \int d\mathbf{x}_i \int d\mathbf{x}_f \Psi_f^*(\mathbf{x}_f) \langle \mathbf{x}_i | e^{-i\hat{H}t/\hbar} | \mathbf{x}_f \rangle \Psi_i(\mathbf{x}_i), \quad (1.13)$$

where \mathbf{x}_i and \mathbf{x}_f represent the initial and final coordinates respectively. Using the van Vleck [61] approximation for the coordinate propagator leads to

$$K_{fi}(t) = \sum_c \int d\mathbf{x}_i \int d\mathbf{x}_f \Psi_f^*(\mathbf{x}_f) \left((2\pi i \hbar)^F \left| \frac{\partial \mathbf{x}_f}{\partial \mathbf{p}_i} \right| \right)^{-1/2} \times e^{\frac{i}{\hbar} S_c(\mathbf{x}_i, \mathbf{x}_f, t)} e^{-iM_c \frac{\pi}{2}} \Psi_i(\mathbf{x}_i) , \quad (1.14)$$

where $S_c(\mathbf{x}_i, \mathbf{x}_f, t)$ represents the classical action along the trajectory, M_c is the Maslov index counting the number of negative eigenvalues of the second derivative matrix of the action S_c , and the momentum \mathbf{p}_i is given by

$$\mathbf{p}_i = - \frac{\partial S_c(\mathbf{x}_i, \mathbf{x}_f, t)}{\partial \mathbf{x}_i} . \quad (1.15)$$

The direct application of Eq. (1.14) is prohibitively impractical for two reasons. First, the determination of $S_c(\mathbf{x}_i, \mathbf{x}_f, t)$ is associated with the notorious root-search problem. Because only the end points \mathbf{x}_i and \mathbf{x}_f are known, all classical trajectories satisfying the condition $\mathbf{x}_f(\mathbf{x}_i, \mathbf{p}_i, t) = \mathbf{x}_f$ need to be located by varying the initial momentum. The second inconvenience comes from the observation that the propagator is singular at caustics or turning points where

$$\frac{\partial \mathbf{x}_f(\mathbf{x}_i, \mathbf{p}_i, t)}{\partial \mathbf{p}_i} = 0 , \quad (1.16)$$

thus rendering its evaluation problematic.

Applications of the semiclassical propagator in the early 1970's were traditionally performed by introducing further semiclassical approximations for the wave functions and evaluating them using the stationary phase approximation (SPA). The birth of the Initial Value Representation (IVR) [62] has revolutionized applications of semiclassical theory. The strategy of the IVR is to evaluate the integrals over \mathbf{x}_i and \mathbf{x}_f numerically rather than by using SPA. To circumvent the root-search problem, SC-IVR employs a transformation of the integration variable from \mathbf{x}_f to \mathbf{p}_i , i.e.,

$$d\mathbf{x}_f = \left| \frac{\partial \mathbf{x}_f(\mathbf{p}_i, \mathbf{p}_i, t)}{\partial \mathbf{p}_i} \right| d\mathbf{p}_i , \quad (1.17)$$

resulting in the following expression for the IVR transition amplitude

$$K_{fi}(t) = \sum_c \int d\mathbf{x}_i \int d\mathbf{p}_i \Psi_f^*(\mathbf{x}_t) \left(\frac{1}{(2\pi i\hbar)^F} \left| \frac{\partial \mathbf{x}_t(\mathbf{x}_i, \mathbf{p}_i)}{\partial \mathbf{p}_i} \right| \right)^{1/2} \times e^{\frac{i}{\hbar} S_c(\mathbf{x}_i, \mathbf{p}_i, t)} e^{-iM_c \frac{\pi}{2}} \Psi_i(\mathbf{x}_i), \quad (1.18)$$

Since $\mathbf{x}_f(\mathbf{x}_i, \mathbf{p}_i, t)$ is given by the trajectory evolving from an initial coordinate \mathbf{x}_i and an initial momentum \mathbf{p}_i , the integral can be evaluated by a Monte Carlo sampling without the need for root-searching. In addition, the singularities that could arise in the original expression are removed since the Jacobian ($\partial \mathbf{x}_t / \partial \mathbf{p}_i$) is now present in the numerator rather than in the denominator as in Eq. (1.14). Eq. (1.18) can be expressed in Dirac notation as

$$\langle \Psi_i | e^{-i\hat{H}t/\hbar} | \Psi_f \rangle = \sum_c \int d\mathbf{x}_i \int d\mathbf{p}_i \langle \Psi_f | \mathbf{x}_t \rangle \left(\frac{1}{(2\pi i\hbar)^F} \left| \frac{\partial \mathbf{x}_t(\mathbf{x}_i, \mathbf{p}_i)}{\partial \mathbf{p}_i} \right| \right)^{1/2} \times e^{\frac{i}{\hbar} S_c(\mathbf{x}_i, \mathbf{p}_i, t)} e^{-iM_c \frac{\pi}{2}} \langle \mathbf{x}_i | \Psi_i \rangle, \quad (1.19)$$

An explicit expression for the IVR propagator can be obtained in terms of the Cartesian coordinates by deleting the wave packets from the above equation

$$e^{-i\hat{H}t/\hbar} = \sum_c \int d\mathbf{x}_i \int d\mathbf{p}_i \left(\frac{1}{(2\pi i\hbar)^F} \left| \frac{\partial \mathbf{x}_t(\mathbf{x}_i, \mathbf{p}_i)}{\partial \mathbf{p}_i} \right| \right)^{1/2} \times e^{\frac{i}{\hbar} S_c(\mathbf{x}_i, \mathbf{p}_i, t)} e^{-iM_c \frac{\pi}{2}} |\mathbf{x}_t\rangle \langle \mathbf{x}_i|, \quad (1.20)$$

Similarly, the propagator can be written in Cartesian momentum representation as

$$e^{-i\hat{H}t/\hbar} = \sum_c \int d\mathbf{x}_i \int d\mathbf{p}_i \left(\frac{1}{(2\pi i\hbar)^F} \left| \frac{\partial \mathbf{p}_t(\mathbf{x}_i, \mathbf{p}_i)}{\partial \mathbf{x}_i} \right| \right)^{1/2} \times e^{\frac{i}{\hbar} \tilde{S}_c(\mathbf{x}_i, \mathbf{p}_i, t)} e^{-iM_c \frac{\pi}{2}} |\mathbf{p}_t\rangle \langle \mathbf{p}_i|, \quad (1.21)$$

where the action is defined in momentum space as

$$S_c(\mathbf{x}_i, \mathbf{x}_f, t) = \int_0^t dt' [-\mathbf{x}(t') \dot{\mathbf{p}}(t') - H(\mathbf{p}(t'), \mathbf{x}(t'))]. \quad (1.22)$$

In 1984, Herman and Kluk [63] derived an expression for the IVR propagator in terms of coherent-states $|g_{\mathbf{p}_i, \mathbf{q}_i}\rangle$. These hybrid states, intermediate between position

and momentum eigenstates, are given in the position representation as

$$\langle \mathbf{x} | g_{\mathbf{p}_i, \mathbf{q}_i} \rangle = \left(\frac{\gamma}{\pi} \right)^{F/4} \exp \left[-\frac{1}{2} (\mathbf{x} - \mathbf{q}_i)^T \gamma (\mathbf{x} - \mathbf{q}_i) + \frac{i}{\hbar} \mathbf{p}_i^T (\mathbf{x} - \mathbf{q}_i) \right]. \quad (1.23)$$

In this picture, every classical point in phase space is represented by a Gaussian wave packet of width γ through its expectation values of the position and momentum operators, corresponding to \mathbf{q}_i and \mathbf{p}_i respectively in the above equation. The wave packets are commonly referred to as frozen Gaussian wave packets [64, 65] in the literature because of their fixed widths. Chapter 2 offers a description of the procedure leading to the generation of the width matrix. In the limit $\gamma \rightarrow \infty$, the coherent-states become position eigenstates and the propagator reduces to Eq. (1.20). Similarly, in the opposite limit of $\gamma \rightarrow 0$, the coherent-states become momentum eigenstates with the description of the propagator afforded by Eq. (1.21). The Herman-Kluk (HK) propagator is expressed as

$$e^{-i\hat{H}t/\hbar} = (2\pi\hbar)^{-F} \int \int d\mathbf{p}_i d\mathbf{q}_i R_{\mathbf{p}_i \mathbf{q}_i t} e^{iS_{\mathbf{p}_i \mathbf{q}_i t}/\hbar} |g_{\mathbf{p}_i \mathbf{q}_i}\rangle \langle g_{\mathbf{p}_i \mathbf{q}_i}|. \quad (1.24)$$

As mentioned above, detailed explanations of the propagator can be found in forthcoming chapters. We will just point out here the appearance of a new term $R_{\mathbf{p}_i \mathbf{q}_i t}$ known as the HK prefactor in the propagator.

The acronym SC-IVR in this thesis refers specifically to Herman and Kluk's version of the Semiclassical Initial Value Representation. Likewise, unless otherwise specified, the SC-IVR propagator is synonymous to HK propagator given by Eq. (1.24).

1.7.2 Features of SC-IVR

Herman and Kluk's contribution has made SC-IVR by far the most popular semiclassical scheme by offering a practical way of adding quantum effects to classical dynamics. The success can also be attributed to the accuracy as well as the simplicity and ease of implementation of the method.

Past studies have shown that SC-IVR is able to capture a variety of quantum effects such as interference, zero-point motion and tunneling, sometimes with very

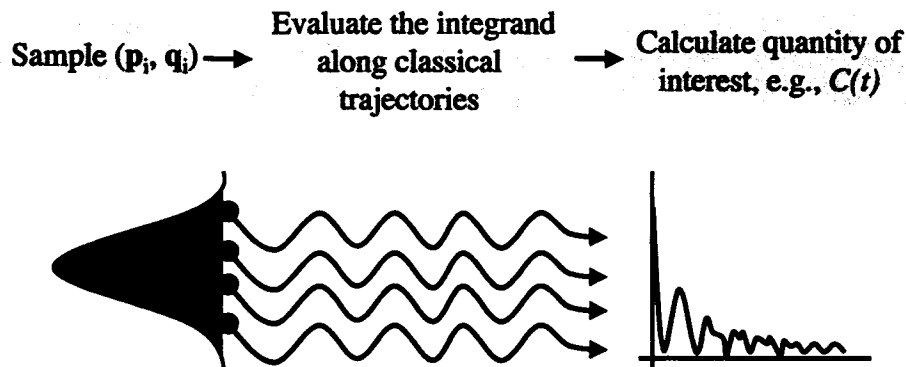


Figure 1.1: Schematic representation of SC-IVR calculation

good accuracy [66, 67, 68]. A concise description of applications of the technique is provided in Sec. 1.7.3. To illustrate the simplicity of SC-IVR calculations, we briefly describe the procedure depicted in Fig. 1.1. The first step involves sampling initial conditions from which trajectories are generated. The integrand is evaluated during the classical dynamics and finally employed to calculate quantities of interest, which are discussed below. The time-averaged SC-IVR employed in Chapter 5 is essentially a single-step procedure. This is as simple as a quantum dynamical calculation can get! In addition, implementations of SC-IVR have wisely taken advantage of established tools such as Monte Carlo for the sampling of initial conditions and MD for the classical dynamics. The latter point is particularly important. Since quantum dynamical quantities are calculated exclusively from classically obtained data, SC-IVR can be integrated into MD software packages without much effort. Too often, quantum systems are studied classically due to the limitations of available quantum mechanical methods. Such implementations of SC-IVR would allow for the possibility of including quantum effects in conventional classical MD simulations. Part of our goal is precisely to implement SC-IVR in the context of the molecular modelling toolkit [69], a software toolkit currently designed for *classical* simulations.

Besides the advantages listed above, SC-IVR is blessed with technical benefits

over other quantum mechanical methods. The fact that the dynamics are performed classically suggests an affordable computational cost compared to exact approaches. Brewer’s study on the scaling of SC-IVR revealed a linear scaling with the number of degrees of freedom [70]. Moreover, the nature of the method, namely the independent generation of classical trajectories from a pool of initial conditions makes it amenable to parallelization of the computational effort during the dynamics and evaluation of the integrand.

The difficulty in SC-IVR lies in the rapidly oscillating nature of the integrand, which slows down the convergence of the calculations. *“The interference between the trajectories with different initial conditions is the source of computational difficulty, but is also the source of quantum effects, so one must deal with it”*, rightly comments W. H. Miller, the father of SC-IVR [71]. Several variants of IVR have been developed to this end, although none have been as successful as the HK formulation. An example is the linearized IVR [72, 73] which makes a rather drastic approximation in the evaluation of the propagator by assuming that the contribution to the integral comes exclusively from trajectories that are closely related in phase space, thereby dampening the integrand. The approach has been tested on model systems where it was shown to correctly reproduce rate constants and the population relaxation in an electron-transfer reaction. However, the effect of the linearized approximation is a purely classical behaviour of the dynamics at long times. Therefore, the method is not suited to the study of more realistic systems where quantum treatment is often required over longer periods of time [71]. A more rigorous and practical way of dealing with oscillatory signals is offered by Forward-Backward IVR (FBIVR) [74, 75, 76]. In this technique the double phase space integral is reduced to a single integral. Two propagators, $e^{-i\hat{H}t/\hbar}$ and $e^{+i\hat{H}t/\hbar}$ are utilized resulting in the time evolution of initial conditions from time 0 to t (forward propagation) and from time t to 0 (backward propagation). As opposed to the linearized IVR, FBIVR has been successfully applied to molecular systems. These applications are listed in the review of applications of SC-IVR at the end of this section. For details concerning the formalism of FBIVR, we refer the reader to the article by Sun and Miller [76] and a recent review [77]. No

perfect solution has been identified yet. Attempts to reduce the computational cost is still a current area of research as illustrated by the recent formulation of a van Vleck SC-IVR [78] or of a new and improved linearized version [79]. The treatment of the oscillatory integrand in our calculations is discussed alongside the specific methods used in the respective chapters.

1.7.3 Applications of SC-IVR

The massive current literature related to SC-IVR attests to its growing popularity. Several reviews have appeared on the general subject in recent years [71, 80, 81, 82, 77]. In broad terms, developmental efforts can be divided into methodological improvements (such as the aforementioned efforts to cut down the computational cost) and their applications. In this section, we provide a mini-review of the large volume and variety of applications of SC-IVR, which ultimately dictates the general and practical nature of any implemented theoretical tool.

The application of a newly developed method generally occurs in stages. Often, initial attempts involve some form of testing on model problems. Successful testing then allows applications to more realistic systems. While each stage of the process is equally important, attention is focused here on applications to atomic and molecular systems because of their greater relevance to our goal of treating complex dynamical molecular systems quantum mechanically.

To fully understand and appreciate the quantum dynamical calculations, it is useful to have a feel for the quantities that are calculated. In this regard, we provide a short description of real-time correlation functions [83].

The dynamical behaviour of molecular systems in general can be studied through time correlation functions. Classical correlation functions relate the value of a property B at time 0 with a property A at time t , i.e.,

$$C(t) = \langle B(0)A(t) \rangle = \frac{1}{Z_{cl}} \int d\mathbf{p} \int d\mathbf{q} e^{-\beta H(\mathbf{p}, \mathbf{q})} A(t) B(0) , \quad (1.25)$$

where Z_{cl} is the classical partition function and $\beta = 1/k_B T$, k_B and T being the Boltzmann constant and the temperature, respectively. Quantum mechanically, the

correlation function is defined as a trace over the operators corresponding to the observables of interest normalized by the partition function Z :

$$C(t) = \frac{1}{Z} \text{Tr} \left[e^{-\beta \hat{H}} \hat{B} e^{i\hat{H}t/\hbar} \hat{A} e^{-i\hat{H}t/\hbar} \right]. \quad (1.26)$$

The quantities or operators A and B are determined by the property that is being investigated. If $A = B$ or ($\hat{A} = \hat{B}$ in the quantum mechanical version), the correlation function is called an autocorrelation function. For example, the eigenvalue spectrum, commonly known as the power spectrum, $I(\omega)$ can be obtained via a Fourier transformation of the survival amplitude (sometimes also called the autocorrelation function)

$$I(\omega) = \frac{1}{2\pi} \int_{-\infty}^{\infty} dt e^{i\omega t} C(t) = \sum_n |\langle \Psi | n \rangle|^2 \delta(\hbar\omega - E_n). \quad (1.27)$$

ω corresponds to the frequency (or eigenvalue) and $C(t)$ is given in SC-IVR formulation by

$$\begin{aligned} C(t) &= \langle \Psi_i | e^{-i\hat{H}t/\hbar} | \Psi_i \rangle \\ &= (2\pi\hbar)^{-3N} \int \int d\mathbf{p}_i d\mathbf{q}_i R_{\mathbf{p}_i \mathbf{q}_i t} e^{iS_{\mathbf{p}_i \mathbf{q}_i t}/\hbar} \langle \Psi_i | g_{\mathbf{p}_i \mathbf{q}_i} \rangle \langle g_{\mathbf{p}_i \mathbf{q}_i} | \Psi_i \rangle, \end{aligned} \quad (1.28)$$

where $3N$ is the total number of degrees of freedom for a system consisting of N atoms. Such an expression has been used to accurately determine the tunneling splitting of the HCl dimer from its eigenvalues [84]. Photodetachment spectra (i.e., photoelectron spectra of negatively charged ions) have been calculated for $\Gamma^- \text{Ar}_n$, $n = 2 - 6$ by Brewer *et al.* [85]. Calculations were performed for systems possessing up to 15 degrees of freedom with $|\Psi_i\rangle$ as the ground vibrational state of the negative ion and with the Hamiltonian \hat{H} describing the dissociation to a neutral molecule. The authors observed very good agreement with the experimentally determined spectrum. Other spectroscopic applications include the photodissociation of carbon dioxide CO_2 [86], ozone [87] O_3 and iodine cyanide ICN [88] and the photoexcitation of pyrazine [89]. Except for CO_2 , all systems involved a coupling of electronic states and therefore necessitated a non-adiabatic treatment of the dynamics. In all cases, the quantum mechanical result was closely reproduced. Ovchinnikov and Apkarian [90] successfully

simulated the absorption spectrum of Cl₂ in solid Ar via mixed-order semiclassical dynamics of a system with a total number of 321 degrees of freedom.

Just as autocorrelation functions enable the calculation of the eigenvalues, they also provide a means of analyzing the eigenfunctions associated with each eigenvalue after minor manipulations:

$$|\Phi_n\rangle \propto \frac{1}{2t} \int_{-t}^t e^{iE_n t'/\hbar} |\Psi(t')\rangle dt' . \quad (1.29)$$

Such an approach offers the possibility of probing the molecular structure and has been applied to a ruthenium dihydrogen complex, [Ru(H...H)(C₅Me₅)(dppm)]⁺, [91]. Conventionally, molecular structures are determined quantum mechanically via electronic structure theory. In the case of the above complex, however, the results from neutron diffraction experiments did not match the predictions from electronic structure methods but have been successfully explained in terms of the delocalisation of the wave function within SC-IVR.

Another type of correlation function that has been extensively studied is the flux flux correlation function. The long time limit of this correlation function affords the rate constant for a chemical reaction. In this case,

$$\begin{aligned} \hat{A} &= \hat{F} = \frac{i}{\hbar} [\hat{H}, h(s(\hat{\mathbf{q}}))] \\ \hat{B} &= h(s(\hat{\mathbf{q}})) , \end{aligned} \quad (1.30)$$

where \hat{F} stands for the flux operator and the Heaviside function, $h(s(\hat{\mathbf{q}}))$ has a value of 1 on the product and 0 on the reactant sides of the dividing surface defined by $s(\hat{\mathbf{q}})$. Alternatively, the reaction survival probability can be calculated as

$$P(t) = \langle \Psi_i | e^{i\hat{H}t/\hbar} h(\mathbf{q}) | \Psi_i \rangle . \quad (1.31)$$

Investigation of the excited state double-proton transfer in 7-azaindole dimers via FBIVR revealed that proton transfer occurs 100 fs after photoexcitation [92]. A similar study was performed for oxazole derivatives (51 degrees of freedom) [93]. In both studies, the authors report that the results are in good agreement with full quantum mechanical results. As well, comparison of SC-IVR treatment of reaction dynamics

with experimental observations has offered valuable insight into the hydroxylation mechanism of alkanes [94].

In conclusion, the impressive number of applications of SC-IVR and the successful extension to systems of increasing complexity in particular makes it an undoubtedly promising approach for the treatment of quantum effects in large complex molecular systems.

1.7.4 The void in SC-IVR

Generality is a major requirement for methods such as SC-IVR which aspire to offer a practical means of adding quantum effects to classical simulations of systems of molecular complexity. In other words, to truly function in conjunction with classical dynamics, SC-IVR needs to be amenable to the treatment of existing classical simulations. However, as SC-IVR is trying to establish itself as a quantum dynamical technique for large complex molecules, one cannot help but note that there lies a significant obstacle in its way: *the treatment of geometrically constrained molecular systems has been neglected.*

The natural question that pops up in the mind of the reader at this point is: *Why is the treatment of constrained molecules so critical?* The majority of MD simulations of large molecules inevitably involve constraining some parts of the systems. For instance, the simulation of solvated proteins generally employs rigid solvent molecules. The rationale for constraining high frequency motions or freezing out degrees of freedom is the same as in the BO approximation: motions occurring on different timescales can be decoupled without seriously compromising the accuracy of the calculations. In MD specifically, there is another more compelling reason for constraining high frequency vibrations, as beautifully illustrated by W. H. Miller's words: *"consider the water molecule, which is ubiquitous in bio simulations: the zero-point energy in its two OH stretching vibrations and its bending vibration is more than 20 times $k_B T$ (at 300 K). If this energy were allowed to behave classically in a simulation with hundreds (or thousands) of water molecules, it is clear that nonsense would result; the energy could leak out of these modes classically (which it cannot do*

quantum mechanically) and boil the system!" [82].

By freezing out certain motions from a system, one is left with a system of reduced dimensionality. Since the computational cost of carrying out a classical or semiclassical simulation is proportional to the dimensionality, the beneficial consequence accompanying the inclusion of constraints is a gain in computer time. By extension, it becomes conceivable to investigate quantum mechanical phenomena in systems of high dimensions which traditionally lie outside the capabilities of semiclassical methods. This lowering of computational cost in semiclassical calculations has two origins. First is a reduction in the computational effort involved in the generation of classical trajectories, through the use of larger timesteps (see Sec. 1.4 for details). The second spin-off is related to the traditional difficulty of handling the oscillatory integrand in semiclassical calculations (mentioned earlier): constraining high frequency modes naturally smoothes out the integrand and leads to a faster convergence of the calculations. Finally, imposing constraints on selected degrees of freedom is desirable in some situations such as kinetic studies where one wishes to focus on a specific reactive mode of interest.

Traditionally, quantum calculations on constrained systems are performed in internal coordinates. This natural choice of coordinate system is however the least general option since a re-definition is required for every new system. Cartesian coordinates, on the other hand, being general, conveniently obviates the need for such a new definition. For this reason, they are also the coordinate system employed in the majority of MD simulation packages. It is therefore desirable to perform SC-IVR calculations of constrained molecules in Cartesian coordinates, particularly if integration within MD framework is to be maintained as a viable goal.

1.7.5 Original contributions to knowledge and overview

To reiterate, our goal is to treat geometrically constrained systems within SC-IVR in Cartesian coordinates. The inclusion of constraints in SC-IVR is a non-trivial problem, especially for systems of high dimensionality. Previous efforts have treated model and simple one dimensional systems [95]. In this thesis, we present the development

of a general and practical approach targeting constrained *multidimensional* systems [96, 97, 98, 99].

Our novel contributions, specifically, are twofold: scientific and technical (or computational). The scientific accomplishment is the extension of the capabilities of SC-IVR to allow for the treatment of geometrically constrained atomic and molecular clusters in Cartesian coordinates. Our method was initially developed and tested on model *atomic clusters* and shown to accurately reproduce the zero-point energy (see Chapter 2) as well as the excited state energies (see Chapter 3). Following the success of the tests, we extended the method to treat *molecular* clusters. The encouraging results of the study are presented in Chapter 4. We also apply our approach to another SC-IVR technique (the time-averaged SC-IVR) which has been proposed as a potential way of studying specifically large quantum dynamical systems. The performance of our method in this context is discussed in Chapter 5. Concluding remarks and future work are presented in Chapter 6.

In addition, the implementation of the developed methodology is carried out in the context of the molecular modelling tooling (MMTK) [69], a software library package for MD simulations. Currently, no quantum dynamical calculations can be performed directly with the software. The planned distribution of our computer codes (a description of the codes is provided in the Appendix C) as open software will offer the possibility of investigating non-equilibrium (dynamical) quantum mechanical properties to users of MMTK.

Bibliography

- [1] P. A. M. Dirac, Proc. R. Soc. London Ser. A **123**, 714 (1929).
- [2] Cambridge advanced learner's dictionary, 1995.
- [3] C. J. Cramer, *Essentials of Computational Chemistry* (Wiley, England, 2002).
- [4] H. Goldstein, C. Poole, and J. Safko, *Classical mechanics*, 3rd edition (Addison-Wesley, San Francisco, 2002).
- [5] R. P. Feynman, *The Feynman Lectures on Physics*, volume 3 of *The Feynman Lectures on Physics* (Addison-Wesley, Boston, 1963).
- [6] T. Engel and P. Reid, *Physical Chemistry* (Pearson Benjamin Cummings, San Francisco, 2006).
- [7] J. Z. H. Zhang, *Theory and Application of Quantum Molecular Dynamics* (World Scientific, Singapore, 1999).
- [8] M. Born and R. Oppenheimer, Ann. Phys. (Berlin) **84**, 457 (1927).
- [9] L. Verlet, Phys. Rev. **159**, 98 (1967).
- [10] R. Car and M. Parrinello, Phys. Rev. Lett. **55**, 2471 (1985).
- [11] M. P. Allen and D. J. Tildesley, *Computer Simulation of Liquids* (Oxford University Press, 1989).
- [12] T. E. Cheatham III and P. A. Kollman, Ann. Rev. Phys. Chem. **51**, 435 (2001).
- [13] H. Gao and Y. Kong, Annu. Rev. Mater. Res. **34**, 123 (2004).

- [14] M. José-Yacamán, E. Pérez-Tijerina, and S. Mejía-Rosales, *J. Mater. Chem.* **17**, 1035 (2007).
- [15] P. Entel et al., Molecular dynamics simulations in biology, chemistry and physics, in *Computational Material Science*, edited by W. Hergert, M. Däne, and A. Ernst, volume 642 of *Lecture Notes in Physics* (Berlin Springer Verlag, 2004).
- [16] J. C. Light, I. P. Hamilton, and J. V. Lill, *Adv. Chem. Phys.* **82**, 1400 (1984).
- [17] J. C. Light and T. Carrington Jr., *Adv. Chem. Phys.* **114**, 263 (2000).
- [18] H.-G. Yu, *J. Chem. Phys.* **120**, 2270 (2004).
- [19] H.-D. Meyer, U. Manthe, and L. S. Cederbaum, *Chem. Phys. Lett.* **165**, 73 (1990).
- [20] U. Manthe, H.-D. Meyer, and L. S. Cederbaum, *J. Chem. Phys.* **97**, 3199 (1992).
- [21] M. H. Beck, A. Jäckle, G. A. Worth, and H.-D. Meyer, *Phys. Rep.* **324**, 1 (2000).
- [22] G. A. Worth, H.-D. Meyer, and L. S. Cederbaum, *J. Chem. Phys.* **105**, 4412 (1996).
- [23] R. P. Feynman, *Mod. Rev. Phys.* **20**, 367 (1948).
- [24] R. P. Feynman and A. R. Hibbs, *Quantum Mechanics and Path Integrals* (McGraw-Hill, New York, 1965).
- [25] N. Metropolis, A. W. Rosenbluth, M. N. Rosenbluth, H. Teller, and E. Teller, *J. Chem. Phys.* **21**, 1087 (1953).
- [26] M. Parrinello and A. M. Rahman, *J. Chem. Phys.* **80**, 860 (1984).
- [27] B. de Raedt, M. Spirik, and M. L. Klein, *J. Chem. Phys.* **80**, 5719 (1984).
- [28] M. E. Tuckerman, B. J. Berne, G. J. Martyna, and M. L. Klein, *J. Chem. Phys.* **99**, 2796 (1993).

- [29] M. E. Tuckerman, D. Marx, M. L. Klein, and M. Parrinello, *J. Chem. Phys.* **275**, 817 (1997).
- [30] A. Kuki and P. G. Wolynes, *Science* **236**, 1647 (1987).
- [31] M. E. Tuckerman, D. Marx, M. L. Klein, and M. Parrinello, *Science* **275**, 817 (1997).
- [32] R. A. Kuharski and P. J. Rossky, *J. Chem. Phys.* **82**, 5164 (1985).
- [33] A. Wallqvist and B. J. Berne, *Chem. Phys. Lett.* **117**, 214 (1985).
- [34] J. Lobaugh and G. A. Voth, *J. Chem. Phys.* **106**, 2400 (1997).
- [35] G. S. D. Buono, P. J. Rossky, and J. Schnitker, *J. Chem. Phys.* **95**, 3728 (1991).
- [36] D. M. Ceperley, *Rev. Mod. Phys.* **67**, 279 (1995).
- [37] Y. Kwon and K. B. Whaley, *Phys. Rev. Lett.* **89**, 273401 (2002).
- [38] N. Blinov, X. Song, and P. N. Roy, *J. Chem. Phys.* **120**, 5916 (2004).
- [39] S. Moroni, N. Blinov, and P. N. Roy, *J. Chem. Phys.* **121**, 3577 (2004).
- [40] Y. Xu, N. Blinov, W. Jäger, and P. N. Roy, *J. Chem. Phys.* **124**, 081101 (2006).
- [41] W. Topic, W. Jäger, N. Blinov, and P. N. Roy, *J. Chem. Phys.* **125**, 144310 (2006).
- [42] D. Thirumalai and B. J. Berne, *J. Chem. Phys.* **79**, 5029 (1983).
- [43] K. Yamashita and W. H. Miller, *J. Chem. Phys.* **82**, 5475 (1985).
- [44] E. Rabani, G. Krilov, and B. J. Berne, *J. Chem. Phys.* **112**, 2605 (2000).
- [45] R. E. Wyatt, *Mixed quantum-classical dynamics* (Springer New York, 2006).
- [46] G. D. Billing, *Int. Rev. Phys. Chem.* **13**, 309 (1994).

- [47] J. C. Tully, *J. Chem. Phys.* **93**, 1061 (1990).
- [48] S. R. Billeter, S. P. Webb, T. Iordanov, P. K. Agarwal, and S. Hammes-Schiffer, *J. Chem. Phys.* **114**, 6925 (2001).
- [49] J. Cao and G. A. Voth, *J. Chem. Phys.* **100**, 5106 (1994).
- [50] S. Jang and G. A. Voth, *J. Chem. Phys.* **111**, 2357 (1999).
- [51] S. Jang and G. A. Voth, *J. Chem. Phys.* **111**, 2371 (1999).
- [52] I. R. Craig and D. E. Manolopoulos, *J. Chem. Phys.* **121**, 3368 (2004).
- [53] E. Geva, Q. Shi, and G. A. Voth, *J. Chem. Phys.* **115**, 9209 (2001).
- [54] Q. Shi and E. Geva, *J. Chem. Phys.* **116**, 3223 (2002).
- [55] L. H. de la Pena, M. S. G. Razul, and P. G. . Kusalik, *J. Chem. Phys.* **123**, 144506 (2005).
- [56] K. Kinugawa, P. B. Moore, and M. L. Klein, *J. Chem. Phys.* **106**, 1154 (1997).
- [57] T. Hone, P. J. Rossky, and G. A. Voth, *J. Chem. Phys.* **124**, 154103 (2006).
- [58] I. R. Craig and D. E. Manolopoulos, *J. Chem. Phys.* **122**, 084106 (2005).
- [59] I. R. Craig and D. E. Manolopoulos, *J. Chem. Phys.* **123**, 034102 (2005).
- [60] T. F. Miller III and D. E. Manolopoulos, *J. Chem. Phys.* **123**, 154504 (2005).
- [61] J. H. V. Vleck, *Proc. Natl. Acad. Sci. U. S. A.* **14**, 178 (1928).
- [62] W. H. Miller, *J. Chem. Phys.* **53**, 3578 (1970).
- [63] M. Herman and E. Kluk, *Chem. Phys.* **91**, 27 (1984).
- [64] E. Heller, *J. Chem. Phys.* **75**, 2923 (1981).
- [65] E. Heller, *Acc. Chem. Res.* **39**, 127 (2006).

- [66] W. H. Miller, Farad. Discuss. Chem. Soc. **110**, 1 (1998).
- [67] S. Garashchuk and D. Tannor, Chem. Phys. Lett. **262**, 477 (1996).
- [68] F. Grossmann, Chem. Phys. Lett. **262**, 470 (1996).
- [69] K. Hinsen, J. Comp. Chem. **21**, 79 (2000).
- [70] M. L. Brewer, J. Chem. Phys. **111**, 6168 (1999).
- [71] W. H. Miller, J. Phys. Chem. A **105**, 2942 (2001).
- [72] X. Sun and W. H. Miller, J. Chem. Phys. **106**, 6347 (1997).
- [73] H. Wang, X. Sun, and W. H. Miller, J. Chem. Phys. **108**, 9726 (1998).
- [74] N. Makri and K. Thompson, Chem. Phys. Lett. **291**, 101 (1998).
- [75] K. Thompson and N. Makri, J. Chem. Phys. **110**, 1343 (1999).
- [76] X. Sun and W. H. Miller, J. Chem. Phys. **110**, 6635 (1999).
- [77] W. H. Miller, J. Chem. Phys. **125**, 132305 (2006).
- [78] C. Venkataraman and W. H. Miller, J. Chem. Phys. **126**, 094124 (2007).
- [79] J. Liu and W. H. Miller, J. Chem. Phys. **126**, 234110 (2007).
- [80] M. Thoss and H. Wang, Annu. Rev. Phys. Chem. **55**, 299 (2004).
- [81] K. G. Kay, Annu. Rev. Phys. Chem. **56**, 255 (2005).
- [82] W. H. Miller, Proc. Natl. Acad. Sci. U. S. A. **102**, 6660 (2005).
- [83] D. Chandler, *Introduction to Modern Statistical Mechanics* (Oxford University Press, 1987).
- [84] X. Sun and W. Miller, J. Chem. Phys. **108**, 8870 (1998).
- [85] M. L. Brewer, J. Hulme, and D. Manolopoulos, J. Chem. Phys. **106**, 4832 (1997).

- [86] A. Walton and D. Manolopoulos, *Chem. Phys. Lett.* **84**, 961 (1996).
- [87] V. S. Batista and W. H. Miller, *J. Chem. Phys.* **108**, 498 (1998).
- [88] E. A. Coronado, V. S. Batista, and W. H. Miller, *J. Chem. Phys.* **112**, 5566 (2000).
- [89] M. Thoss, W. H. Miller, and G. Stock, *J. Chem. Phys.* **112**, 10282 (2000).
- [90] M. Ovchinnikov and V. A. Apkarian, *J. Chem. Phys.* **108**, 2277 (1998).
- [91] L. Torres, R. Gelabert, X. Gimenez, M. Moreno, and J. Lluch, *J. Chem. Phys.* **117**, 7094 (2002).
- [92] V. Guallar, V. S. Batista, and W. H. Miller, *J. Chem. Phys.* **110**, 9922 (1999).
- [93] V. Guallar, V. S. Batista, and W. H. Miller, *J. Chem. Phys.* **113**, 9510 (2000).
- [94] V. Guallar, B. F. Gherman, W. H. Miller, S. J. Lippard, and R. A. Friesner, *J. Am. Chem. Soc.* **124**, 3377 (2001).
- [95] B. B. Harland and P.-N. Roy, *J. Chem. Phys.* **118**, 4791 (2003).
- [96] B. B. Issack and P.-N. Roy, *J. Chem. Phys.* **123**, 084103 (2005).
- [97] B. B. Issack and P.-N. Roy, *J. Chem. Phys.* **126**, 024111 (2007).
- [98] B. B. Issack and P.-N. Roy, *J. Chem. Phys.* **127**, 054105 (2007).
- [99] B. B. Issack and P.-N. Roy, *J. Chem. Phys.* **submitted** (2007).

Chapter 2

Ground state

Article 1. Geometric constraints in semiclassical initial value representation calculations in Cartesian coordinates: Accurate reduction in zero-point energy

Reused with permission from Bilkiss B. Issack and Pierre-Nicholas Roy, *Journal of Chemical Physics* **123**, 084103 (2005). Copyright 2005, American Institute of Physics.

2.1 Introduction

Considerable progress has been made in semiclassical (SC) theory and its applicability to quantum dynamics since the development of van Vleck's [1] standard SC approximation. The approximation involves evaluating the time evolution of the quantum propagator from observables obtained from classical trajectories. Early applications of van Vleck's propagator proved to be problematic because of the "root-search" procedure that was required: all trajectories with different initial momenta that satisfied the initial and time-evolved coordinates had to be located. The problem was circumvented with the birth of the initial value representation (IVR) of the SC propagator over three decades ago [2, 3, 4]. Since then, there has been numerous applications of SC-IVR [5, 6, 7, 8]. The Herman-Kluk [5] (HK) or coherent-state version has been the most popular in terms of applications to quantum dynamics. The HK version of the SC-IVR will be referred to as HK-SC-IVR throughout this paper.

SC-IVR theory offers a means of adding quantum effects to classical trajectories. Semiclassical dynamics have been shown to provide a description, although approx-

imate, of quantum effects such as tunneling, interference, and zero-point energy, in chemical dynamics [9, 10, 11]. Since exact quantum calculations are not feasible for complex systems with many degrees of freedom, SC methods provide an attractive alternative to include quantum effects in such systems. For instance, SC approaches present the advantage of avoiding the exponential scaling of computational cost with the number of degrees of freedom that is seen in quantum mechanical calculations.

Many SC-IVR calculations are carried out in the internal coordinates of the molecular systems being investigated. While this choice can be practical for systems with few atoms, it requires the definition of a different coordinate system for every new molecular system. Cartesian coordinates, on the other hand, conveniently obviates the need for a redefinition of the coordinate system. It is our aim to develop a general approach to perform SC dynamics in Cartesian coordinates with geometric constraints. It is often desirable to apply holonomic constraints to large complex systems for several reasons. Firstly, the computational cost is reduced by freezing high-frequency motions, as longer time steps can be employed during molecular-dynamics (MD) simulations. In addition, specifically to SC calculations, the presence of constraints makes the SC propagator less oscillatory and consequently, the calculations become less computationally demanding. Secondly, the application of constraints strips off irrelevant degrees of freedom, thus making it possible to focus on some specific modes of interest. The latter is especially useful in the study of reaction dynamics.

A first implementation of the HK-SC-IVR with constraints in Cartesian coordinates has recently been reported [12]. Energy states of a model constrained water bender were calculated using an approximate form of the so-called HK prefactor. The approximation is the one proposed in Ref. [13] and is also called the Johnson’s “multichannel Wentzel Kramers Brillouin (WKB)” approximation. Details of the approximation are provided in the Sec. 2.2. As a common practice, the phase-space integral over the initial coordinates and momenta of the SC expression was evaluated through Monte Carlo sampling to reduce computational effort. It was observed that a large proportion of the sampled initial conditions did not obey the bond constraints, and one had to resort to an approximate method to force back the constraints on the

initial conditions. It is our belief that, to extend the applicability of the approach, a systematic method needs to be developed to sample constrained initial conditions. We remedy these problems in the current work which endeavors at presenting a general approach to perform Monte Carlo sampling of constrained initial conditions that falls out from the representation of the wave function.

The remainder of the paper is organized as follows: Sec. 2.2 reviews the HK-SC-IVR theory and provides details of our approach to represent the wave function. The implications, on the dynamics, of imposing constraints to a system are outlined in the last part of the section. Section 2.3 provides a description of the rare-gas trimers, the system we choose to test our method. Sampling results and details of trajectory calculations are also included. In Sec. 2.3.3, the SC results for the various trimers are presented. Finally, Sec. 2.4 provides concluding remarks.

2.2 Theoretical approach

The eigenvalues of the quantum Hamiltonian \hat{H} can be determined from the power spectrum, the result of a Fourier transform of the quantum-mechanical autocorrelation function,

$$I(\omega) = \frac{1}{2\pi} \int_{-\infty}^{\infty} dt e^{i\omega t} C(t) , \quad (2.1)$$

where

$$C(t) = \langle \Psi_i | e^{-i\hat{H}t/\hbar} | \Psi_i \rangle , \quad (2.2)$$

and Ψ_i stands for the initial wave function. The HK-SC-IVR propagator in the coherent-state representation for a $3N$ -dimensional system is given by

$$\begin{aligned} e^{-i\hat{H}t/\hbar} &= (2\pi\hbar)^{-3N} \int \int d\mathbf{p}_i d\mathbf{q}_i R_{\mathbf{p}_i\mathbf{q}_i t} \\ &\times e^{iS_{\mathbf{p}_i\mathbf{q}_i t}/\hbar} |g_{\mathbf{p}_i\mathbf{q}_i}\rangle \langle g_{\mathbf{p}_i\mathbf{q}_i}| , \end{aligned} \quad (2.3)$$

where \mathbf{q}_i and \mathbf{p}_i are the $3N$ -dimensional vectors corresponding to the position and momentum, respectively, at time $t = 0$. Similarly, \mathbf{q}_t and \mathbf{p}_t denote the corresponding variables at time t . $g_{\mathbf{p}_i\mathbf{q}_i}$ and $g_{\mathbf{p}_t\mathbf{q}_t}$ represent the coherent-state, minimum uncertainty

wave packets before and after their time evolution, respectively. $S_{\mathbf{p}_i, \mathbf{q}_i t}$ is the classical action along each trajectory, i.e.,

$$S_{\mathbf{p}_i, \mathbf{q}_i t} = \int_0^t dt' [\mathbf{p}_{t'} \cdot \dot{\mathbf{q}}_{t'} - H]. \quad (2.4)$$

Formally, the Herman-Kluk prefactor $R_{\mathbf{p}_i, \mathbf{q}_i t}$ is given by

$$R_{\mathbf{p}_i, \mathbf{q}_i t} = \left| \frac{1}{2} \left[\frac{\partial \mathbf{q}_t}{\partial \mathbf{q}_i} + \frac{\partial \mathbf{p}_t}{\partial \mathbf{p}_i} - i\gamma\hbar \frac{\partial \mathbf{q}_t}{\partial \mathbf{p}_i} + \frac{i}{\gamma\hbar} \frac{\partial \mathbf{p}_t}{\partial \mathbf{q}_i} \right] \right|^{1/2}. \quad (2.5)$$

The partial derivatives of the time-evolved coordinates and momenta with respect to their initial values are elements of the monodromy matrix and γ is a $3N \times 3N$ matrix related to the width of the Gaussian wave packet. In this paper, the HK prefactor was computed using the log-derivative formulation as well as its approximate form, the Johnson's multichannel WKB version [13].

The log-derivative form of the prefactor is given by

$$R_{\mathbf{p}_i, \mathbf{q}_i t} = \sqrt{\det \left[\frac{1}{2} \left(\mathbf{1} + \frac{i}{\hbar} \gamma^{-1} \mathbf{A}_t \right) \right]} \exp \left[\frac{1}{2} \int_0^t dt' \text{Tr}(\mathbf{A}_{t'}) \right]. \quad (2.6)$$

The evaluation of the above expression involves the integration of a log-derivative matrix \mathbf{A}_t , according to the differential Riccati equation

$$\dot{\mathbf{A}}_t = -\mathbf{F}_t - \mathbf{A}_t^2. \quad (2.7)$$

The initial value of \mathbf{A} is given by $\hbar\gamma/i$ and \mathbf{F}_t is the matrix of force constants, or the Hessian, at time t .

The approximate form of the prefactor is based on the assumption that the Riccati matrix is independent of time. It is calculated from the phase resulting from the local harmonic zero-point energy along the trajectory, i.e.,

$$R_{\mathbf{p}_i, \mathbf{q}_i t} \approx \exp \left[-\frac{i}{\hbar} \int_0^t dt' \sum_{j=1}^{3N} \frac{\hbar\omega_j(t')}{2} \right]. \quad (2.8)$$

In the above expression, $\omega_j(t')$, the frequency corresponding to the normal mode defined by the index j , is obtained from the eigenvalues of the matrix of force constants.

Combination of Eqs. (2.2) and (2.3) leads to the following expression for the SC autocorrelation function:

$$C(t) = (2\pi\hbar)^{-3N} \int \int d\mathbf{p}_i d\mathbf{q}_i R_{\mathbf{p}_i, \mathbf{q}_i t} e^{iS_{\mathbf{p}_i, \mathbf{q}_i t}/\hbar} \langle \Psi_i | g_{\mathbf{p}_i, \mathbf{q}_i} \rangle \langle g_{\mathbf{p}_i, \mathbf{q}_i} | \Psi_i \rangle . \quad (2.9)$$

The overlaps between the initial wave function and the initial and time-evolved Gaussian wave packets are denoted by $\langle g_{\mathbf{p}_i, \mathbf{q}_i} | \Psi_i \rangle$ and $\langle \Psi_i | g_{\mathbf{p}_i, \mathbf{q}_i} \rangle$, respectively. Overlap terms are explained in greater detail in Sec. 2.2.1. Suffice it to say at this point that the phase-space integral of $\langle g_{\mathbf{p}_i, \mathbf{q}_i} | \Psi_i \rangle$ is generally evaluated by Monte Carlo sampling.

2.2.1 Representation of the wave function

We choose to represent the initial wave function in the position representation as a product of Gaussian functions of the normal coordinates $\mathbf{Q} = \{Q_k\}$, i.e.,

$$\langle \mathbf{x} | \Psi_i \rangle = \prod_{k=1}^{3N} c_k \exp(-\alpha_k Q_k^2) , \quad (2.10)$$

where $\alpha_k = \omega_k/2\hbar$ and c_k is the normalizing factor $(2\alpha/\pi)^{1/4}$ [14].

Conversion to mass-weighted Cartesian coordinates leads to,

$$\langle \mathbf{x} | \Psi_i \rangle = c \exp[-(\mathbf{x} - \mathbf{x}_e)^T L \alpha L^T (\mathbf{x} - \mathbf{x}_e)] . \quad (2.11)$$

In the above expression, α and c are $3N \times 3N$ diagonal matrices. L is the transformation matrix that converts normal coordinates to mass-weighted Cartesian coordinates. \mathbf{x} and \mathbf{x}_e are both $3N$ -dimensional vectors of the mass-weighted Cartesian coordinates, with \mathbf{x}_e referring specifically to the minimum-energy configuration.

The Gaussian wave packet of Sec. 2.2 in the position representation has the form

$$\langle \mathbf{x} | g_{\mathbf{p}_i, \mathbf{q}_i} \rangle = \left(\frac{\gamma}{\pi} \right)^{3N/4} \exp \left[-\frac{1}{2} (\mathbf{x} - \mathbf{q}_i)^T \gamma (\mathbf{x} - \mathbf{q}_i) + \frac{i}{\hbar} \mathbf{p}_i^T (\mathbf{x} - \mathbf{q}_i) \right] . \quad (2.12)$$

The overlap between the Gaussian wave packet and the wave function is obtained by combining Eqs. (2.11) and (2.12) and integrating

$$\begin{aligned} \langle g_{\mathbf{p}_i, \mathbf{q}_i} | \Psi_i \rangle &= \int d\mathbf{x} \langle g_{\mathbf{p}_i, \mathbf{q}_i} | \mathbf{x} \rangle \langle \mathbf{x} | \Psi_i \rangle \\ &= \exp \left[-\frac{1}{4} (\mathbf{q}_i - \mathbf{x}_e)^T \gamma (\mathbf{q}_i - \mathbf{x}_e) - \frac{1}{4\hbar^2} \mathbf{p}_i^T \gamma^{-1} \mathbf{p}_i - \frac{i}{\hbar} \mathbf{p}_i^T (\mathbf{q}_i - \mathbf{x}_e) \right] . \end{aligned} \quad (2.13)$$

Note that here, the γ matrix is not restricted to a diagonal form. We choose to define γ as a symmetric matrix related to the frequencies of the system:

$$\gamma = 2L\alpha L^T . \quad (2.14)$$

2.2.2 Inclusion of constraints

The SC-IVR autocorrelation function for a constrained system with a reduced number of degrees of freedom, $F = 3N - N_c$, where N_c is the number of constraints, can be expressed as [12]

$$\begin{aligned} C(t) &= \langle \Psi_i | e^{-i\hat{H}^c t/\hbar} | \Psi_i \rangle \\ &= (2\pi\hbar)^{-F} \int \int d\mathbf{p}_i^c d\mathbf{q}_i^c R_{\mathbf{p}_i^c \mathbf{q}_i^c}^c e^{iS_{\mathbf{p}_i^c \mathbf{q}_i^c}^c/\hbar} \langle \Psi_i | g_{\mathbf{p}_i^c \mathbf{q}_i^c}^c \rangle \langle g_{\mathbf{p}_i^c \mathbf{q}_i^c}^c | \Psi_i \rangle . \end{aligned} \quad (2.15)$$

The integration is now performed over constrained coordinates and momenta indicated by the superscript c . The equations of motion can be integrated using the RATTLE (Ref. [15]) or the SHAKE (Ref. [16]) algorithm. The procedure used here is identical to the one used in classical simulations studies where one wishes to impose constraints while keeping a Cartesian coordinate system and therefore builds on existing tools.

As explained in Sec. 2.2, the approximate form of the HK prefactor is evaluated from the sum of the frequencies of the system. As a result of the introduction of constraints, however, the frequencies $\omega_j^c(t')$ are now obtained from a projected Hessian matrix \mathbf{F}^c , i.e., a Hessian matrix of the allowed motions only.

$$R_{\mathbf{p}_i^c \mathbf{q}_i^c}^c \approx \exp \left[-\frac{i}{\hbar} \int_0^t dt' \sum_{j=1}^F \frac{\hbar\omega_j^c(t')}{2} \right] . \quad (2.16)$$

The projection is performed by using the approach devised by Hinsen and Kneller [17]. First, a subspace is built by specifying the displacement vectors $\mathbf{d}^{(i)}$ corresponding to the desired motions. The M displacement vectors are combined into the columns of a $3N \times M$ displacement matrix \mathbf{D} , i.e.,

$$\mathbf{D} = (\mathbf{d}^{(1)}, \dots, \mathbf{d}^{(m)}) . \quad (2.17)$$

As an example, consider the stretching motion of atoms about their molecular bond. If \mathbf{R}_j is a vector which describes the positions of the atoms, where j is the atomic index (i.e., $j = 1, \dots, N$), the displacement vectors are given by the general expression

$$\mathbf{d}_j = (\mathbf{R}_k - \mathbf{R}_l)(\delta_{jk} - \delta_{kl}) . \quad (2.18)$$

The matrix \mathbf{D} is then orthonormalized by singular value decomposition to a basis \mathbf{U} with orthonormal columns, spanning the same subspace:

$$\mathbf{D} = \mathbf{U} \cdot \mathbf{\Sigma} \cdot \mathbf{V}^T . \quad (2.19)$$

$\mathbf{\Sigma}$ is an $M \times M$ diagonal matrix which contains the singular values of \mathbf{D} . The number of nonzero singular values corresponds to the dimension of the subspace, d^s . \mathbf{V}^T is an orthogonal matrix of the same size as $\mathbf{\Sigma}$. The d^s columns of the matrix \mathbf{U} which contain nonzero singular values constitute the orthonormal basis of the subspace. The projection of the mass-weighted Hessian is carried out by the projection matrix, $\mathbf{\Delta}$

$$\mathbf{F}^c = \mathbf{\Delta} \mathbf{F} \mathbf{\Delta} , \quad (2.20)$$

where $\mathbf{\Delta}$ is defined as $\mathbf{U} \cdot \mathbf{U}^T$.

The overlaps between the initial wave function and the initial and time-evolved Gaussian wave packets, i.e., $\langle g_{p_i q_i}^c | \Psi_i \rangle$ and $\langle \Psi_i | g_{p_i q_i}^c \rangle$ are also calculated with constrained coordinates and momenta. The implication for a geometrically constrained system is that initial conditions need to obey the constraints. This is achieved to some extent by our choices of the wave function and the Gaussian widths. As for ω_j^c , the matrix γ^c is also derived from the diagonalization of the projected Hessian matrix such that Eq. (2.14) becomes

$$\begin{aligned} \mathbf{F}^c L^c &= L^c \Lambda^c , \\ \gamma^c &= 2L^c \alpha L^{c T} . \end{aligned} \quad (2.21)$$

In addition, the evaluation of the exact HK prefactor becomes a nontrivial operation in the presence of constraints. As mentioned earlier, the log-derivative formulation of the HK prefactor is based on the integration of the Riccati equation, which

involves both the γ and Hessian matrices. For the constrained systems, we used the matrices in their reduced subspace instead, that is, the projection given by Eq. (2.20) was omitted and the basis was used directly. This is achieved by

$$\begin{aligned}\mathbf{F}^s &= \mathbf{U}^T \mathbf{F} , \mathbf{U} \\ \mathbf{F}^s L^s &= L^s \Lambda^s , \\ \gamma^s &= 2L^s \alpha^s L^{s T} .\end{aligned}\tag{2.22}$$

The superscripts s denote the matrices with reduced dimensionality d^s . The HK prefactor can be rewritten for the constrained system as a function of the matrices in their reduced space

$$R_{\mathbf{p}_i^s \mathbf{q}_i^s t} = \sqrt{\det \left[\frac{1}{2} \left(\mathbf{1} + \frac{i}{\hbar} \gamma^{s-1} \mathbf{A}_t^s \right) \right]} \exp \left[\frac{1}{2} \int_0^t dt' \text{Tr} (\mathbf{A}_{t'}^s) \right] ,$$

where

$$\dot{\mathbf{A}}_t^s = -\mathbf{F}_t^s - (\mathbf{A}_t^s)^2 \text{ and } \mathbf{A}_0^s = \hbar \gamma^s / i .\tag{2.23}$$

An obvious advantage of using the smaller matrices compared with projected matrices is a reduction in the computer time required for the integration of the differential equation.

2.3 Numerical example: Rare-gas trimers

We study argon and neon trimers to test and illustrate our approach. The interactions between the atoms are described by the Lennard-Jones potential $4\epsilon[(\sigma/r)^{12} - (\sigma/r)^6]$. The atomic masses and the parameters ϵ and σ employed in the calculations are provided in Table 2.1. We study two variants of each trimer: the regular trimer, labeled Ar_3 and Ne_3 and the constrained trimer, designated by $\text{Ar}_2^{\text{rigid}} \text{Ar}$ and $\text{Ne}_2^{\text{rigid}} \text{Ne}$. In the regular trimers, stretches are allowed between all three pairs of atoms. In the constrained trimers, the internuclear distance between two chosen atoms is fixed at their equilibrium value $2^{1/6}\sigma$, such that interatomic stretching is permitted along two directions only. Rotation and translation are excluded from the subspace of all clusters, so the number of degrees of freedom is given by the vibrational contribution

Table 2.1: Masses and parameters for the Lennard-Jones potential for argon and neon.

	Mass (amu)	$\epsilon/k_B(\text{K})$	$\sigma(\text{\AA})$
Argon	39.948	120	3.4
Neon	20.1797	35.6	2.75

only. Consequently, the regular trimers have three degrees of freedom while those of the constrained trimers are reduced to two. All of the following calculations were performed using the molecular modelling toolkit (MMTK), an open source software toolkit based on the object-oriented PYTHON [18].

2.3.1 Sampling of initial conditions

The integral over phase space was evaluated by Monte Carlo sampling. The initial positions and momenta were generated in Cartesian coordinates from the phase-space integral of the product of the overlap terms at initial times by performing a multivariate Gaussian sampling. The sampling function is described by

$$\rho(\mathbf{p}_i^c, \mathbf{q}_i^c) = \langle \Psi_i | g_{\mathbf{p}_i, \mathbf{q}_i}^c \rangle \langle g_{\mathbf{p}_i, \mathbf{q}_i}^c | \Psi_i \rangle = \exp \left[\frac{-(\mathbf{q}_i^c - \mathbf{x}_e)^2}{2\sigma_q^2} - \frac{\mathbf{p}_i^c{}^2}{\sigma_p^2} \right] \quad (2.24)$$

and has covariance matrices defined as

$$\begin{aligned} \sigma_q^2 &= \gamma^{c-1}, \\ \sigma_p^2 &= \hbar^2 \gamma^c. \end{aligned} \quad (2.25)$$

Initial conditions were generated from a mass-weighted matrix of width parameters and were transformed into regular Cartesian coordinates prior to the dynamics. The center-of-mass motions and rigid body rotations were removed from the sampled positions and momenta. Only the initial conditions with total energies corresponding to bound trajectories were retained as highly energetic trajectories that quickly escape the potential-energy surface offer hardly any contributions to the correlation function. The number of rejected initial conditions amounted to less than 10% of the generated

positions and momenta for the argon trimers. The acceptance ratio for the neon trimers was about 60%.

We analyzed the sampled initial conditions by plotting the distribution of interatomic distances. The plots for the constrained trimers $\text{Ar}_2^{\text{rigid}}\text{Ar}$ and $\text{Ne}_2^{\text{rigid}}\text{Ne}$ are shown in Fig. 2.1. The distributions for the regular trimers are rather monotonous and are not presented. They indicate a uniform spread in the interatomic positions about their equilibrium value. As mentioned above, the interatomic distance between two atoms of the constrained trimer is held constant at its equilibrium distance. This feature is reflected in the nonuniform distribution of the distance between pairs of atoms in the trimers. The distribution along the constrained direction is highly localized for both constrained trimers, as desired. The sampling results provide evidence for constrained sampling of initial conditions. The key to the successful sampling lies in the use of the subspace. The constraints are introduced in our system by specifying a subspace of allowed motions or equivalently removing undesired motions as outlined in Sec. 2.2. The resulting projected Hessian matrix is used in the calculation of the constrained width matrix. The information about the constraints are thus preserved in the covariance matrices, consequently affecting the sampling of initial conditions.

2.3.2 Dynamics

Trajectories were generated from 5000 sampled initial conditions for each of the regular and constrained trimers and autocorrelation functions were computed using the two previously discussed versions of the HK prefactor. The constrained equations of motion were integrated every femtosecond using the RATTLE algorithm (Ref. [15]) and data were collected over a period of 2 ps for each trajectory. The load of data collection was divided on a number of computers.

The Ricatti equation in the log-derivative version of the prefactor was propagated with a very simple Euler integrator with a time step of 0.03 fs. The size of the log-derivative matrix is determined by the dimensionality of the subspace d^s . In our case, this also corresponds to the number of vibrational degrees of freedom since no rotation and translation are possible in the subspace. We noted earlier that the subspace of

a regular trimer such as Ar_3 or Ne_3 has three dimensions and that of a constrained trimer has only two dimensions. Consequently, their log-derivative matrices are 3×3 and 2×2 matrices, respectively. As was previously reported [13, 19], the branch cut problem traditionally encountered in the exact calculation of the HK prefactor is avoided in the log-derivative version by the choice of the width matrix to match the frequencies of the constrained trimers. We observed a branch cut problem arising from the evaluation of the square root in the expression for the HK prefactor in Eq. (2.6) in about 1% of the generated trajectories for the regular trimer Ar_3 or Ne_3 . In these cases, the branch cut problem was fixed by inspection.

2.3.3 Reduction in zero point energy

We now analyze the power spectra obtained from the Fourier transform of the autocorrelation function and assess the accuracy of the reduction in zero-point energy (ZPE) that results from the inclusion of constraints. The peaks of the power spectrum correspond to the energies of the eigenstates of the system. The peaks shown in Fig. 2.2 represent the ZPE of the regular and constrained trimers. Our SC approach fares well in describing the ZPE of the trimers. The expected, almost linear, decrease in the SC ZPE is observed with a decrease in the number of degrees of freedom for both systems. Exact results were obtained using the methods outlined in Ref. [20] for the regular trimers and using the method of Ref. [21] for the constrained trimers.

Both the approximate and the exact forms of the prefactor in the semiclassical autocorrelation function result in comparable ZPEs for the rare-gas trimers as indicated by Table 2.2. When compared with the exact result, both prefactors give rise to energies that are in very good agreement. Although sometimes small, the differences between the results from the two prefactors show that the ZPE calculated using the exact prefactor is superior in accuracy to the approximate prefactor for all cases with the exception of the constrained argon trimer.

The harmonic approximation to the ZPE is included in Table 2.2 for comparison purposes. In all cases, the SC method consistently outperforms the simple harmonic

Table 2.2: Zero-Point Energies (in kJ mol^{-1}). Results of exact quantum mechanical, and SC-IVR treatment based on the exact log-derivative HK (SCIVR^E) and the approximate (SCIVR^A) prefactors. The result from the harmonic approximation (HA) is included for reference. The difference, δ , between the various approximations and the exact results is also given. The energies are given with respect to the bottom of the total potential.

System	Exact	SCIVR ^E	δ_{SCIVR^E}	SCIVR ^A	δ_{SCIVR^A}	HA	δ_{HA}
Ar ₃	0.445	0.439	-0.006	0.433	-0.012	0.467	0.022
Ar ₂ ^{rigid} Ar	0.290	0.301	0.011	0.299	0.009	0.320	0.030
Ne ₃	0.379	0.354	-0.025	0.333	-0.046	0.442	0.063
Ne ₂ ^{rigid} Ne	0.248	0.245	-0.003	0.232	-0.016	0.303	0.055

approximation at describing the energies of the system. In addition, the harmonic results overestimate the true ZPE while the SC results underestimate the ZPE for all trimers excluding the constrained argon trimer again. Anharmonicity is of greater relevance to the neon trimers than to the argon trimers. As a result the discrepancy between the exact result and the harmonic approximation to the ZPE is larger for the neon system than for the argon system. The same trend is also observed for the SC result obtained from the approximate prefactor. This can be understood by referring to Eq. (2.8). The phase is calculated by assuming a local harmonic approximation.

In general, the harmonic approximation is reasonable at low kinetic energies. However, as more modes become available for vibrations and the kinetic energies increase, anharmonicity becomes more significant. Based on this reasoning one would expect the difference between the SC and the harmonic results to increase with the number of degrees of freedom. We observe such an increase in the differences for the neon system. The argon trimers, however, do not display the same behavior. The deviation with respect to the exact ZPE for the SC result is nearly doubled with the addition of a constraint when the log-derivative formulation of the prefactor is employed. Interestingly, the harmonic result also shows an increase in the discrepancy upon the decrease in the number of degrees of freedom for the argon trimers. We point out that

the approximate prefactor makes use of an additional local harmonic approximation. So, the observed decrease in the magnitude of the difference with the exact ZPE could also be fortuitous.

We further analyze our results by comparing their dissociation energies D_0 . We calculate the difference between the dissociation energies of the neon and argon trimers for each of the constrained and regular trimers. The calculation, done at different levels of approximation, is related to the measure of anharmonicity present in the calculated results. For ease of comparison, we show in Table 2.3 the differences per number of vibrational degree of freedom. The calculated quantity is a constant for every method and is independent of the number of vibrational degrees of freedom. In contrast to the harmonic value, both SC values are lower than the exact value. The SC value computed from the exact prefactor is closest to the exact value.

Table 2.3: The difference in dissociation energies between the argon and neon trimers per number of vibrational degree of freedom d .

	Exact	SCIVR ^E	SCIVR ^A	HA
$D_0(\text{Ar}_2^{\text{rigid}}\text{Ar})$	1.705	1.694	1.696	1.675
$D_0(\text{Ne}_2^{\text{rigid}}\text{Ne})$	0.344	0.347	0.360	0.289
$\Delta D_0/(d = 2)$	0.680	0.674	0.668	0.693
$D_0(\text{Ar}_3)$	2.548	2.554	2.560	2.526
$D_0(\text{Ne}_3)$	0.509	0.533	0.555	0.445
$\Delta D_0/(d = 3)$	0.680	0.674	0.668	0.694

2.4 Conclusion and Outlook

We have developed a general method to sample initial conditions in Cartesian coordinates to study the SC dynamics of geometrically constrained systems. In this work, the sampling of initial conditions was performed from a multivariate Gaussian form. We observed the retention of constraints in the sampled initial conditions.

Compared to our initial effort [12], which lead to accurate energies, we now have an approach that additionally yields the correct distribution directly. The SC autocorrelation function was calculated from an approximate form of the HK prefactor as well as from its exact log-derivative form which is a novel aspect of the current work. In the latter version, we performed the calculation of the prefactor in the subspace of permissible motions. Only the approximate form of the prefactor was used in the earlier work on the inclusion of constraints in HK-SC-IVR [12].

We tested the approach on model rare-gas trimers in their constrained and unconstrained forms. The zero-point energies obtained from the Fourier transform of the correlation function for all trimers show good to excellent agreements with the exact counterparts. In the present work, the integration of the Riccati equation was performed by a simplistic Euler integrator. Future work will involve the implementation of a better-performing integrator for the time evolution of the prefactor, especially for larger constrained systems. Our approach, being a general one, can easily be extended the study to analyse the quantum dynamical properties of more complicated constrained systems. Since our approach is implemented in the context of MMTK [18], the code can currently be used to study a wide variety of systems described, for example, by the AMBER (Ref. [22]) force field, Lennard-Jones interactions, or the TIP3P (Ref. [23]) water model. This generality is an important step towards making semiclassical initial value representation methods, a practical tool for the simulation of complex molecular systems. The application to the complexes of rigid molecular monomers will be considered in the future. The performance of our Cartesian method could for instance be benchmarked by comparing to the results obtained in curvilinear coordinates as in the case of the HCl dimer [9].

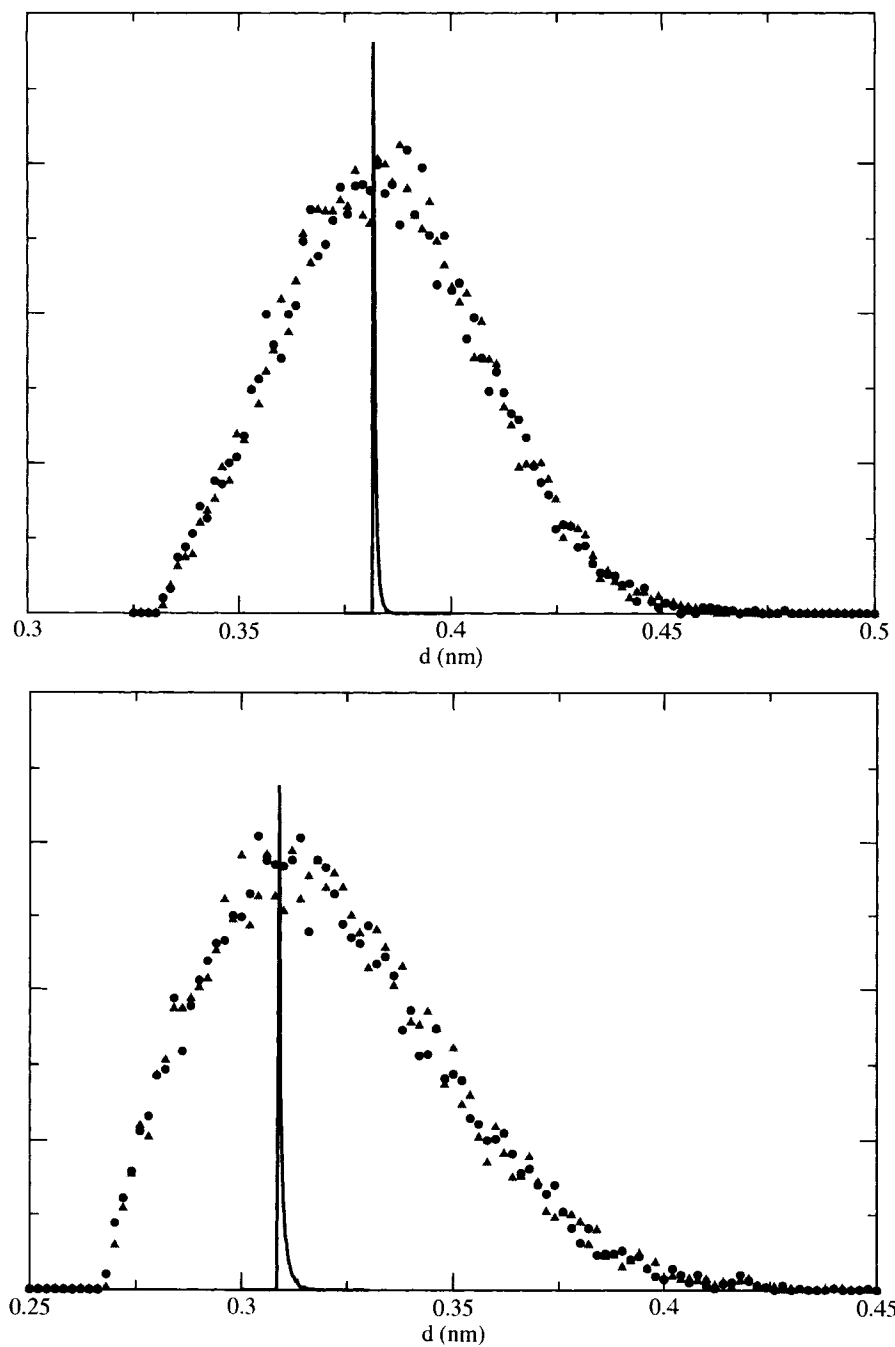


Figure 2.1: Distribution of atomic distances for $\text{Ar}_2^{\text{rigid}} + \text{Ar}$ (top) and $\text{Ne}_2^{\text{rigid}} + \text{Ne}$ (bottom). The circles and the triangles represent the unconstrained interatomic distances. The solid line indicates the distribution of distances along the constrained direction. A sample size of 10000 configurations is used.

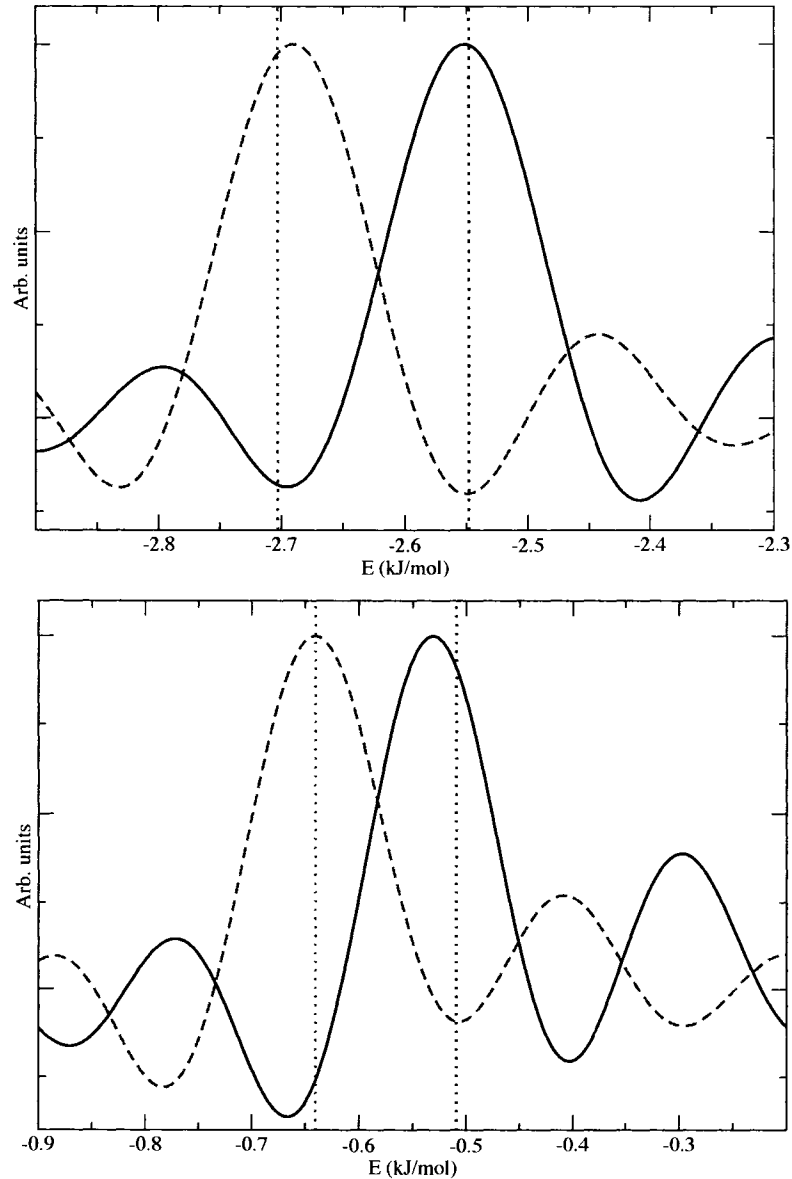


Figure 2.2: Power spectra for the argon (top panel) and neon (lower panel) trimers. The solid line corresponds to the results for the regular trimer and the broken line shows results for the constrained trimer. The results are obtained based on the exact log-derivation expression for the HK prefactor. The exact results (dotted vertical lines) are also included.

Bibliography

- [1] J. H. van Vleck, Proc. Natl. Acad. Sci. U. S. A. **14**, 178 (1928).
- [2] W. H. Miller, J. Chem. Phys. **53**, 3578 (1970).
- [3] W. H. Miller, J. Chem. Phys. **95**, 9428 (1991).
- [4] E. Heller, J. Chem. Phys. **94**, 2723 (1991).
- [5] M. Herman and E. Kluk, Chem. Phys. **91**, 27 (1984).
- [6] K. Kay, J. Chem. Phys. **101**, 2250 (1994).
- [7] M. Sepulveda and E. Heller, J. Chem. Phys. **101**, 8004 (1994).
- [8] A. Walton and D. Manolopoulos, Mol. Phys. **84**, 961 (1996).
- [9] W. H. Miller, Farad. Discuss. Chem. Soc. **110**, 1 (1998).
- [10] S. Garashchuk and D. Tannor, Chem. Phys. Lett. **262**, 477 (1996).
- [11] F. Grossmann, Chem. Phys. Lett. **262**, 470 (1996).
- [12] B. Harland and P.-N. Roy, J. Chem. Phys. **118**, 4791 (2003).
- [13] R. Gelabert, X. Gimenez, M. Thoss, H. Wang, and W. Miller, J. Phys. Chem. A **104**, 10321 (2000).
- [14] E. B. Wilson, J. C. Decius, and P. C. Cross, *Molecular Vibrations: The Theory of Infrared and Raman Vibrational Spectra* (Dover, Inc. New York, 1955).
- [15] H. C. Andersen, J. Comput. Phys. **52**, 24 (1983).

- [16] J. P. Ryckaert, G. Ciccotti, and H. J. C. Berendsen, *J. Comp. Phys.* **23**, 327 (1977).
- [17] K. Hinsen and G. R. Kneller, *Mol. Sim.* **23**, 275 (2000).
- [18] K. Hinsen, *J. Comp. Chem.* **21**, 79 (2000).
- [19] L. Torres, R. Gelabert, X. Gimenez, M. Moreno, and J. Lluch, *J. Chem. Phys.* **117**, 7094 (2002).
- [20] P. N. Roy, *J. Chem. Phys.* **119**, 5437 (2003).
- [21] N. Blinov, X. Song, and P. N. Roy, *J. Chem. Phys.* **120**, 5916 (2004).
- [22] W. D. Cornell et al., *J. Am. Chem. Soc.* **117**, 5179 (1995).
- [23] W. L. Jorgensen, J. Chandrasekhar, J. D. Madura, R. W. Impey, and M. L. Klein, *J. Chem. Phys.* **79**, 926 (1983).

Chapter 3

Excited states

Article 2. *Geometric constraints in semiclassical initial value representation calculations in Cartesian coordinates: excited states*

Reused with permission from Bilkiss B. Issack and Pierre-Nicholas Roy, *Journal of Chemical Physics*, **126**, 024111 (2007). Copyright 2007, American Institute of Physics.

3.1 Introduction

Dynamical simulations of high-dimensional complex molecular systems are essentially restricted to a classical description. Indeed, such systems represent a challenge to study quantum mechanically since the Schrödinger equation cannot be solved exactly for all their degrees of freedom. However, purely classical dynamics fail to provide an accurate description and understanding of processes where quantum mechanical effects are significant. For instance, it is not possible to explain the kinetics of some proton transfer reactions without taking tunneling into account. Other examples of quantum effects include fundamental concepts such as zero-point energy and energy quantization, which form the cornerstone of spectroscopy. Quantum effects are also of relevance to complex systems: they play an important role in biological interactions and enzymatic reactions that rely on hydrogen bonding. Owing to the limitations of both extreme levels of theory, namely classical mechanics and full quantum calculations, it is imperative to develop approximate methods which allow one to treat

dominant quantum effects within molecular dynamics simulations.

Semiclassical initial value representation (SC-IVR) is a method which uses semiclassical theory to incorporate quantum effects in classical dynamics [1, 2, 3]. Over the years, it has proven to be a robust and attractive approach capable of, at least approximately, capturing quantum effects. The main appeal of the method lies in its practical use of classical mechanics to determine the quantities of interest [4]. SC-IVR has been applied in the popular Herman-Kluk [5] (HK) version to treat a variety of systems and phenomena. Spectroscopic applications include simulations of the photodissociation spectrum of CO_2 (Ref. [6]) and the photodetachment spectra of ArI_n^- (Ref. [7]) and I_2^- [8]. Partial use of the method in a mixed-order semiclassical dynamics calculation has also been reported to provide an understanding of the spectral features of the electronic absorption spectrum of Cl_2 in solid Ar at the molecular level. Additional implementations of the HK SC-IVR method range from the study of quantum tunneling in the HCl dimer, [9] to the successful description of the molecular geometry of a ruthenium complex [10].

Despite considerable progress in the field, illustrated by the long list of examples, applications of SC-IVR are still limited to system sizes well below the reach of classical dynamics. Such restrictions can seriously compromise the potential of the method as a practical tool for the study of quantum effects in classical simulations. Yet, compared to quantum mechanical calculations, SC-IVR is known to scale favorably with the dimensionality of the systems under investigation. In principle, one should be able to exploit this feature together with the simplicity and relatively low cost of well-refined classical simulations to increase the practicability of the approach.

One commonly used technique to reduce computational effort in classical molecular dynamics simulations involves selectively imposing geometric constraints on separable motions of lower importance in the system. Freezing certain modes of motion effectively reduces the number of degrees of freedom and therefore the computational cost. Alternatively, the study of systems of higher complexity becomes more accessible upon application of constraints. The consequences of imposing constraints in a semiclassical calculation are twofold. Firstly, the computational effort involved

in integrating the equations of motion during the dynamics is reduced when high-frequency motions are excluded. Secondly, the semiclassical propagator becomes less oscillatory and therefore a faster convergence can be achieved.

We developed a general method which implements the inclusion of constraints in SC-IVR calculations in Cartesian coordinates [11, 12]. Our choice for the coordinate system gives the method immediate appeal in terms of generality since it is directly applicable to any system without a redefinition of the coordinate system. It is also worth pointing out that the majority of software available for molecular dynamics simulations also makes use of the Cartesian coordinate system. This is particularly relevant to the efforts being invested in making SC-IVR a practical tool to be used in conjunction with classical simulations for the treatment of quantum effects [13, 4].

To test our approach, we recently carried out a calculation of the zero-point energy of constrained weakly bound clusters. The calculations of the Herman-Kluk prefactor were performed using the approach described by Gelabert *et al.* [14] both in its exact and approximate forms. The computation of the exact prefactor is based on the integration of a log-derivative matrix, obtained by solving a differential Riccati equation. The simpler and less computationally demanding approximate form makes use of Johnson’s “multichannel WKB” approximation. We demonstrated that both forms of the prefactor gave an accurate reduction in the zero-point energy upon reduction in the number of degrees of freedom when compared to full quantum mechanical calculations. Given its highly reasonable performance for weakly bound systems, the approximate form of the prefactor was selected for the present calculations. The goal of the current work is to assess the performance of our approach in the determination of *excited states* of constrained weakly bound clusters.

In the remaining sections, the paper describes the aspect of the SC-IVR theory pertaining specifically to the extraction of excited states in Sec. 3.2. Calculations are performed for small argon clusters. Technical details regarding the systems and the calculations are provided in Sec. 3.3. In Sec. 3.3.3, we present and compare results for the excited states obtained semiclassically and from full quantum treatment. The final part, Sec. 3.4 presents concluding remarks.

3.2 Theoretical approach

The dynamics of complex systems can be probed by analyzing the time-dependent survival amplitude $C(t)$. In quantum mechanics, the survival amplitude for a system with $3N$ degrees of freedom described by the Hamiltonian \hat{H} is given by

$$C(t) = \langle \Psi_i | e^{-i\hat{H}t/\hbar} | \Psi_i \rangle, \quad (3.1)$$

where Ψ_i represents the initial wave function and $e^{-i\hat{H}t/\hbar}$ is the quantum mechanical propagator. Its semiclassical counterpart in the initial value representation can be expressed in terms of coherent states as

$$e^{-i\hat{H}t/\hbar} = (2\pi\hbar)^{-3N} \int \int d\mathbf{p}_i d\mathbf{q}_i R_{\mathbf{p}_i, \mathbf{q}_i t} e^{iS_{\mathbf{p}_i, \mathbf{q}_i t}/\hbar} |g_{\mathbf{p}_t, \mathbf{q}_t}\rangle \langle g_{\mathbf{p}_i, \mathbf{q}_i}|. \quad (3.2)$$

In the above expression, \mathbf{q}_i and \mathbf{p}_i represent the initial positions and momenta for classical trajectories; \mathbf{q}_t and \mathbf{p}_t are their time-evolved values. $|g_{\mathbf{p}_i, \mathbf{q}_i}\rangle$ and $|g_{\mathbf{p}_t, \mathbf{q}_t}\rangle$ are the coherent state, minimum uncertainty wave packets prior to and after their time evolution, respectively. The initial wave packet in the position representation has the following analytical form:

$$\langle \mathbf{x} | g_{\mathbf{p}_i, \mathbf{q}_i} \rangle = \left(\frac{\gamma}{\pi} \right)^{3N/4} \exp \left[-\frac{1}{2} (\mathbf{x} - \mathbf{q}_i)^T \gamma (\mathbf{x} - \mathbf{q}_i) + \frac{i}{\hbar} \mathbf{p}_i^T (\mathbf{x} - \mathbf{q}_i) \right], \quad (3.3)$$

with γ being a matrix representing the Gaussian widths. The classical action $S_{\mathbf{p}_i, \mathbf{q}_i t}$ is computed during the dynamics according to

$$S_{\mathbf{p}_i, \mathbf{q}_i t} = \int_0^t dt' [\mathbf{p}_{t'} \cdot \dot{\mathbf{q}}_{t'} - H]. \quad (3.4)$$

Finally, the quantity $R_{\mathbf{p}_i, \mathbf{q}_i t}$ is the Herman-Kluk prefactor. As mentioned in the previous section, an approximate form of the prefactor known as Johnson's "multichannel WKB" (Ref. [14]), is employed during the calculations. In this formulation, the prefactor is calculated from the phase resulting from the local harmonic zero-point energy along the trajectory as

$$R_{\mathbf{p}_i, \mathbf{q}_i t} \approx \exp \left[-\frac{i}{\hbar} \int_0^t dt' \sum_{j=1}^{3N} \frac{\hbar \omega_j(t')}{2} \right]. \quad (3.5)$$

The sum in the expression runs over the $3N$ frequencies $\omega_j(t')$ associated with the normal modes of motion.

The present work aims at calculating the bound energy states of geometrically constrained systems. In general, these can be extracted by performing a Fourier transform on the survival amplitude to produce the power spectrum,

$$I(\omega) = \frac{1}{2\pi} \int_{-\infty}^{\infty} dt e^{i\omega t} C(t) . \quad (3.6)$$

The computation of the semiclassical survival amplitude for a geometrically constrained system is far from being trivial. An extensive discussion of the implications of constraints on SC-IVR calculations is provided elsewhere [12]. We only provide a brief overview in the current report for the sake of completeness.

The semiclassical survival amplitude for a geometrically constrained system with a reduced dimensionality F is given by

$$C(t) = (2\pi\hbar)^{-F} \int \int d\mathbf{p}_i^c d\mathbf{q}_i^c R_{i\mathbf{p}_i^c \mathbf{q}_i^c}^c e^{iS_{\mathbf{p}_i^c \mathbf{q}_i^c}^c / \hbar} \langle \Psi_i | g_{\mathbf{p}_i^c \mathbf{q}_i^c}^c \rangle \langle g_{\mathbf{p}_i^c \mathbf{q}_i^c}^c | \Psi_i \rangle . \quad (3.7)$$

The superscript c indicates that the calculation of the quantities contained in the expression is performed under the existence of constraints. In particular, constrained classical trajectories are generated by the time evolution of constrained initial conditions, \mathbf{q}_i^c and \mathbf{p}_i^c . In addition, the construction of the initial Gaussian wave packet is performed by taking into account the geometric constraints on the system. While the expression retains the same form as Eq. (3.3), γ^c , the matrix of Gaussian widths itself is significantly changed. As described in our previous work [12], the width matrix is derived from the F eigenvalues of a projected force constant matrix. The projection refers to the exclusion of constrained modes from the force constant matrix according to a procedure developed by Hinsen and Kneller [15]. The approach is briefly described below. The projected force constant matrix is also employed in the calculation of the Herman-Kluk prefactor, particularly in the determination of the frequencies of the unconstrained modes $\omega_j^c(t')$ in the equation,

$$R_{\mathbf{p}_i^c \mathbf{q}_i^c}^c \approx \exp \left[-\frac{i}{\hbar} \int_0^t dt' \sum_{j=1}^F \frac{\hbar \omega_j^c(t')}{2} \right] . \quad (3.8)$$

The first step in the projection procedure involves the construction of a subspace of allowed motions, \mathbf{D} , from the corresponding vectors describing these motions. The subspace is subsequently orthonormalized by singular value decomposition to remove any dependencies between the vectors forming the subspace, *i.e.*,

$$\mathbf{D} = \mathbf{U} \cdot \mathbf{\Sigma} \cdot \mathbf{V}^T . \quad (3.9)$$

Of the resulting matrices, only the basis \mathbf{U} is pertinent to the discussion. It is used to form the projector $\mathbf{\Delta}$ as follows:

$$\mathbf{\Delta} = \mathbf{U} \cdot \mathbf{U}^T . \quad (3.10)$$

The projection of the mass-weighted force constant matrix \mathbf{F} is then carried out according to

$$\mathbf{F}^c = \mathbf{\Delta} \mathbf{F} \mathbf{\Delta} \quad (3.11)$$

to produce the projected force constant matrix \mathbf{F}^c . We would like to point out that the procedure is very similar to existing projection methods used in geometry optimization techniques in *ab initio* codes. The projection procedure used in our calculations indeed compares with projection approaches in redundant internal coordinates developed by Pulay and Fogarasi [16] and by Ayala and Schlegel [17] when the gradient correction is neglected.

Both the constrained width matrix and the frequencies of the Herman-Kluk prefactor are determined from the diagonalization of the projected force constant matrix:

$$\begin{aligned} \mathbf{F}^c L^c &= L^c \Lambda^c \\ \omega^c &= \sqrt{\Lambda^c} \\ \gamma^c &= \frac{1}{\hbar} L^c \omega^c L^{c T} . \end{aligned} \quad (3.12)$$

Specifically, the frequencies of the free modes ω^c are derived from the corresponding nonzero eigenvalues Λ^c of the projected force constant matrix. The mass-weighted width matrix on the other hand is additionally related to the eigenvectors L^c .

3.3 Numerical example: Small Argon clusters

Our recent work has demonstrated the success of our method in extracting the zero-point energies of argon and neon trimers and particularly in catching the reduction in energy upon application of constraints. In the current work, we study argon clusters to test and illustrate the applicability of our approach in extracting the excited energy states. A mass of 39.948 amu is used to represent the argon atoms in our system. The interactions between the atoms are described by the Lennard-Jones potential

$$V(r) = 4\epsilon[(\sigma/r)^{12} - (\sigma/r)^6], \quad (3.13)$$

where r refers to the interatomic distance. The well depth ϵ and the van der Waals radius σ are equal to 0.998 kJ mol⁻¹ and 3.4 Å, respectively.

We study three forms of the clusters: the dimer, the regular trimer, and the constrained trimer.

The dimer is the simplest system, designated by Ar₂. The subspace of the dimer is defined by a single interatomic stretching motion ($F = 1$) and excludes overall rotations and translations.

The regular trimer is labeled Ar₃ and has three degrees of freedom ($F = 3$) corresponding to stretches between all three pairs of atoms. The constraints on the regular trimer are similar in nature to those of the dimer since both subspace definitions prohibit overall rotational and translational motions.

In the constrained trimer, Ar₂^{rigid}Ar, the internuclear distance between two chosen atoms is fixed at its equilibrium value such that interatomic stretching is permitted along two directions only. As a result, the number of degrees of freedom is reduced to two compared to the regular trimer ($F = 2$). The constrained trimer can alternatively be viewed as the combination of a constrained dimer and a single argon atom. Beside rotational and translational constraints, there also exists an additional constraint on the system: the constraint on the dimer, which is analogous to a geometric bond constraint. All calculations were performed using the molecular modeling toolkit (MMTK) [18].

3.3.1 Sampling of initial conditions

The integral over phase space in Eq. (3.7) was evaluated by Monte Carlo sampling. Initial positions and momenta were generated in Cartesian coordinates from the phase space integral of the product of the overlap terms at initial times. A multivariate Gaussian sampling was performed using

$$\rho(\mathbf{p}_i^c, \mathbf{q}_i^c) = \langle \Psi_i | g_{\mathbf{p}_i, \mathbf{q}_i}^c \rangle \langle g_{\mathbf{p}_i, \mathbf{q}_i}^c | \Psi_i \rangle = \exp \left[\frac{-(\mathbf{q}_i^c - \mathbf{x}_{\text{ref}})^2}{2\sigma_q^2} - \frac{\mathbf{p}_i^c{}^2}{\sigma_p^2} \right] \quad (3.14)$$

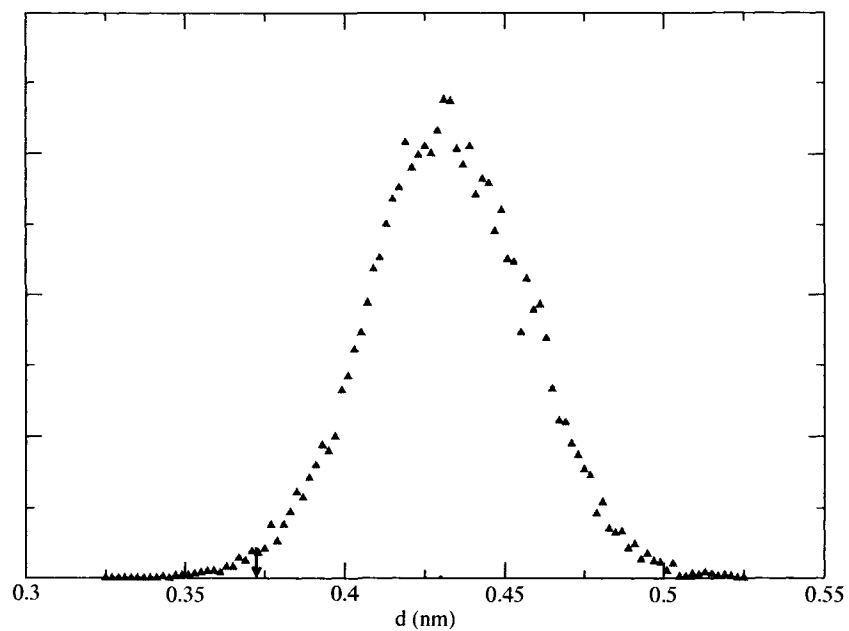
as a sampling function with covariance matrices given by

$$\begin{aligned} \sigma_q^2 &= \gamma^{c-1} \\ \sigma_p^2 &= \hbar^2 \gamma^c. \end{aligned} \quad (3.15)$$

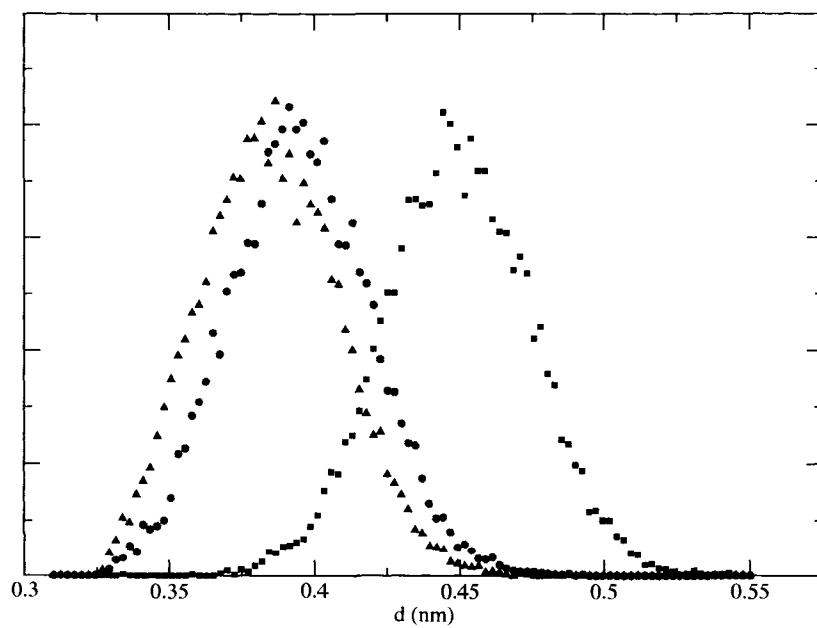
Equations (3.14) and (3.15) are expressed in terms of mass-weighted quantities. The quantity \mathbf{x}_{ref} specifically represents the mass-weighted coordinates of the center of the wave function. Consequently the sampling procedure yielded mass-weighted initial conditions which were transformed into regular Cartesian coordinates prior to the dynamics. Center-of-mass motions and rigid-body rotations were removed from the sampled positions and momenta. Initial conditions with total energies exceeding the binding energy were discarded as such highly energetic trajectories quickly escape the potential energy well and do not contribute significantly to the survival amplitude (with regard to the bound states). The number of rejected initial conditions amounted to less than 10% of the generated positions and momenta for all the argon clusters.

We show in Fig. 3.1 the distribution of initial conditions along interatomic distances for the three model systems under study. The distribution of distances for the Ar₂ dimer is peaked away from the minimum of the potential well as shown in Fig. 3.1(a). Such a displaced wavefunction will have greater overlap with excited states. A similar distribution is seen in Fig. 3.1(b) for the Ar₃ trimer.

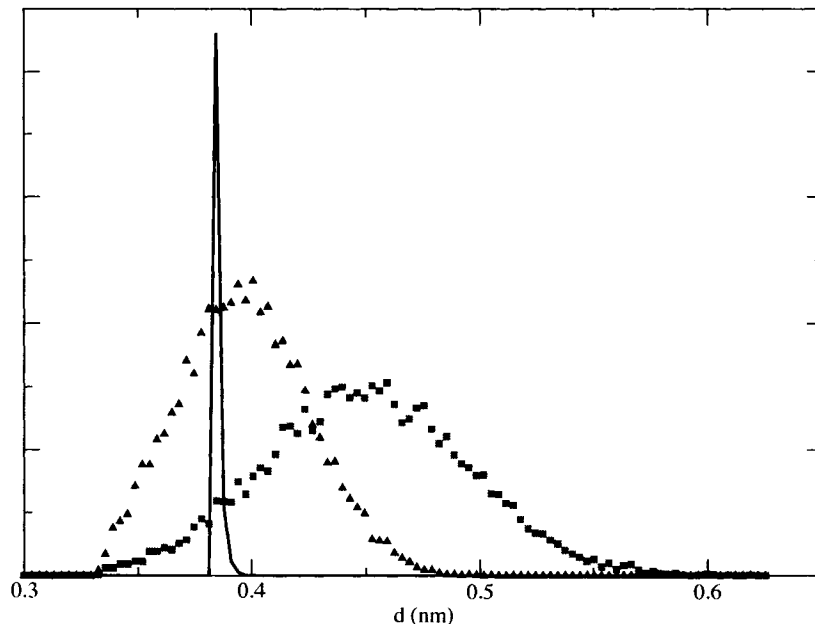
This time, there are three possible pair distances and we see that they have different distributions. Such an uneven distribution will also be useful in the extraction of excited states. For the constrained trimer, Ar₂^{rigid}Ar, the preservation of the geometric “bond constraint” in the sampled initial conditions is illustrated in the distribution of



(a)



(b)



(c)

Figure 3.1: Sampling distribution of atom pair distances, d , for the three model systems. (a) Ar_2 dimer: the arrow indicates the position of the potential minimum. (b) Ar_3 trimer: the filled triangles, circles, and squares represent the pair distance between the three possible atom pairs. (c) $\text{Ar}_2^{\text{rigid}}\text{Ar}$ complex: the solid line corresponds to the constrained distance while the filled triangle and squares correspond the remaining two unconstrained distances.

interatomic distances in Fig. 3.1(c). The distances corresponding to the two unconstrained stretches are uniformly spread compared to the highly localized distribution along the constrained direction. We refer the interested reader to our previous work for a detailed description of constrained sampling [12].

3.3.2 Dynamics

The dynamical quantities in the survival amplitude were calculated from the time-evolution of 10 000 sampled initial conditions. Equations of motion were integrated at every femtosecond with the velocity-Verlet algorithm for the dimer and the regular

trimer and with the RATTLE algorithm [19] for the constrained trimer, $\text{Ar}_2^{\text{rigid}}\text{Ar}$. The time lengths of propagation were 15 ps for the dimer and 30 ps for both trimers. The load of data collection was divided on a number of computers.

The survival amplitude was computed using the approximate form of the HK prefactor. The latter quantity is calculated from the frequencies of permissible motions as given by Eq. (3.8) after projection of undesired motions. As mentioned in the last part of Sec. 3.2 the projection procedure requires the construction of a subspace. The subspace of allowed motions for the argon clusters is defined as a combination of interparticle stretches. In a multidimensional system, the subspace definition (and therefore the basis) is dependent on the geometry of the cluster. The one-dimensional subspace of the dimer is made up of a single normalized vector describing the translation of the two argon atoms and is therefore unaffected by the geometry. For systems of higher dimensionalities, the orientation of the vectors in the subspace changes with time during the dynamics depending on the geometry. Consequently, the frequency calculations along the trajectory require the costly computation of a basis at every time step. Our calculations employ the zero-time approximation to the basis to save on the computational cost by bypassing the diagonalization involved in the generation of the basis.

3.3.3 Bound state energies

Eigenvalues of the system under investigation are revealed from its power spectrum following the Fourier transform of the survival amplitude. A Gaussian filtering procedure was applied to the survival amplitudes prior to the Fourier transform to reduce the noise level in the power spectra and therefore facilitate the identification of the true eigenvalues of the systems. The power spectra of the smoothed survival amplitudes were obtained as

$$I(\omega) = \frac{1}{\pi} \text{Re} \int_0^\infty dt e^{i\omega t} C(t) e^{-\alpha^2 t^2} \quad (3.16)$$

where the parameter α determines the degree of smoothing.

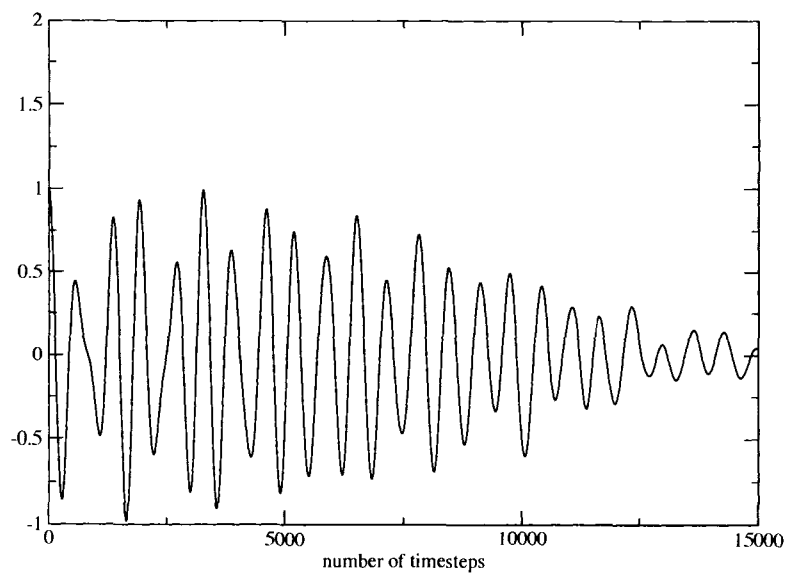
Figures 3.2(a), 3.3(a) and 3.4(a) contain the semiclassical survival amplitudes for

the dimer, trimer, and constrained trimer respectively. Their corresponding power spectra are provided in Figs. 3.2(b), 3.3(b), and 3.4(b). In order to obtain the bound state energies, we extracted the positions of the peaks of the power spectra. During this procedure, we varied the integration time interval to identify peaks of the power spectrum that correspond to true bound state energies. The peaks whose position was not affected by this procedure were deemed good bound states.

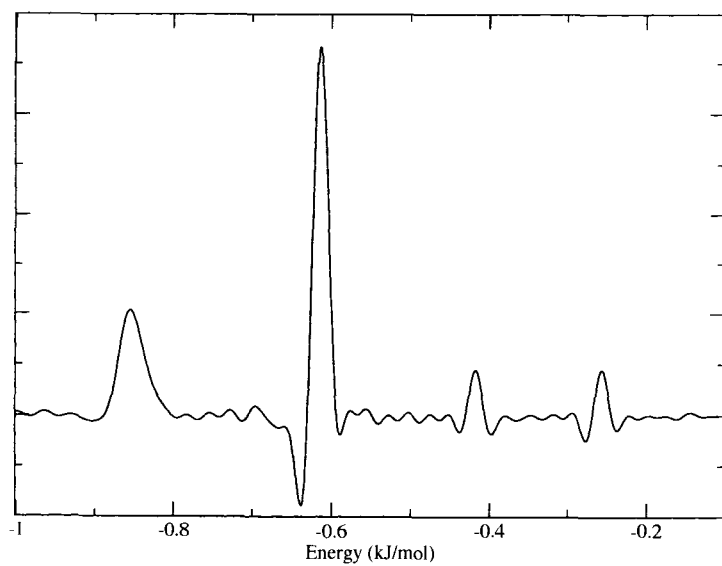
The semiclassical energies of the first few bound states are tabulated and compared with exact results in Table 3.1. Exact calculations were performed using the methods outlined in Ref. [20] for the regular clusters and using the method of Ref. [21] for the constrained trimer. In general, the semiclassical energies show good agreement with their exact counterparts.

Table 3.1: Comparison of exact quantum mechanical bound state energies and the corresponding SC-IVR results for argon clusters. Energies are given with reference to the minimum of the potential in kJ mol^{-1} . Calculations are performed using the full approximate HK prefactor (SC-IVR^A) as well as the absolute value (SC-IVR^{abs}) approximation. The percentage difference, δ , between the exact and SC-IVR calculations is also provided

System	n	Exact	SC-IVR ^A	$\delta\%$	SC-IVR ^{abs}	$\delta\%$
Ar ₂	0	0.15	0.14	6.6	0.15	2.0
	1	0.41	0.39	5.4	0.41	0.2
	2	0.61	0.58	4.5	0.62	2.0
	3	0.76	0.74	2.2	0.77	2.1
Ar ₃	0 (A1)	0.44	0.43	2.7	0.43	2.7
	1 (E)	0.66	0.64	2.9	0.66	0.3
	2 (A1)	0.75	0.74	0.8	0.75	0.1
	3 (E)	0.86	0.85	1.8	0.88	1.4
Ar ₂ ^{rigid} Ar	0	0.29	0.30	3.0	0.30	2.7
	1	0.52	0.52	1.0	0.52	1.6
	2	0.56	0.56	0.4	0.57	1.4
	3	0.72	0.72	0.3	0.74	3.6

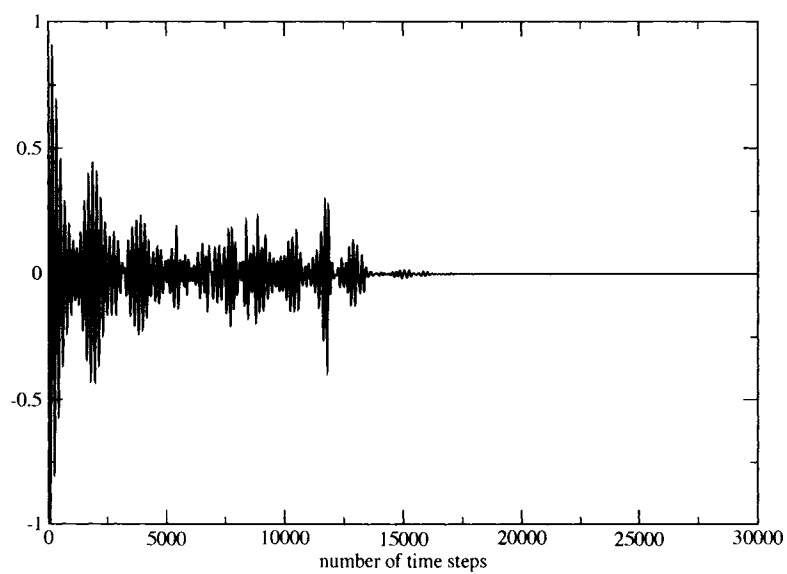


(a)

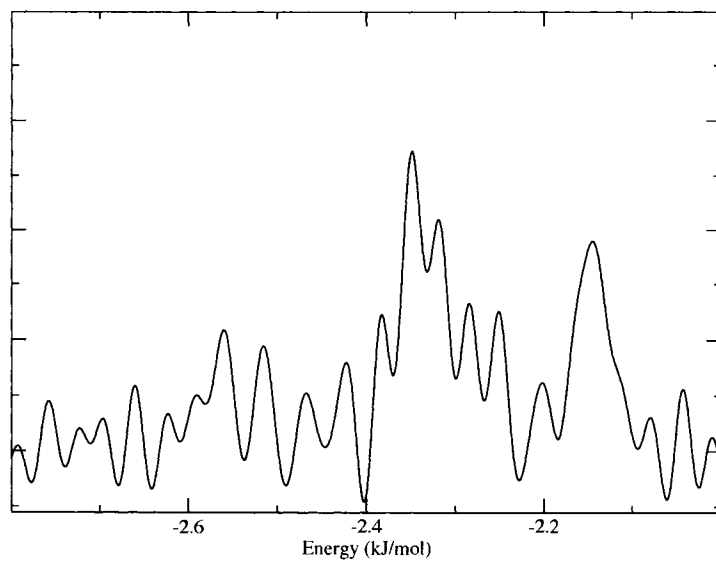


(b)

Figure 3.2: Real part of the survival amplitude (a), and associated power spectrum (b) for the Ar_2 dimer.

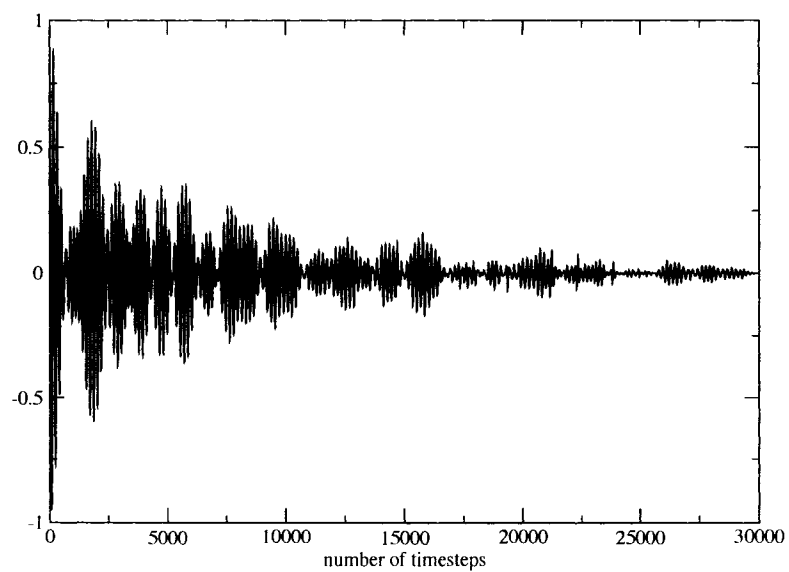


(a)

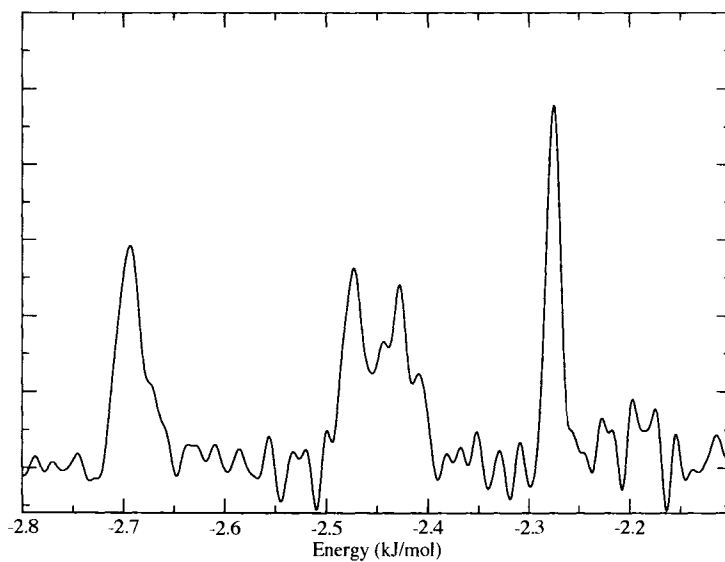


(b)

Figure 3.3: Real part of the survival amplitude (a), and associated power spectrum (b), for the Ar₃ trimer.



(a)



(b)

Figure 3.4: Real part of the survival amplitude (a), and associated power spectrum (b), for the $\text{Ar}_2^{\text{rigid}}\text{Ar}$ complex.

A high degree of accuracy is noted in the calculated energies of the trimers. The deviation in energies between the two levels of theory amounts to a maximum of 3%. The dimer shows a larger discrepancy. Also note that exact calculations of the energies of the regular trimers were performed by taking inversion symmetry into account. Figure 3.3(b) and Table 3.1 reveal that the semiclassical energy calculations are capable of capturing and reproducing the energies of states of different symmetries, namely A_1 and E .

Aside from the zero-time approximation to the basis, we additionally calculated the HK prefactor using the absolute values of the square frequencies. This is equivalent to converting imaginary frequencies into real ones. The practical advantage which results from this *ad hoc* approximation is a reduction in the oscillatory behavior of the prefactor. In such cases, no abnormally large prefactors are encountered at long propagation times. The resulting survival amplitude is “naturally” dampened and can be Fourier transformed directly without Gaussian filtering. In addition, the calculations required a shorter propagation time: the length of trajectories was reduced to half of the time required for the full approximation prefactor calculations. Energies calculated with the extra approximation are included in Table 3.1. The results compare favorably with those of the full prefactor calculation for the dimer. As for the trimers, the values obtained for the energies are similar in accuracy to the full prefactor calculation results.

3.4 Conclusion and Outlook

We previously reported a general method to study the SC dynamics of geometrically constrained systems in Cartesian coordinates. The approach involves the sampling of constrained initial conditions from a multivariate Gaussian form prior to dynamics. Our earlier study showed that the method is able to accurately capture the zero-point energies of constrained weakly bound clusters. In addition the reduction in zero-point energies upon application of constraints or reduction in dimensionality was successfully reproduced. The current work shows that this approach can also be

used to accurately obtain excited state energies of constrained systems. Not only does the method deliver in terms of accuracy but is also able to capture the symmetry of the different states for the argon trimer.

With an appropriate description of excited states, we can envisage applying our approach to problems in kinetics and spectroscopy. The method could, for example, be used to study the *real-time* dynamics of a rigid impurity embedded in a quantum solvent and address questions related to the onset of superfluidity [22, 23]. Such questions are currently addressed using imaginary-time path integral techniques (see Ref. [24] for a recent overview). From a more general point of view, one could say that we are a step closer to having a practical approach for the inclusion of quantum effects in molecular dynamics simulations. For computing the spectra of complex systems, a promising approach is the combination of our constraint techniques with the time averaging method of Kaledin and Miller [25, 26].

Bibliography

- [1] W. H. Miller, J. Chem. Phys. **53**, 3578 (1970).
- [2] W. H. Miller, J. Chem. Phys. **95**, 9428 (1991).
- [3] E. Heller, J. Chem. Phys. **94**, 2723 (1991).
- [4] W. H. Miller, J. Chem. Phys. **125**, 132305 (2006).
- [5] M. Herman and E. Kluk, Chem. Phys. **91**, 27 (1984).
- [6] A. Walton and D. Manolopoulos, Chem. Phys. Lett. **84**, 961 (1996).
- [7] M. L. Brewer, J. Hulme, and D. Manolopoulos, J. Chem. Phys. **106**, 4832 (1997).
- [8] V. S. Batista, M. T. Zanni, B. J. Greenblatt, D. M. Neumark, and W. H. Miller, J. Chem. Phys. **110**, 3736 (1999).
- [9] W. H. Miller, Farad. Discuss. Chem. Soc. **110**, 1 (1998).
- [10] L. Torres, R. Gelabert, X. Gimenez, M. Moreno, and J. Lluch, J. Chem. Phys. **117**, 7094 (2002).
- [11] B. Harland and P.-N. Roy, J. Chem. Phys. **118**, 4791 (2003).
- [12] B. Issack and P.-N. Roy, J. Chem. Phys. **123**, 084103 (2005).
- [13] W. H. Miller, J. Phys. Chem. A **105**, 2942 (2001).
- [14] R. Gelabert, X. Gimenez, M. Thoss, H. Wang, and W. Miller, J. Phys. Chem. A **104**, 10321 (2000).

- [15] K. Hinsen and G. R. Kneller, *Mol. Sim.* **23**, 275 (2000).
- [16] P. Pulay and G. Fogarasi, *J. Chem. Phys.* **96**, 2856 (1992).
- [17] P. Y. Ayala and H. B. Schlegel, *J. Chem. Phys.* **108**, 2314 (1998).
- [18] K. Hinsen, *J. Comp. Chem.* **21**, 79 (2000).
- [19] H. C. Andersen, *J. Comput. Phys.* **52**, 24 (1983).
- [20] P. N. Roy, *J. Chem. Phys.* **119**, 5437 (2003).
- [21] N. Blinov, X. Song, and P. N. Roy, *J. Chem. Phys.* **120**, 5916 (2004).
- [22] J. Tang, Y. Xu, A. R. W. McKellar, and W. Jäger, *Science* **297**, 2030 (2002).
- [23] Y. Xu, W. Jäger, J. Tang, and A. R. W. McKellar, *Phys. Rev. Lett.* **91**, 163401 (2003).
- [24] P.-N. Roy, *Theo. Chem. Acc.* **116**, 274 (2006).
- [25] A. L. Kaledin and W. H. Miller, *J. Chem. Phys.* **118**, 7174 (2003).
- [26] A. L. Kaledin and W. H. Miller, *J. Chem. Phys.* **119**, 3078 (2003).

Chapter 4

Extension to hydrogen bonded molecular systems: water dimer dynamics

Article 3. *Quantum molecular dynamics of hydrogen bonded complexes of rigid molecules using the semiclassical initial value representation in Cartesian coordinates* Reused with permission from Bilkiss B. Issack and Pierre-Nicholas Roy, Journal of Chemical Physics, **127**, 054105 (2007). Copyright 2007, American Institute of Physics.

4.1 Introduction

Proteins and protein-ligand interactions typically take place in aqueous media under physiological conditions. These interactions, which rely mostly on hydrogen bonding or the hydrophobic effect, play a significant role on the energetics of the system. An accurate understanding of hydrogen bonding requires a quantum mechanical treatment because it involves a light hydrogen atom. Yet, the majority of biomolecular simulations are carried out at a classical level of theory owing to the limitations of currently available quantum dynamical methods. Biomolecular systems are not the only victims; the problem also arises in dynamical studies of nanostructures and in any large complex system in general. The challenge is therefore to develop *practical* quantum dynamical methods that allow for the treatment of key quantum effects in

high-dimensional systems by a broader base of users.

A truly practical method should have the ability of combining simplicity, generality and ease of implementation with affordability. In that respect, the semiclassical initial value representation (SC-IVR) offers a promising method of performing quantum dynamics [1, 2, 3, 4, 5, 6]. As a result of considerable developmental efforts, SC-IVR has been implemented in several forms including forward-backward SC-IVR [7, 8, 9], the thawed gaussian approach [10, 11], and the Herman-Kluk (HK) form [12]. HK SC-IVR, in particular, is able to boast a number of applications ranging from molecular structure determination [13] to quantum tunneling in the HCl dimer [14] to studies of the photodetachment and photoionization spectrum of small molecules and clusters [15, 16, 17]. The simplicity of the approach lies in the use of classical trajectories to compute quantities of interest. One of its strongest assets is the fact that any classical simulation can, in principle, be extended albeit with additional effort to include quantum effects. In addition, it presents a favorable scaling with system size as opposed to the prohibitive exponential scaling of exact quantum mechanical methods.

However, to date, the high generality that SC-IVR aspires to achieve remains circumscribed to some extent. Classical simulations of large systems are commonly carried out with constraints. Imposing geometric constraints on a system provides the benefit of reducing computational effort. In a classical system, constraints are used to freeze out high frequency modes since those should be treated quantum mechanically for a proper description. For large complex dynamical systems specifically, the gain in computation time can be substantial, sometimes to the extent of bringing otherwise intractable simulations into the realm of feasibility. SC-IVR calculations of constrained systems are usually performed in internal coordinates, which are perhaps the simplest and most intuitive choice of coordinate system. This advantage is, however, accompanied by a significant drawback: a redefinition of the coordinates is required for every new system. In other words, the simplest choice of coordinates is also the less general option. Cartesian coordinates, on the other hand, offer the generality that internal coordinates lack and are therefore often the coordinate system

employed by the majority of classical molecular dynamics software packages.

In an effort to extend the capabilities of SC-IVR as a practical tool to include quantum effects in classical simulations, we have developed a method that allows for constrained calculations in Cartesian coordinates [18, 19, 20]. Our approach, based on HK SC-IVR, has been successfully tested on the intramolecular interaction of the water bender as well as on small constrained weakly bound atomic clusters of argon. In all cases, the zero-point energy and other bound state energies of the investigated systems were accurately reproduced. Motivated by the encouraging results, we now investigate the accuracy of our method in treating systems of higher complexity.

More specifically, the current work aims at gauging the ability of our approach in capturing quantum effects in molecular clusters through the calculation of the bound states of a dimer of rigid water molecules. The rationale for our choice of the system is twofold. Firstly, being the archetypal hydrogen bonded molecule, the constrained water dimer provides an ideal ground for investigating the quantum nature of hydrogen bonding without the interference of intramolecular interactions. Secondly, water molecules are probably the most frequently constrained species in any molecular dynamics simulations making use of explicit water molecules. In that respect, the calculation of constrained water clusters represents a stepping-stone to the application of SC-IVR to solvated systems and by extension, to the quantum simulations of large complex molecular systems in general.

The following section of the paper (Sec. 4.2) describes the SC-IVR theory and associated methods employed in the calculation of bound state energies of constrained molecules. The methods rest on the approaches developed in our earlier reports [18, 19, 20], along with the key technical improvement in the computation of the time-dependent Herman-Kluk prefactor. In the remaining sections, we provide details of the calculations along with a description of the water model in Sec. 4.3. Energy levels determined for the constrained water dimer, along with the results of the isotopic substitution study are presented in Sec. 4.3.2. The final part (Sec. 4.4) presents concluding remarks.

4.2 Theory and Methods

The energy levels of a system of N atoms can be determined from the time-dependent survival amplitude $C(t)$ via a Fourier transform. The result, called the power spectrum, is mathematically expressed as

$$I(\omega) = \frac{1}{2\pi} \int_{-\infty}^{\infty} dt e^{i\omega t} C(t) . \quad (4.1)$$

For a geometrically constrained system, with F degrees of freedom, the survival amplitude or wave packet autocorrelation function is defined as

$$C(t) = \langle \Psi_i | e^{-i\hat{H}^c t/\hbar} | \Psi_i \rangle , \quad (4.2)$$

where Ψ_i is the initial state wave function propagated by the Hamiltonian of the constrained system, \hat{H}^c .

The semiclassical propagator in the initial value representation is expressed in terms of coherent state bases, $g_{\mathbf{p}\mathbf{q}}^c$. These are minimum uncertainty wave packets which are Gaussian in position and momentum space, centered at vectors \mathbf{q} and \mathbf{p} . In the position representation, the coherent state takes the following form:

$$\langle \mathbf{x} | g_{\mathbf{p}\mathbf{q}}^c \rangle \propto \exp \left[-\frac{\gamma^c}{2} (\mathbf{x} - \mathbf{q}^c)^2 + \frac{i}{\hbar} \mathbf{p}^c (\mathbf{x} - \mathbf{q}^c) \right] , \quad (4.3)$$

where γ^c is a matrix defining the widths of the Gaussian for the constrained system.

The SC-IVR time propagator for a system is given by

$$e^{-i\hat{H}^c t/\hbar} = (2\pi\hbar)^{-F} \int \int d\mathbf{p}_i^c d\mathbf{q}_i^c R_{\mathbf{p}_i^c \mathbf{q}_i^c}^c e^{iS_{\mathbf{p}_i^c \mathbf{q}_i^c}^c/\hbar} |g_{\mathbf{p}_t^c \mathbf{q}_t}^c\rangle \langle g_{\mathbf{p}_i^c \mathbf{q}_i}^c| . \quad (4.4)$$

The integral in the above expression is performed over constrained initial conditions of the classical trajectories, i.e, constrained positions and momenta, \mathbf{p}_i^c and \mathbf{q}_i^c . The corresponding classically evolved phase space coordinates are represented by \mathbf{p}_t^c and \mathbf{q}_t^c . $g_{\mathbf{p}_i^c \mathbf{q}_i}^c$ and $g_{\mathbf{p}_t^c \mathbf{q}_t}^c$ are the coherent states prior to and after their time evolution respectively. $S_{\mathbf{p}_i^c \mathbf{q}_i^c}^c$ is the action computed during the constrained classical dynamics as

$$S_{\mathbf{p}_i^c \mathbf{q}_i^c}^c = \int_0^t dt' [\mathbf{p}_{t'}^c \cdot \dot{\mathbf{q}}_{t'}^c - H^c] . \quad (4.5)$$

The quantity $R_{\mathbf{p}_i, \mathbf{q}_i, t}^c$ is the Herman-Kluk prefactor [12] and represents the contribution of a trajectory to the overall wave function. It can be calculated from the local harmonic approximation [21]

$$R_{\mathbf{p}_i, \mathbf{q}_i, t}^c \approx \exp \left[-\frac{i}{\hbar} \int_0^t dt' \sum_{j=1}^F \frac{\hbar \omega_j^c(t')}{2} \right]. \quad (4.6)$$

The sum in the expression runs over the number of normal modes of vibrations and $\omega_j^c(t')$ is the frequency corresponding to the j th unconstrained mode and is determined from the eigenvalues of a projected matrix of force constants. A description of the projection method employed in our calculations is given below.

Using the definition of the propagator from Eq. (4.4), one obtains the following expression for the survival amplitude:

$$C(t) = (2\pi\hbar)^{-F} \int \int d\mathbf{p}_i^c d\mathbf{q}_i^c R_{\mathbf{p}_i, \mathbf{q}_i, t}^c e^{iS_{\mathbf{p}_i, \mathbf{q}_i, t}^c/\hbar} \langle \Psi_i | g_{\mathbf{p}_i, \mathbf{q}_i}^c \rangle \langle g_{\mathbf{p}_i, \mathbf{q}_i}^c | \Psi_i \rangle. \quad (4.7)$$

The integration over phase space is evaluated by Monte Carlo sampling of the wave function. In other words, the actual calculation of the survival amplitude is performed according to

$$C(t) = (2\pi\hbar)^{-F} \sum_{\rho(\mathbf{p}_i^c, \mathbf{q}_i^c)} R_{\mathbf{p}_i, \mathbf{q}_i, t}^c e^{iS_{\mathbf{p}_i, \mathbf{q}_i, t}^c/\hbar} \frac{\langle \Psi_i | g_{\mathbf{p}_i, \mathbf{q}_i}^c \rangle}{\langle \Psi_i | g_{\mathbf{p}_i, \mathbf{q}_i}^c \rangle}, \quad (4.8)$$

with mass-weighted constrained initial conditions generated from the sampling function,

$$\rho(\mathbf{p}_i^c, \mathbf{q}_i^c) = \langle \Psi_i | g_{\mathbf{p}_i, \mathbf{q}_i}^c \rangle \langle g_{\mathbf{p}_i, \mathbf{q}_i}^c | \Psi_i \rangle = \exp \left[\frac{-(\mathbf{q}_i^c - \mathbf{x}_{\text{ref}})^2}{2\sigma_q^2} - \frac{\mathbf{p}_i^c{}^2}{\sigma_p^2} \right]. \quad (4.9)$$

The parameters σ_q and σ_p are the covariance matrices defined as

$$\begin{aligned} \sigma_q^2 &= \gamma^{c-1} \\ \sigma_p^2 &= \hbar^2 \gamma^c, \end{aligned} \quad (4.10)$$

and \mathbf{x}_{ref} is the reference geometry. It specifically refers to the mass-weighted position vector representing the center of the initial wave function. If the reference coordinate is chosen to coincide with the center of the wave function in the position representation, given by Eq. (4.3), it is clear that the sampled distribution of positions is

equivalent to the probability associated with the wave function, except for a factor of 2 in the width of the Gaussian function.

The effective sampling of phase space for a constrained system is achieved through a judicious choice of the width matrix, as described in our earlier work [19]. The elements of the width matrix are obtained from a vibrational analysis of the projected matrix of force constants or Hessian at the equilibrium geometry.

In the present calculations, we choose to perform the projection according to the methods proposed by Pulay and Fogarasi [22] and Ayala and Schlegel [23]. The approaches, originally developed for the purpose of geometry optimization in electronic structure calculations, provide a means of creating a subspace of allowed motions by projecting unwanted motions from the Hessian in redundant coordinates. We provide a short description of the approach as employed in our calculations.

The transformation from Cartesian displacement coordinates to redundant internal displacement coordinates is carried out through the Wilson B matrix [24], defined as

$$\delta\mathbf{q} = B\delta\mathbf{x} . \quad (4.11)$$

The first step of the procedure involves the transformation of the gradient \mathbf{g} and Hessian H ,

$$\mathbf{g}_q = B^{-1}\mathbf{g}_x \quad (4.12)$$

and

$$H_q = B^{-1}H_x(B^{-1})^T , \quad (4.13)$$

where \mathbf{g}_x and H_x are the gradient and Hessian in Cartesian coordinates and \mathbf{g}_q and H_q are the corresponding quantities in internal coordinates. B is a rectangular matrix whose inverse is given by

$$B^{-1} = G^{-1}Bu . \quad (4.14)$$

G^{-1} is the generalized inverse of the matrix $G = BuB^T$, i.e.,

$$V^T G V = \begin{bmatrix} \Lambda & 0 \\ 0 & 0 \end{bmatrix}; \quad G^{-1} = V \begin{bmatrix} \Lambda^{-1} & 0 \\ 0 & 0 \end{bmatrix} V^T , \quad (4.15)$$

and u is a diagonal matrix of inverse masses. Equation (4.13) holds true when the Hessian is calculated at infinitesimal displacements from stationary points on the potential energy surface. For larger displacements, a gradient correction term is required and the equation becomes

$$H_q = B^{-1} \left(H_x - \frac{dB}{d\mathbf{x}} \mathbf{g}_q \right) (B^{-1})^T . \quad (4.16)$$

We would like to point out that the inclusion of the gradient correction in the calculation of the projected Hessian constitutes an improvement over our previous calculations, where the gradient correction was neglected [19, 20],

A subspace of allowed motions in the nonredundant part of internal coordinates is then constructed from the projection procedure. The function of the projector is to remove the redundancies and forbidden motions from the Hessian. A primary projector is built from the G matrix and its generalized inverse as $P = GG^-$. It is then modified to account for the constraints according to

$$P^c = P - PC(CPC)^{-1}CP , \quad (4.17)$$

where the constrained projector C is given by

$$C_{ij} = \delta_{ij}\zeta \quad (4.18)$$

where

$$\zeta = \begin{cases} 1 & \text{for constraints} \\ 0 & \text{otherwise.} \end{cases}$$

Redundancies and constraints are projected from the G matrix in an identical fashion

$$G^c = G - GC(CGC)^{-1}CG . \quad (4.19)$$

The actual projection of the Hessian is written as

$$H_q^c = P^c H_q P^c + a(1 - P^c) . \quad (4.20)$$

The second term of the equation ensures that no displacement occurs in the remainder of the space by setting the constant a to an arbitrarily large value (e.g., 1000 a.u.).

Finally, the projected Hessian is mass weighted and diagonalized as follows:

$$G^c H_q^c L_q^c = \lambda^c L_q^c \quad (4.21)$$

$$(G^c)^{1/2} H_q^c (G^c)^{1/2} L_q^c = \lambda^c L_q^c . \quad (4.22)$$

The resulting eigenvectors L_q^c span the subspace of allowed motions, as desired. Since our calculations are carried out in Cartesian coordinates, they need to be transformed back into non-mass-weighted Cartesian displacement coordinates via the transformation matrix F according to

$$L_x^c = F (G^c)^{1/2} L_q^c ; \quad F = u B^T G^- . \quad (4.23)$$

Once the eigenvalues and eigenvectors are determined, the width matrix is constructed as

$$\gamma^c = 2 L_x^c \alpha (L_x^c)^T , \quad (4.24)$$

where $\alpha = \frac{\sqrt{\lambda^c}}{h}$. The projection method is also used in the evaluation of the constrained HK prefactor $R_{\mathbf{p}_i, \mathbf{q}_i t}^c$ described by Eq. (4.6), particularly in the determination of the frequencies of the unconstrained modes of motion $\omega^c = \sqrt{\lambda^c}$.

4.3 Calculations for the water dimer

Bound state energies are calculated for a constrained water dimer, where the interactions are represented by the TIP3P water model [25]. Along with the SPC/E model [26], the TIP3P model is the most widely used water model in simulations of solvated biomolecules. The main reasons for their popularity include their ability to deliver a reasonable description of the solvation and dielectric properties of water as well as a high computational efficiency. Apart from the calculation of energy levels of the water dimer, we additionally carry out an investigation of the effect of isotopic substitution on the bound state energies in the current work.

The TIP3P water monomer is a three-site model with partial positive charges located on the hydrogen atoms and a partial negative charge on the oxygen atom. The intermolecular interaction is represented by a Lennard-Jones potential between

the oxygen atoms and a Coulombic contribution from interacting atomic charges q_i and q_j on monomers, a and b , respectively,

$$U_{ab} = \sum_i^{on\ a} \sum_j^{on\ b} \frac{q_i q_j e^2}{4\pi\epsilon_0 r_{ij}} + 4\epsilon \left[\left(\frac{\sigma}{r_{OO}} \right)^{12} - \left(\frac{\sigma}{r_{OO}} \right)^6 \right]. \quad (4.25)$$

r_{ij} is the Cartesian separation of two atomic sites and r_{OO} is the distance between the two oxygen atoms. The values of the parameters used in our calculations are provided in Ref. [25].

The effect of isotopic substitution was also investigated in the present work. Both monomer geometry of the deuterated TIP3P water model and intermolecular interactions in the dimer are identical to those of H_2O .

The B matrix defined in Eq. (4.11) was built from all possible pair distances of the water dimer. Subsequent projection of redundancies and constraints yielded the desired subspace. The subspace specifically excluded intramolecular motion as well as overall rotation and translation. Consequently, the only permitted motions in the rigid water dimer were the six intermolecular vibrational modes of motion, i.e., $F = 6$.

4.3.1 Calculation of the survival amplitude

The first step of the SC-IVR calculation consisted of sampling initial positions and momenta of the constrained water dimer for the classical trajectories. The Monte Carlo method described in the previous section generated initial conditions in mass-weighted Cartesian coordinates, which were transformed to non-mass-weighted coordinates and further modified to exclude center-of-mass motion and rigid body rotation. A filtering procedure was then applied to the sampled initial positions and momenta based on their total energies. Highly energetic trajectories that quickly escape the potential energy surface and do not contribute significantly to the survival amplitude were cast aside. The acceptance ratio resulting from the filtering procedure was greater than 75%. The sampling of initial conditions for constrained simple atomic clusters was previously demonstrated [19, 20]. We show here the first application of our sampling method to treat intermolecular interactions in constrained molecular clusters. The

distributions of interatomic distances derived from a pool of 100 000 sampled initial positions are shown in Fig. 4.1.

All unconstrained intermolecular atomic pair distances are distributed about the pair distances in the reference geometry, \mathbf{x}_{ref} of Eq. (4.9), while the intramolecular pair distances are held fixed, as desired, at the equilibrium bond geometries. This is further depicted in the three-dimensional representation of atomic densities given in Fig. 4.2. In general, the atomic distribution of lighter hydrogen atoms tends to be more spread than the heavier oxygen atoms in the water dimer. Compared to other hydrogen atoms, the distribution around the hydrogen atom involved in hydrogen bonding spans a smaller volume as a result of the localizing effect of hydrogen bonding. The survival amplitude was calculated from 10 000 sampled positions and momenta, corresponding to bound trajectories, which were classically evolved for 400 fs. Constrained equations of motion were integrated at intervals of 0.1 fs using the Rattle algorithm [27]. The semiclassical calculation was completely carried out using computational classes (or routines) we have developed for the molecular modelling toolkit (MMTK), an open source program library for molecular simulations [28].

The calculation of the constrained HK prefactor was performed from the sum of frequencies corresponding to permissible motions using the approximate method described in Sec. 4.2. These frequencies were obtained from the square root of the eigenvalues of a projected Hessian matrix computed along the trajectories. At the equilibrium geometry, all frequencies are real by definition. However, as the trajectory explores the potential energy surface, deviations from the equilibrium geometry can give rise to imaginary frequencies. In our calculations, frequencies were determined from the absolute value of the eigenvalues, and were therefore always real. This reduced the oscillatory behavior of the prefactor and conveniently led to a more rapid convergence of the calculations. The performance of this approximation proved to be highly comparable to the full approximate form of the HK prefactor in our earlier work [20].

The evolution of trajectories and the calculation of the survival amplitude for the constrained water dimers were divided on a number of computers. The real and

imaginary parts of the resulting signal for the water dimer are shown in Fig. 4.3.

4.3.2 Bound state energies

Bound state energies of the constrained water dimer can be determined from peaks of the power spectrum, obtained through the Fourier transform of its survival amplitude. The power spectrum and its identified energy levels for the constrained water dimer are displayed in Fig. 4.4 and Table 4.1, respectively.

Table 4.1: SC-IVR bound state energies (in kJ mol^{-1}) for $(\text{H}_2\text{O})_2$ and $(\text{D}_2\text{O})_2$ calculated with reference to the minimum of the potential ($D_e = -27.36 \text{ kJ mol}^{-1}$).

n	$(\text{H}_2\text{O})_2$	$(\text{D}_2\text{O})_2$
0	8.28	6.50
1	10.50	8.71
2	12.61	10.77

We take a closer look at the zero-point energy (ZPE) of the constrained water dimer in particular, by comparing the semiclassical value to the value obtained from the harmonic approximation, as highlighted in Table 4.2. The harmonic calculation considerably overshoots the ZPE with a discrepancy of 87%. Likewise, an overestimation trend was observed in the study of constrained van der Waals clusters [19]. A direct comparison of our approach with other available quantum mechanical methods is unfortunately not possible, since no record of a calculation of the zero-point energy of a dimer of rigid TIP3P water molecules was found in the literature. The constrained water dimer has been studied, however, using the TIP4P water model by the rigid body diffusion Monte Carlo (RBDMC) technique [29]. The harmonic ZPE for this model also corresponds to an overestimate of 70% over the reported RBDMC value of 9.17 kJmol^{-1} . The similar trends as well as the relatively comparable anharmonicity exhibited by the two calculations indicate the accuracy of our approach in capturing the correct quantum effect in the interactions between the water molecules.

Quantum mechanical effects in hydrogen bonded moieties or entities are sensitive

Table 4.2: Comparison of zero point energies (kJ mol^{-1}) of the water dimer using the TIP3P and TIP4P potentials. Energies are given with reference to the minimum of the potential.

Water Model	Quantum	Harmonic	Δ
TIP4P	9.17 ^a	15.61	70%
TIP3P	8.28	15.46	87%

^aRigid body diffusion Monte Carlo result (Ref [29])

to the mass of the participating atoms and can therefore be probed through isotopic substitution. We repeated the SC-IVR calculation of bound state energies for a deuterated dimer of rigid water molecules $(\text{D}_2\text{O})_2$. The results are shown in Fig. 4.5 and Table 4.1. Table 4.3 compares the ZPEs of the intermolecular interaction in both the water dimer and its deuterated counterpart. As expected, we observe a lowering of the ZPE upon substitution by the heavier isotope. The vibrational motion in a diatomic molecule can be described by the Morse potential energy function

$$E = D_e[1 - e^{\beta(r_e - r)}]^2, \quad (4.26)$$

where D_e is the dissociation energy, r_e is the equilibrium bond distance, and β is a constant specific to the molecule under investigation. The solution of the Schrödinger equation for the Morse oscillator yields an expression of the following form for vibrational transitions between two consecutive energy levels, with vibrational quantum numbers n and $n + 1$, respectively

$$\begin{aligned} \varepsilon_{n+1 \leftarrow n} &= E_{n+1} - E_n \\ &= \left(n + \frac{1}{2}\right) \hbar\omega_e + \left(n + \frac{1}{2}\right)^2 \hbar\omega_e x_e, \end{aligned} \quad (4.27)$$

where ω_e is the (hypothetical) equilibrium frequency of vibration, i.e., the frequency of infinitesimal vibrations about the equilibrium point and x_e is the corresponding anharmonicity constant. The above equation has found wide applications in the analysis of spectroscopic data. It can also be used to fit the calculated bound state energies

from Table 4.1 to solve for x_e and therefore quantitatively provide an estimate of the anharmonic contribution to the hydrogen bond vibration. The resulting anharmonic constants for the intermolecular interactions of the constrained $(\text{H}_2\text{O})_2$ and $(\text{D}_2\text{O})_2$ water dimer are 0.024 and 0.034, respectively, indicating greater anharmonicity in the latter over the former. Table 4.3 contains the SC-IVR along the harmonic results for both isotopes for comparison purposes.

Table 4.3: Comparison of SC-IVR and harmonic zero point energies (kJ mol^{-1}) of $(\text{H}_2\text{O})_2$ and $(\text{D}_2\text{O})_2$. Energies are given with reference to the minimum of the potential.

System	SC-IVR	Harmonic
$(\text{H}_2\text{O})_2$	8.28	15.46
$(\text{D}_2\text{O})_2$	6.50	15.43

4.4 Conclusions

We previously reported the development of a general approach for the treatment of geometrically constrained systems in SC-IVR calculations in Cartesian coordinates. Early applications of our method successfully reproduced the ZPE and higher energy levels of constrained small van der Waals clusters. In this work we applied, for the first time, our approach to the determination of bound state energies of a constrained *molecular* cluster. We also report a more accurate way of generating the projected Hessian matrix from which the time-dependent constrained HK prefactor is evaluated. The present calculations included a gradient correction term to account for displacements away from the equilibrium geometry.

ZPEs and excited energy levels were calculated for a dimer of rigid TIP3P water monomers and its deuterated counterpart. We assessed the accuracy of our method by comparing with an existing ZPE calculation of the constrained dimer and by investigating the effect of isotopic substitution on the ZPE. Comparison of our results

with the harmonic oscillator model shows a reduction in ZPE. The reduction is in good agreement with the decrease observed in the ZPE of the constrained TIP4P water dimer, thus demonstrating the correct predictive ability of our approach. This is further supported by the observation of the expected reduction in the ZPE of the deuterated dimer upon isotopic substitution. A quantitative measure of the anharmonicity, given by the anharmonicity constant, was determined from the Morse oscillator model. The results indicate the deuterated dimer possesses a stronger anharmonic character than the lighter isotope dimer.

The positive results of the present work on the application of SC-IVR to a constrained molecular dimer in Cartesian coordinates opens the way to the treatment of larger clusters and molecular systems, in general, with the same method. The time-averaging approach of Kaledin and Miller [30, 31] is particularly appealing for systems of higher complexity. The straightforward implementation of our constraint techniques in that context is currently being carried out. An immediate application of interest is the extension of the present study to larger constrained water clusters. Other possible applications include real-time quantum spectroscopic and kinetic studies.

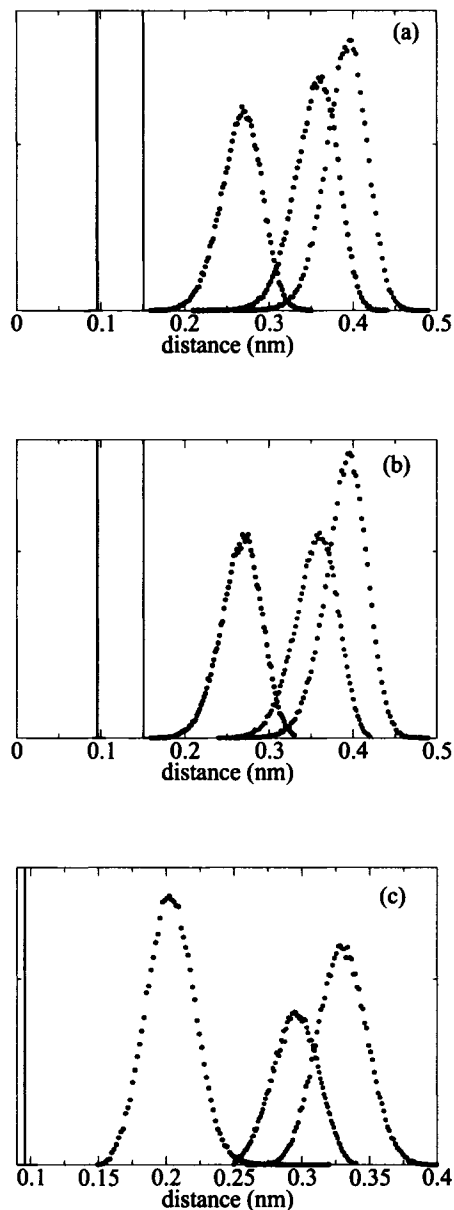


Figure 4.1: Distribution of atomic distances for $(\text{H}_2\text{O})_2$ for the pairs (a) XH1, (b) XH2, and (c) YO1, where $X=\text{O1, H1 or H2, H3, O2 and H4}$ and $Y= \text{H1 and H2, H3, O2 and H4}$ in this order, from left to right. Atomic labels on each of the two water monomers are H1, H2, and O1 and H3, H4, and O2, respectively. Distributions of intramolecular pair distances are truncated along the vertical axis for clarity.



Figure 4.2: Three-dimensional atomic densities generated from sampled positions of the water dimer wave function.

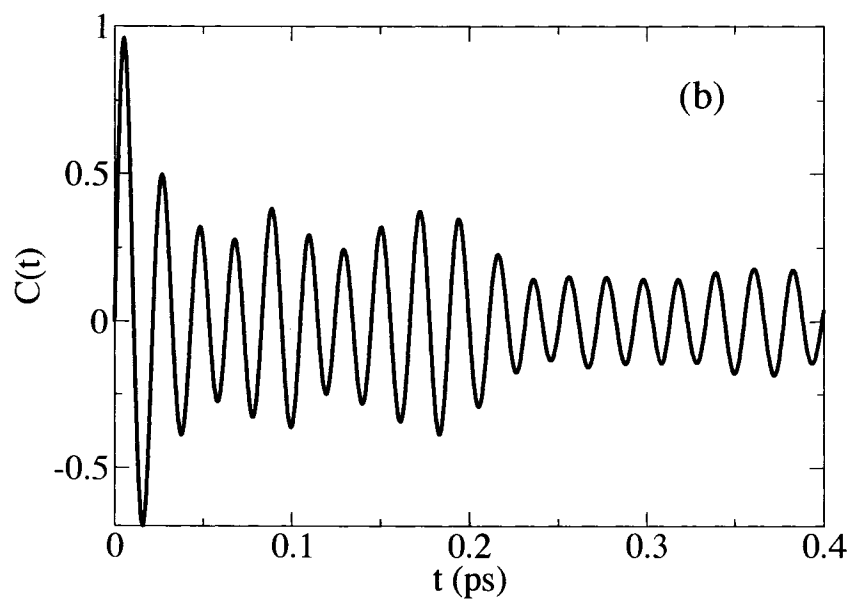
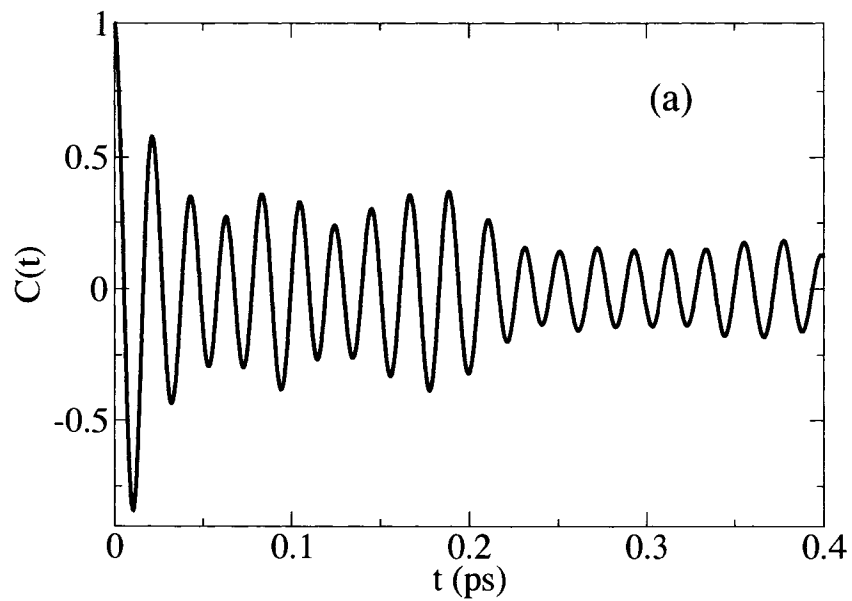


Figure 4.3: (a) Real and (b) imaginary parts of the survival amplitude for $(\text{H}_2\text{O})_2$.

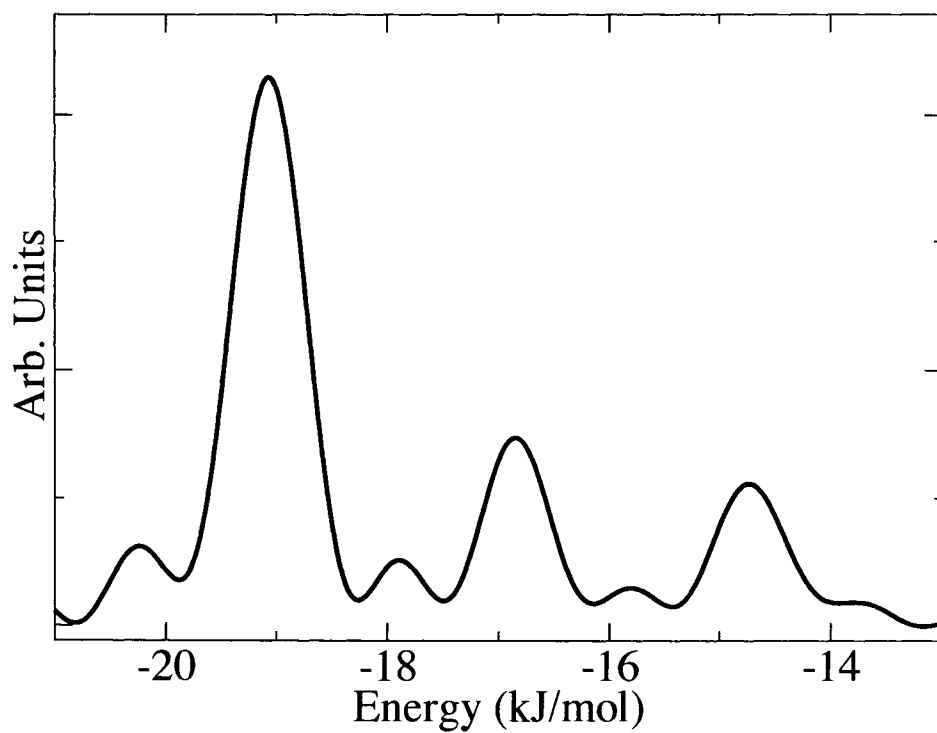


Figure 4.4: Power spectrum showing the bound state energies of $(\text{H}_2\text{O})_2$.

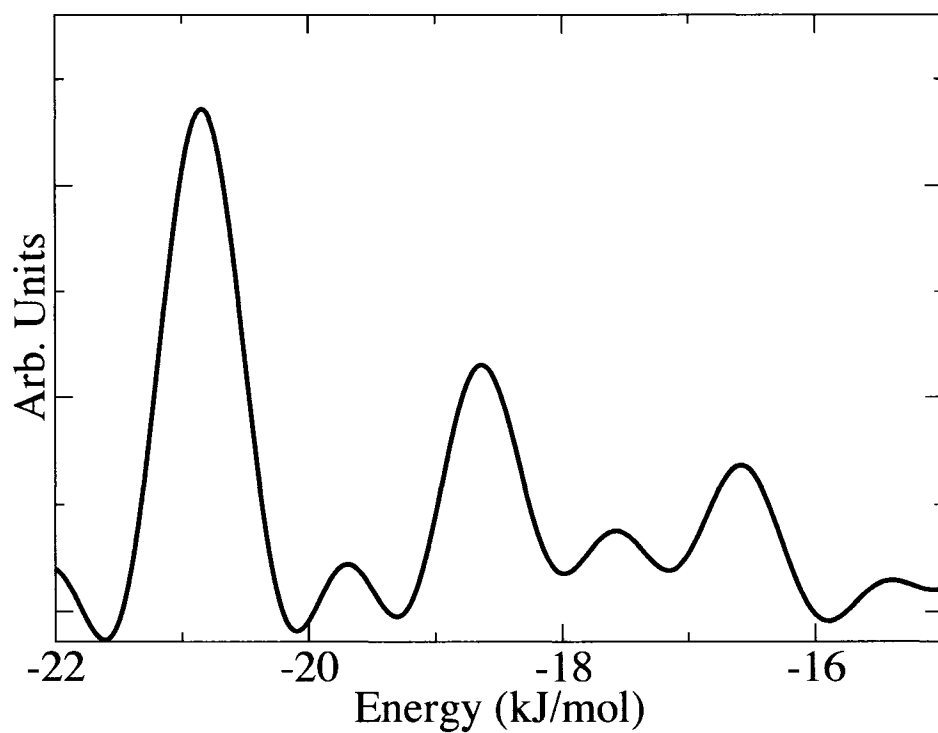


Figure 4.5: Power spectrum showing the bound state energies of $(D_2O)_2$.

Bibliography

- [1] W. H. Miller, *J. Chem. Phys.* **53**, 3578 (1970).
- [2] W. H. Miller, *J. Chem. Phys.* **95**, 9428 (1991).
- [3] E. Heller, *J. Chem. Phys.* **94**, 2723 (1991).
- [4] M. Thoss and H. Wang, *Annu. Rev. Phys. Chem.* **55**, 299 (2004).
- [5] K. G. Kay, *Annu. Rev. Phys. Chem.* **56**, 255 (2005).
- [6] W. H. Miller, *J. Chem. Phys.* **125**, 132305 (2006).
- [7] N. Makri and K. Thompson, *Chem. Phys. Lett.* **291**, 101 (1998).
- [8] K. Thompson and N. Makri, *J. Chem. Phys.* **110**, 1343 (1999).
- [9] X. Sun and W. H. Miller, *J. Chem. Phys.* **110**, 6635 (1999).
- [10] E. Heller, *J. Chem. Phys.* **75**, 2923 (1981).
- [11] M. Baranger, M. A. M. de Aguiar, F. Keck, H. J. Korsch, and B. Schellhass, *J. Phys. A* **34**, 7227 (2001).
- [12] M. Herman and E. Kluk, *Chem. Phys.* **91**, 27 (1984).
- [13] L. Torres, R. Gelabert, X. Gimenez, M. Moreno, and J. Lluch, *J. Chem. Phys.* **117**, 7094 (2002).
- [14] W. H. Miller, *Farad. Discuss. Chem. Soc.* **110**, 1 (1998).
- [15] A. Walton and D. Manolopoulos, *Chem. Phys. Lett.* **84**, 961 (1996).

- [16] M. L. Brewer, J. Hulme, and D. Manolopoulos, *J. Chem. Phys.* **106**, 4832 (1997).
- [17] V. S. Batista, M. T. Zanni, B. J. Greenblatt, D. M. Neumark, and W. H. Miller, *J. Chem. Phys.* **110**, 3736 (1999).
- [18] B. Harland and P.-N. Roy, *J. Chem. Phys.* **118**, 4791 (2003).
- [19] B. Issack and P.-N. Roy, *J. Chem. Phys.* **123**, 084103 (2005).
- [20] B. Issack and P.-N. Roy, *J. Chem. Phys.* **126**, 024111 (2007).
- [21] R. Gelabert, X. Gimenez, M. Thoss, H. Wang, and W. Miller, *J. Phys. Chem. A* **104**, 10321 (2000).
- [22] P. Pulay and G. Fogarasi, *J. Chem. Phys.* **96**, 2856 (1992).
- [23] P. Y. Ayala and H. B. Schlegel, *J. Chem. Phys.* **108**, 2314 (1998).
- [24] E. B. Wilson, J. C. Decius, and P. C. Cross, *Molecular Vibrations: The Theory of Infrared and Raman Vibrational Spectra* (Dover, Inc. New York, 1955).
- [25] W. L. Jorgensen, J. Chandrasekhar, J. D. Madura, R. W. Impey, and M. L. Klein, *J. Chem. Phys.* **79**, 926 (1983).
- [26] H. J. C. Berendsen, J. R. Grigera, and T. P. Straatsma, *J. Phys. Chem.* **91**, 6269 (1987).
- [27] H. C. Andersen, *J. Comput. Phys.* **52**, 24 (1983).
- [28] K. Hinsen, *J. Comp. Chem.* **21**, 79 (2000).
- [29] D. C. Clary, D. M. Benoit, and T. V. Mourik, *Acc. Chem. Res.* **33**, 441 (2000).
- [30] A. I. Kaledin and W. H. Miller, *J. Chem. Phys.* **118**, 7174 (2003).
- [31] A. I. Kaledin and W. H. Miller, *J. Chem. Phys.* **119**, 3078 (2003).

Chapter 5

Quantum molecular dynamics from a single trajectory

Article 4. *Semiclassical initial value representation treatment of hydrogen bonded complexes of rigid molecules from a single trajectory in Cartesian coordinates*

Reused with permission from Bilkiss B. Issack and Pierre-Nicholas Roy, Journal of Chemical Physics, **submitted** (2007). Copyright 2007, American Institute of Physics.

5.1 Introduction

Correlation functions are a versatile group of functions which offer a means of probing dynamical systems. Quantum mechanically, they are generically given as

$$C(t) = \frac{1}{Z} \text{Tr} \left[e^{-\beta \hat{H}} \hat{B} e^{i\hat{H}t/\hbar} \hat{A} e^{-i\hat{H}t/\hbar} \right], \quad (5.1)$$

where $e^{-\beta \hat{H}}$ is the thermal density operator, $Z = \text{Tr}(e^{-\beta \hat{H}})$ is the partition function, and $e^{i\hat{H}t/\hbar} \hat{A} e^{-i\hat{H}t/\hbar} = \hat{A}(t)$ is the Heisenberg representation of operator \hat{A} . The exact expression for a correlation function depends on the property investigated. For example, the rate constant of a reaction can be determined if the operators \hat{A} and \hat{B} correspond to the flux operator. Similarly, the velocity autocorrelation (i.e., $\hat{A} = \hat{B} = \hat{v}$) provides insight about transport properties.

Semiclassical initial value representation (SC-IVR) [1, 2] is a method of performing quantum dynamics based on classically determined variables. A simple and practical approach, the Herman-Kluk (HK) version in particular [3], holds great promise for the

investigation of dynamical properties (via the calculation of correlation functions) in large molecular systems, a class of chemical entities that falls outside the capabilities of current quantum dynamical methods.

SC-IVR calculations call for the integration of an oscillating function, with an oscillatory behaviour which increases with the system size. As a result, the number of trajectories required in order to achieve converged results grows as a function of the complexity and dimensionality of the problem. One foresees therefore, that the treatment of large complex molecular systems by SC-IVR will eventually become impractical. Recent developments have been geared towards optimizing SC-IVR calculations with the objective of extending the applicability of the method [4, 5, 6]. To this end, we proposed a means of reducing the computational cost associated with the generation of classical trajectories via the introduction of constraints in SC-IVR by reducing the effective number of degrees of freedom. Originally formulated for interatomic interactions [7, 8, 9], we recently extended our method to treat intermolecular interactions between rigid molecules [10]. Calculations are performed in Cartesian coordinates with the purpose of keeping a general approach. We point out that constraints are ubiquitous in classical molecular dynamics and easily implemented through well-developed existing constraint techniques in Cartesian coordinates. The integration of our approach into molecular dynamics software therefore comes at a very affordable price.

Kaledin and Miller [6] proposed an alternative method of performing SC-IVR calculations which involves the time-averaging of correlation functions. They showed that, while introducing no additional approximation *per se*, the time-averaging procedure conveniently led to a reduction in the number of trajectories required for convergence though an inherent smoothing of the traditionally oscillatory integrand. The method was tested through the calculation of the bound vibrational states of simple molecules such as hydrogen and water. Going to the extreme, single trajectory calculations were sufficient in some instances, in producing reasonably accurate zero-point energies (ZPEs), although the resulting excited state energies were reported to be of poorer quality.

In this work, we combine our constraint approach with the time-averaged (TA) SC-IVR with the aim of investigating the possibility of furthering the gain in computational time. More specifically, we calculate the ZPE for a dimer of rigid water molecules, $(\text{H}_2\text{O})_2$, using the TA single trajectory method and compare our results to the traditional constraint calculations of Ref [10]. Previous applications of TA SC-IVR have considered exclusively single molecules. To our knowledge, this work represents the first application to intermolecular problems.

The article is organized as follows. Sec. 5.2 outlines the theory behind the time-averaging procedure and is followed by a description of the constrained water dimer and of the computational methods in Sec. 5.3. We also present and discuss results of the ZPE calculations in the same section. Concluding remarks can be found in Sec. 5.4.

5.2 Theory

In the current work, the quantity of interest is a particular type of correlation function called the survival amplitude

$$C(t) = \langle \Psi_i | e^{-i\hat{H}^c t/\hbar} | \Psi_i \rangle . \quad (5.2)$$

This quantity is calculated for a constrained molecular system, described by the wave function Ψ_i , evolving according to the Hamiltonian of the system \hat{H}^c . From the survival amplitude, it is possible to extract the eigenvalues of the Hamiltonian via a simple Fourier transform

$$I(\omega) = \frac{1}{2\pi} \int_{-\infty}^{\infty} dt e^{i\omega t} C(t) . \quad (5.3)$$

Using the SC-IVR formulation of the propagator in coherent-state representation [1, 3]

$$e^{-i\hat{H}^c t/\hbar} = (2\pi\hbar)^{-F} \int \int d\mathbf{p}_i^c d\mathbf{q}_i^c R_{\mathbf{p}_i^c \mathbf{q}_i^c}^c e^{iS_{\mathbf{p}_i^c \mathbf{q}_i^c}^c/\hbar} |g_{\mathbf{p}_i^c \mathbf{q}_i^c}^c\rangle \langle g_{\mathbf{p}_i^c \mathbf{q}_i^c}^c| , \quad (5.4)$$

one arrives at the following expression for the survival amplitude of a constrained

molecular system with F degrees of freedom

$$C(t) = (2\pi\hbar)^{-F} \int \int d\mathbf{p}_i^c d\mathbf{q}_i^c R_{\mathbf{p}_i^c \mathbf{q}_i^c}^c e^{iS_{\mathbf{p}_i^c \mathbf{q}_i^c}^c / \hbar} \langle \Psi_i | g_{\mathbf{p}_i^c \mathbf{q}_i^c}^c \rangle \langle g_{\mathbf{p}_i^c \mathbf{q}_i^c}^c | \Psi_i \rangle . \quad (5.5)$$

The integration variables \mathbf{q}_i^c and \mathbf{p}_i^c correspond to constrained initial positions and initial momenta respectively from which constrained classical trajectories are generated. $g_{\mathbf{p}_i^c \mathbf{q}_i^c}^c$ and $g_{\mathbf{p}_i^c \mathbf{q}_i^c}^c$ are the coherent-state bases prior to and after time evolution. These are minimum uncertainty wave packets which are Gaussian in position and momentum space with average values of \mathbf{q}_i^c or \mathbf{q}_i^c and \mathbf{p}_i^c or \mathbf{p}_i^c respectively. They have the following general form in the position representation:

$$\langle \mathbf{x} | g_{\mathbf{p}_i^c \mathbf{q}_i^c}^c \rangle \propto \exp \left[-\frac{\gamma^c}{2} (\mathbf{x} - \mathbf{q}^c)^2 + \frac{i}{\hbar} \mathbf{p}^c (\mathbf{x} - \mathbf{q}^c) \right] , \quad (5.6)$$

where γ^c is a matrix defining the widths of the Gaussian for the constrained system. The quantities $S_{\mathbf{p}_i^c \mathbf{q}_i^c}^c$ and $R_{\mathbf{p}_i^c \mathbf{q}_i^c}^c$ are computed along the trajectories. Specifically, $S_{\mathbf{p}_i^c \mathbf{q}_i^c}^c$ is the classical action calculated as

$$S_{\mathbf{p}_i^c \mathbf{q}_i^c}^c = \int_0^t dt' [\mathbf{p}_{t'}^c \cdot \dot{\mathbf{q}}_{t'}^c - H] , \quad (5.7)$$

and $R_{\mathbf{p}_i^c \mathbf{q}_i^c}^c$ is the HK prefactor, a quantity related to the stability of the trajectories, defined by Herman and Kluk [3] as

$$R_{\mathbf{p}_i^c \mathbf{q}_i^c}^c = \left| \frac{1}{2} \left[\frac{\partial \mathbf{q}_t^c}{\partial \mathbf{q}_i^c} + \frac{\partial \mathbf{p}_t^c}{\partial \mathbf{p}_i^c} + i\gamma\hbar \frac{\partial \mathbf{q}_t^c}{\partial \mathbf{p}_i^c} - \frac{i}{\gamma\hbar} \frac{\partial \mathbf{p}_t^c}{\partial \mathbf{q}_i^c} \right] \right|^{1/2} . \quad (5.8)$$

Traditionally, the multidimensional integral in Eq. (5.5) is evaluated by Monte Carlo sampling of initial conditions. For a constrained molecular system, extra care is required to ensure that the initial conditions do not violate the constraints. We previously reported on the development of a method that allows for constrained sampling of initial conditions [8, 10]. In this work we investigate an alternative formulation of the SC-IVR expression for the survival amplitude which is based on a time-averaging procedure [6]. Kaledin and Miller showed that any quantity determined from the phase space average

$$B = \int d\mathbf{p}_i \int d\mathbf{q}_i A_{\mathbf{p}_i \mathbf{q}_i} , \quad (5.9)$$

can be re-expressed in a time averaged form

$$B_{TA} = \int d\mathbf{p}_i \int d\mathbf{q}_i \frac{1}{T} \int_0^T dt A_{\mathbf{p}_i \mathbf{q}_i} . \quad (5.10)$$

By analogy, the correlation function can be written as

$$C(t) = \int d\mathbf{p}_i \int d\mathbf{q}_i D_{\mathbf{p}_i \mathbf{q}_i, t} = \int d\mathbf{p}_i \int d\mathbf{q}_i \frac{1}{T} \int_0^T dt_1 D_{\mathbf{p}_{t_1} \mathbf{q}_{t_1}, t} . \quad (5.11)$$

Using the above formulation, the TA survival amplitude for a constrained system is explicitly given by

$$\begin{aligned} C_{TA}(t) &= (2\pi\hbar)^{-F} \int \int d\mathbf{p}_i^c d\mathbf{q}_i^c \frac{1}{T} \int_0^T dt_1 R_{\mathbf{p}_{t_1}^c \mathbf{q}_{t_1}^c, t_2}^c \\ &\times e^{iS_{\mathbf{p}_{t_1}^c \mathbf{q}_{t_1}^c, t_2}^c / \hbar} \langle \Psi_i | g_{\mathbf{p}_{t_2}^c \mathbf{q}_{t_2}^c}^c \rangle \langle g_{\mathbf{p}_{t_1}^c \mathbf{q}_{t_1}^c}^c | \Psi_i \rangle , \end{aligned} \quad (5.12)$$

where $t_2 = t_1 + t$ and

$$\begin{aligned} \mathbf{p}_{t_1}^c &\equiv \mathbf{p}_{t_1}^c(\mathbf{p}_i^c, \mathbf{q}_i^c) \\ \mathbf{p}_{t_2}^c &\equiv \mathbf{p}_{t_2}^c(\mathbf{p}_i^c, \mathbf{q}_i^c) \equiv \mathbf{p}_{t_1+t}^c(\mathbf{p}_i^c, \mathbf{q}_i^c) \\ \mathbf{q}_{t_1}^c &\equiv \mathbf{q}_{t_1}^c(\mathbf{p}_i^c, \mathbf{q}_i^c) \\ \mathbf{q}_{t_2}^c &\equiv \mathbf{q}_{t_2}^c(\mathbf{p}_i^c, \mathbf{q}_i^c) \equiv \mathbf{q}_{t_1+t}^c(\mathbf{p}_i^c, \mathbf{q}_i^c) . \end{aligned} \quad (5.13)$$

In words, $(\mathbf{p}_{t_1}^c, \mathbf{q}_{t_1}^c)$ are the constrained phase space variables which have evolved from initial conditions $(\mathbf{p}_i^c, \mathbf{q}_i^c)$ over the time period t_1 while $(\mathbf{p}_{t_2}^c, \mathbf{q}_{t_2}^c)$ have evolved from the same initial conditions for a total time $t_1 + t$. The action $S_{\mathbf{p}_{t_1}^c \mathbf{q}_{t_1}^c, t_2}^c$ is now calculated along trajectories running to t_2 with t_1 as time origin

$$S_{\mathbf{p}_{t_1}^c \mathbf{q}_{t_1}^c, t_2}^c = \int_{t_1}^{t_2} dt' [\mathbf{p}_{t'}^c \cdot \dot{\mathbf{q}}_{t'}^c - H^c] . \quad (5.14)$$

The current calculations were performed using an approximate form [4] of the HK prefactor rather than its formal definition given in Eq. (5.8). We previously showed that the approximate prefactor performed well for constrained atomic trimers [8, 9]. The same prefactor was utilized in the determination of bound states of water clusters using the traditional constraint approach in Ref. [10]. $R_{\mathbf{p}_{t_1}^c \mathbf{q}_{t_1}^c, t_2}^c$ is given by

$$R_{\mathbf{p}_{t_1}^c \mathbf{q}_{t_1}^c, t_2}^c \approx \exp \left[-\frac{i}{\hbar} \int_{t_1}^{t_2} dt' \sum_{j=1}^F \frac{\hbar \omega_j^c(t')}{2} \right] . \quad (5.15)$$

The sum in the expression runs over the number of normal modes of vibrations. $\omega_j^c(t')$ is the frequency corresponding to the j -th unconstrained mode and is determined from the eigenvalues of a projected matrix of force constants. We employed the projection methods of Pulay and Fogarasi (Ref. [11]) and Ayala and Schlegel (Ref. [12]), to exclude the constrained modes from the normal modes analysis. The projection procedure has been thoroughly discussed elsewhere [10]. A noteworthy point regarding the approximate form of the prefactor is that it is equivalent to the separable approximation discussed in Ref. [6]. In the current work, the prefactor is calculated with an additional rather *ad hoc* approximation where $\omega_j^c(t')$ is always real. The latter form is advantageous for practical reasons since by construction, it possesses a smoother integrand.

Although time-averaging of the integrand necessitates an additional step in the SC-IVR calculation and may deceptively suggest an increase in the computational cost, Kaledin and Miller mention that the effect is actually quite the opposite [6]. Since the time-averaging process leads to a smoothing of the integrand, fewer trajectories are, in principle, required to converge the calculations.

5.3 Methods and Results

Calculations were performed for $(\text{H}_2\text{O})_2$ using a rigid TIP3P water model. The constrained system has six degrees of freedom corresponding to the intermolecular vibrational modes of motion. The TIP3P water monomer is a three-site model with partial positive charges located on the hydrogen atoms and a partial negative charge on the oxygen atom. The intermolecular interaction is described by the sum of a Lennard-Jones potential between the oxygen atoms and a Coulombic contribution from interacting atomic charges q_i and q_j on monomers, a and b respectively,

$$U_{ab} = \sum_i^{\text{on } a} \sum_j^{\text{on } b} \frac{q_i q_j e^2}{4\pi\epsilon_0 r_{ij}} + 4\epsilon \left[\left(\frac{\sigma}{r_{OO}} \right)^{12} - \left(\frac{\sigma}{r_{OO}} \right)^6 \right]. \quad (5.16)$$

r_{ij} is the Cartesian separation of two atomic sites and r_{OO} is the distance between the two oxygen atoms. Using values from Ref. [13] for the parameters, the energy at

the equilibrium geometry (D_e) was calculated to be $-27.36 \text{ kJ mol}^{-1}$.

The calculations were completely carried out using the molecular modelling toolkit (MMTK), an open source program library for molecular simulations [14]. In particular, a single trajectory was generated from an initial condition ($\mathbf{p}_i^e, \mathbf{q}_i^e$) corresponding to the average values of the coherent-state parameters and chosen as a zero momentum vector and the equilibrium geometry respectively. Constrained equations of motion were integrated with the RATTLE algorithm [15] using a time step of 0.1 fs. A correlation length of only 80 fs was sufficient to catch the ZPE. The correlation functions were then time-averaged and Fourier transformed to extract the ZPE. Figure 5.1 shows an example of a power spectrum with a unique peak corresponding to the ZPE of the intermolecular vibration of the water dimer. To reduce noise levels, a Gaussian smoothing function was applied to the TA correlation function prior to the Fourier transform

$$I(\omega) = \frac{1}{\pi} \text{Re} \int_0^\infty dt e^{i\omega t} C_{TA}(t) e^{-\alpha^2 t^2}, \quad (5.17)$$

where the parameter α determines the degree of smoothing.

As mentioned earlier, traditional SC-IVR calculations require the time evolution of a pool of sampled initial conditions representative of the initial wave function. In TA SC-IVR, the phase space points corresponding to the time origins of the correlation functions provides an analogous representation of the initial wave function. Figure 5.2 displays the wave function from over 500 000 positions visited during the phase space exploration of the trajectory. We note a similarity between the distributions of the atomic positions during the dynamics and the distributions of sampled initial atomic positions reported in our recent study [10]. In particular, the distributions of the two hydrogen atoms on the left display identical delocalization, as a consequence of their equivalency, while the hydrogen atom directly involved in hydrogen bonding is more localized in space. All distributions are consistent with the bond and bond angle constraints imposed on the water molecules. The time-averaging length T for the constrained water dimer was determined at 50 ps from a convergence plot of the variation of the ZPE (reported with respect to D_e) with T as displayed in

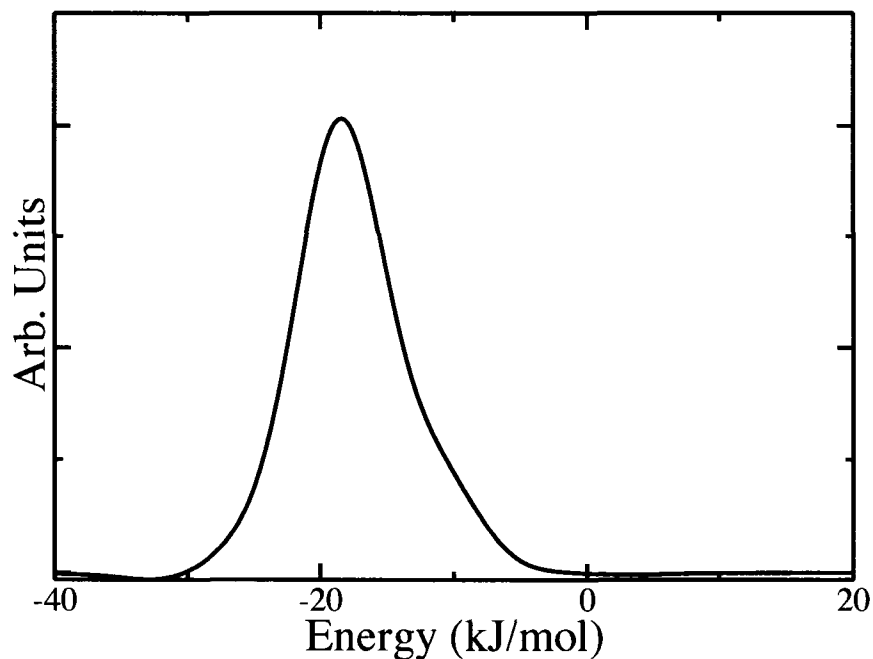


Figure 5.1: Zero-point energy determination from the power spectrum in kJ mol^{-1} for $T=0$ (i.e., no time-averaging).

Fig. 5.2. The resulting ZPE has a value of 8.33 kJ mol^{-1} and compares favourably to our previously reported value of 8.28 kJ mol^{-1} . We therefore conclude that the single trajectory fares reasonably well at describing the ZPE. We also point out that simulations run time for the TA calculations were shortened by an order of magnitude when compared with our original constraint SC-IVR approach.

5.4 Conclusions

We report the first successful implementation of our previously developed constraint technique [8, 9, 10] in the context of TA SC-IVR to treat geometrically constrained systems in Cartesian coordinates. We show that the method affords a reasonably accurate prediction of the ZPE of the water dimer. Although the present study has



Figure 5.2: Three-dimensional atomic densities generated from the dynamical sampling of positions along the trajectory.

focused on the calculation of the ZPE, it can directly be extended to the extraction of excited state energies by simply modifying the initial wave function and increasing the correlation time. A significant practical benefit of the approach is the relatively low cost of carrying out the calculations. Compared to regular SC-IVR calculations, the computational effort is doubly reduced: through the inclusion of constraints and through the time-averaging procedure. Thus, the current work represents a new and fruitful attempt at improving the practicality of SC-IVR with the purpose of treating systems of high dimensionality and complexity.

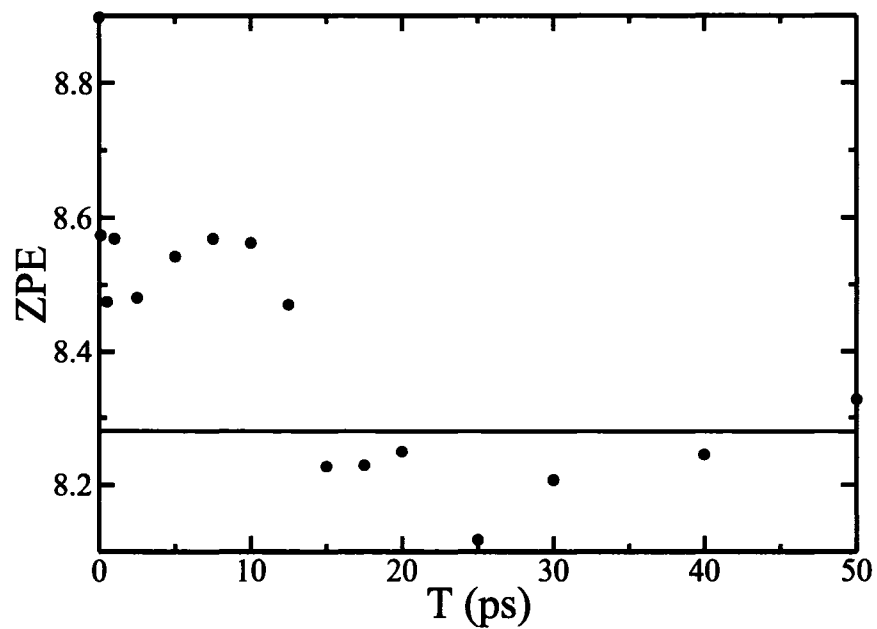


Figure 5.3: Convergence of ZPE in kJ mol^{-1} with time-averaging length T . The horizontal line represents the ZPE obtained from the full SC-IVR calculation of Ref. [10].

Bibliography

- [1] W. H. Miller, *J. Chem. Phys.* **53**, 3578 (1970).
- [2] E. Heller, *J. Chem. Phys.* **75**, 2923 (1981).
- [3] M. Herman and E. Kluk, *Chem. Phys.* **91**, 27 (1984).
- [4] R. Gelabert, X. Gimenez, M. Thoss, H. Wang, and W. Miller, *J. Phys. Chem. A* **104**, 10321 (2000).
- [5] S. Zhang and E. Pollak, *J. Chem. Phys.* **119**, 11058 (2003).
- [6] A. I. Kaledin and W. H. Miller, *J. Chem. Phys.* **118**, 7174 (2003).
- [7] B. B. Harland and P.-N. Roy, *J. Chem. Phys.* **118**, 4791 (2003).
- [8] B. B. Issack and P.-N. Roy, *J. Chem. Phys.* **123**, 084103 (2005).
- [9] B. B. Issack and P.-N. Roy, *J. Chem. Phys.* **126**, 024111 (2007).
- [10] B. B. Issack and P.-N. Roy, *J. Chem. Phys.* **127**, 054105 (2007).
- [11] P. Pulay and G. Fogarasi, *J. Chem. Phys.* **96**, 2856 (1992).
- [12] P. Y. Ayala and H. B. Schlegel, *J. Chem. Phys.* **108**, 2314 (1998).
- [13] W. L. Jorgensen, J. Chandrasekhar, J. D. Madura, R. W. Impey, and M. L. Klein, *J. Chem. Phys.* **79**, 926 (1983).
- [14] K. Hinsen, *J. Comp. Chem.* **21**, 79 (2000).
- [15] H. C. Andersen, *J. Comput. Phys.* **52**, 24 (1983).

Chapter 6

Conclusions

The dynamical behaviour of atomic and molecular systems can be accurately determined in principle by solving the Schrödinger equation. In practice though, the exponential scaling plaguing real-time exact dynamical methods limits applications to small system size. It is hoped that continuing developmental efforts and the increasing computational power and memory will allow the treatment of larger and larger molecules of interest in the future. However, unless a method is developed with a non-exponential scaling, the treatment of large complex molecules will remain outside the boundaries of quantum dynamics in the foreseeable short term.

This bitter reality has motivated the development of alternative approximate methods which allow for the description of key quantum effects in systems that are untreatable by quantum mechanics. We provided in Chapter 1 a brief review of a few approaches developed to that effect. In general, these techniques have been successfully tested and benchmarked against exact quantum mechanical calculations for small systems. The challenge currently lies in the extension to larger systems. In our view, SC-IVR represents a particularly promising approach for the treatment of problems of high complexity and dimensionality. Based on the ingenious incorporation of quantum mechanical effects into classical simulations, the method conveniently takes advantage of existing well-established tools (developed for classical MD) without re-inventing the wheel. However, one is forced to recognise that the applicability of SC-IVR in terms of system size is well under that of classical MD. In the latter approach, the computational burden associated with large system sizes is commonly

alleviated via the introduction of constraints. Prior to our work, a rigorous and general way of constraining degrees of freedom in molecular systems was lacking in SC-IVR. Our contribution towards extending the applicability of SC-IVR is precisely the development and implementation of a *general* method that allows for the treatment of geometrically constrained systems in SC-IVR. The generality of the approach draws on the fact that calculations are performed in Cartesian coordinates.

We presented in Chapter 2 the theoretical formalism we have developed to include constraints in a Cartesian formulation of the SC-IVR. This chapter also includes proposed algorithms for the practical implementation of the theory. In order to test our new theoretical and methodological developments, we presented a benchmark application to model systems consisting of free and constrained van der Waals clusters, modelled by the Lennard-Jones potential. For such systems, exact quantum mechanical calculations are possible and thus provide a way of assessing the accuracy of the new approach. Comparison of results revealed that the constraint SC-IVR was able to correctly catch the reduction in ZPE upon inclusion of constraints. In Chapter 3, we achieved an important step by demonstrating how our new approach could be extended to the calculation of bound excited state energies and we further illustrated the correct predictive ability of our ideas via the reproduction of the exact quantum mechanical bound state energies. The positive benchmarking tests for the *atomic* van der Waals clusters led to further developments and extension to *molecular* systems. Following a successful implementation, we presented in Chapter 4 the calculation of intermolecular vibrational energies for a dimer of rigid water molecules, the archetypical hydrogen bonded cluster, using the TIP3P water model [1]. In this case, exact quantum calculations of the bound state energies were unfortunately not available for comparison. Instead, we compared our results with the exact zero-point energy of the intermolecular vibration of a water dimer computed using a slightly different model from the same family [2] and concluded that the method performed well. In keeping with our efforts towards making quantum dynamical methods, SC-IVR in particular, applicable large complex systems, we combined the constraint technique with a recently proposed time-averaged version of the SC-IVR [3]. Being computa-

tionally cheaper, the latter approach has been qualified by its developers as a method which “*goes a long way towards making such calculations practical for molecular systems of an interesting size*” [3]. We showed in Chapter 5 that the implementation of constraints in TA SC-IVR enables the determination of the ZPE to reasonable accuracy while further reducing the simulation run time, thus amplifying the preceding statement.

Before concluding this section, it is appropriate to point out that for small systems such as the argon clusters, constraint SC-IVR presents no gain in computer time compared to full quantum calculations. In fact, for such small systems exact quantum mechanical methods are by far more advantageous, both in terms of accuracy and cost. However, the computational effort associated with exact methods (which exhibit an exponential dependence on system size) quickly outgrows the linearly scaled SC-IVR as the number of atoms increases. Consequently, SC-IVR remains a perfectly viable option for the target systems of high complexity and dimensionality. The computational bottleneck of SC-IVR calculations in general rests with the evaluation of the HK prefactor: a diagonalisation is required at each timestep. For constraint SC-IVR, the HK prefactor is obtained from a hessian of reduced dimensionality as forbidden modes are projected out. In other words, the computational effort associated with the determination of eigenvalues and eigenvectors of the hessian is lowered. However, part of the difficulty is transferred elsewhere, namely to projection procedure, which also involves either a singular value decomposition or an additional diagonalisation. In this respect, an alternative formulation of the constraint HK prefactor with improved efficiency is perhaps desirable from a technical point of view.

6.1 Complementary discussion of the results

In this section, we provide a discussion of the results which is complementary to the contents of the earlier chapters. The successful treatment of atomic as well as molecular clusters is extremely encouraging for future applications of our constraint approach to larger systems. So far the accuracy has been gauged with respect to cal-

culated results from exact quantum mechanical methods. Besides accuracy, generality is another non-negligible requirement in making a method truly practical. According to Christopher Cramer, “*The generality of any given model can only be established by comparison to experiment for a wider and wider variety of systems.*” [4]. While also pertinent to theoretical/computational methods, comparison to experimentally determined data is often not as simple a procedure as one might think, particularly in the testing phases of a newly developed approach. Models tend to be simplistic and often prohibit direct comparison with experiments. Alternatively, other systems such as the weak van der Waals clusters encountered in Chapters 2 and 3 are very challenging to probe experimentally and can sometimes only be studied theoretically.

6.1.1 van der Waals clusters

The particular issue of weakly bound clusters is addressed by Karlicky *et al.* in a recent article: “*Experimental spectroscopic studies of small neutral argon clusters are difficult, due to the small optical activity of these species. The dimer has no electric dipole and no infrared spectra can be measured for these systems*” [5]. However, the Raman [6] and ultraviolet electronic spectra [7] of the dimer have been measured; the latter is compared to results previously presented in this thesis in Table 6.1. Comparison with the experimental measurements indicates a systematic blue shift in our calculations by $\sim 0.4\text{-}0.5$ kJ mol⁻¹. There are two main reasons for the discrepancies: the limitations of the method and of the model. Being an approximate method, SC-IVR is inherently limited in accuracy due to its use of classically obtained quantities to achieve a quantum mechanical description of the dynamics of systems. Similarly, the Lennard-Jones potential provides a good description of the interactions, but is certainly not the best available model. However, the use of the most accurate model was irrelevant since the objective of the test was to gauge the accuracy of the method rather than the reproducibility of experimental data. For that reason, comparison with exact quantum mechanical results remains the best criterion in judging the performance of the method for the model systems.

Regarding the argon trimer, Karlicky and co-workers write that “*the trimer does*

Table 6.1: Comparison of the predictions of our method using the Lennard-Jones potential with experimentally determined vibrational spacings for the argon dimer in kJ mol^{-1} .

D_0	SC-IVR	Experiment ^a
	0.85	1.01
Transition		
$\nu = 0 \rightarrow 1$	0.31	0.26
$\nu = 1 \rightarrow 2$	0.25	0.21
$\nu = 2 \rightarrow 3$	0.19	0.15

^aVibrational spacings of the argon dimer determined by vacuum ultraviolet laser spectroscopy by Herman *et al.* [7]. Error bars are on the order of $1 \times 10^{-4} \text{ kJ mol}^{-1}$.

have a small electric dipole for configurations distorted from the equilibrium equilateral triangular one. This dipole results mainly from the interaction of each of the three polarizable Ar atoms with the electric field created by the exchange quadrupole of the two other overlapping atoms. These three electric fields cancel for equilateral triangular configurations. We are not aware of experimental spectroscopic studies for the trimer of any type, infrared, Raman or ultraviolet." [5]. The constrained trimers are evidently non-physical and hence cannot be hoped to be studied experimentally.

6.1.2 Water clusters

The intermolecular hydrogen bonded interaction between water molecules has been studied by Curtiss and co-workers back in 1979 [8]. The authors determined the enthalpy of association (alternatively the dissociation energy) of a water dimer through thermal conductivity measurements. They additionally calculated the electronic binding energy from the experimental enthalpy by applying corrections for vibrational, rotational and translational motions. Their study considered both $(\text{H}_2\text{O})_2$ and its the deuterated cluster $(\text{D}_2\text{O})_2$. A comparison of their determination of the ZPE with the SC-IVR results is provided in Table 6.2. The table compares the calculated ZPEs of the intermolecular interaction between H_2O molecules and D_2O molecules with

their experimentally determined counterparts. As expected, we observe a lowering of the ZPE upon substitution by the heavier isotope. The large error bars on the experimental data unfortunately do not allow us to comment further on the effect of isotopic substitution or on the accuracy of the results.

Table 6.2: Comparison of SC-IVR ZPEs of $(\text{H}_2\text{O})_2$ and $(\text{D}_2\text{O})_2$. Energies are given in kJ mol^{-1} with reference to the minimum of the potential.

System	SC-IVR	Experiment ^a
$(\text{H}_2\text{O})_2$	8.28	7.74 (± 2.9)
$(\text{D}_2\text{O})_2$	6.50	7.45 (± 2.9)

^aExperimental values of ZPE are determined from equilibrium and zero-point dissociation energies from thermal conductivity measurements by Curtiss *et al.* [8]

Now that we have rigorously tested the method for a correct description of the bound state energies for several weakly bound clusters, it can be extended to more realistic (and typically larger) systems of interest for the prediction and assignment of spectroscopic data. Examples of such applications are discussed below in Sec. 6.2. Although studies of the novel constraint SC-IVR considered in this thesis have focused on calculations of eigenvalues of the Hamiltonian, they are in no way restricted to such investigations. In principle, its applicability encompasses the multitude of problems that are traditionally studied through SC-IVR and even extends beyond, since constrained and larger systems can additionally be treated. Even more powerful in terms of potential for applications is the method's ability to determine the wave function itself as a function of propagation time. As the wave function completely defines the state of a system, virtually any property of interest can be calculated.

6.1.3 Software development

A significant portion of the work involved in this thesis has required the development and implementation of algorithms and computer codes. As mentioned previously,

computer software codes were designed and programmed ¹. The majority were implemented within the MMTK framework [9]. We present in Appendix C a compilation of some of the key methods and classes, with an accompanying documentation. The run times of simulations performed on a parallel computer cluster varied from hours to days, depending on the system and the type of calculation. Parallelization of the computational effort resulted in a huge practical gain; many of the calculations would have been unrealistically slow on single processors.

6.2 Future Directions

In the last part of the thesis, we offer suggestions for two possible future applications of the developed constraint SC-IVR approach to systems currently in need of computational work in order to rationalize experimental observations and measurements.

6.2.1 Larger water clusters: the hexamer

As a first application, we propose the direct extension of the constraint SC-IVR study of the water dimer to larger water complexes. The motivation behind experimental and computational investigations of water clusters lies in the fact that the acquired information *permits us to systematically untangle the intricacies associated with cooperative hydrogen bonding and promises to lead to a more complete molecular description of the liquid and solid phases* [10]. Among larger water clusters, the water hexamer in particular, presents several features which make it an interesting candidate. Calculations on the stability of the hexamer have revealed the existence of several stable conformers including the book, boat, cage, cyclic and prism structures, all within close energetic proximity [11]. Three isomers of the water hexamer are depicted in Fig. 6.1.

The first experimental measurement of the water hexamer by far-infrared laser supersonic jet spectroscopy identified a cage structure [11, 12] in agreement with RBDMC calculations [11, 13, 14] and an independent spectroscopic characterisation

¹For this project, over 10000 lines of code were written in *python* and *C++* by the author



Figure 6.1: The cyclic, book and boat conformations of the water hexamer, courtesy of N. Oro, unpublished (2005).

also using slit-jet techniques [15]. Smaller clusters ranging from the dimer to the pentamer display cyclic structures with two-dimensional hydrogen bond network as their most stable conformer while the hexamer presents a stable three-dimensional cage structure. Representing a transition point, the cage has been proposed as a model to quantify the intermolecular forces and hydrogen bond rearrangements that occur in condensed phases (i.e., liquid water) via studies of its structural and dynamical properties. More recent spectroscopic investigations of the hexamer trapped in liquid helium droplets [16], solid para-hydrogen matrices [17] and solid neon matrices [18] all reveal a stable cyclic conformation. Attempts to explain the discrepancy have highlighted the role of the conditions under which the clusters are generated [16, 19]. It has been suggested that the isomerization of the book, cage and cyclic conformers holds the key to the puzzle. For a better understanding, the book \leftrightarrow cage \leftrightarrow cyclic interconversion needs to be studied in more details by including quantum effects, since the energy ordering is sensitive to the inclusion of the ZPE [11, 19].

As a first step, the constraint SC-IVR calculation of the water dimer could be extended to the hexamer for the determination of the relative stabilities of the different isomers. The previously used TIP3P water model [1] is however inadequate at the level of the hexamer since it fails to describe the cage structure. A more accurate intermolecular potential is required; TIP4P [1] would be a good starting point since

it has been used in previous studies of the hexamer [20]. As part of a more in-depth study, the isomerization process and the timescales of hydrogen bond rearrangement in particular can be investigated via the calculation of the flux-flux correlation function. The single-trajectory approach is especially appealing in this situation since it can be used in conjunction with “on-the-fly” techniques.

6.2.2 CH_5^+

Although first characterised in the 1950’s by mass-spectrometry [21] protonated methane, CH_5^+ , was considered until recently [22, 23], as “*one of the Holy Grails of rotational-vibrational molecular spectroscopy*” [24]. Due to its unique properties, the molecule has generated massive interest, both from the experimental and theoretical viewpoints. CH_5^+ has no real (fixed) structure, rather, it is a fluxional molecule constantly undergoing structural rearrangements or scrambling of hydrogen atoms at room temperature. The global minimum on the PES can be described as a CH_3 tripod with an H_2 moiety connected to the carbon atom in an eclipsed configuration [24]. The PES additionally contains several low-lying stationary points, all of which are accessible upon the inclusion of ZPE [25, 26, 27], thus explaining the floppy nature of the system. Figure 6.2 illustrates the delocalization of protons in the CH_3 tripod and in the H_2 unit. Besides its peculiar structural properties, it also displays unconventional bonding: three-centre two-electron bonding in the equilibrium geometry. Consequently, CH_5^+ represents the dual prototype of this type of bonding and of hypercoordinated carbon compounds.

The first resolved IR spectrum of bare CH_5^+ measured in 1999 was reported virtually unassigned [22]. The fluxional nature of the molecule obscures the identification of the ro-vibrational modes and complicates the assignment of the recorded spectrum. The challenge of assigning the spectrum of CH_5^+ was finally tackled via simulations based on *ab initio* dynamics [23]. The vibrational spectrum was calculated from the classical dipole-dipole correlation function, with a quantum correction [28]. The low-frequency region of the spectrum was not recorded due to limitations of the experimental technique [23]. As a result, the scrambling dynamics were probed

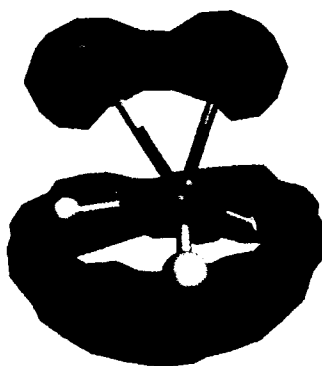


Figure 6.2: The delocalisation of the hydrogen atoms in CH_5^+

during classical simulations via artificial cooling, i.e. at a low temperature. The cooling procedure however, is accompanied by a slowdown in the rate of proton exchange, consequently providing a slightly distorted picture of the scrambling process. The method developed in this thesis, on the other hand, provides a more accurate way of probing the fluxionality of CH_5^+ without affecting the scrambling dynamics and yet avoiding the interference of stretching modes by constraining the CH bonds. We propose to investigate the delocalization of hydrogen atoms through the extraction of the dynamical wave function by SC-IVR using a recently developed *ab initio* potential [29]. In addition, the low-frequency vibrational spectrum can be directly predicted from the semiclassical calculation of the dipole-dipole correlation function $C(t) = \langle \hat{\mu} \hat{\mu}(t) \rangle$.

We have discussed here two possible applications of the constraint SC-IVR approach presented in this thesis. The technique could also be applied to gain insight into the dynamics of a rotating rigid molecule inside superfluid environment or any quantum system, in general, where constraints are of relevance.

Bibliography

- [1] W. L. Jorgensen, J. Chandrasekhar, J. D. Madura, R. W. Impey, and M. L. Klein, *J. Chem. Phys.* **79**, 926 (1983).
- [2] D. M. Benoit and D. C. Clary, *J. Phys. Chem. A* **104**, 5590 (2000).
- [3] A. I. Kaledin and W. H. Miller, *J. Chem. Phys.* **118**, 7174 (2003).
- [4] C. J. Cramer, *Essentials of Computational Chemistry* (Wiley, England, 2002).
- [5] F. Karlicky, B. Lepetit, R. Kalus, and F. X. Gadea, *J. Chem. Phys.* **126**, 174305 (2007).
- [6] P. R. Herman, P. E. Godfriend, and B. P. Stoicheff, *Phys. Rev. A* **27**, 3008 (1983).
- [7] P. R. Herman, P. E. LaRocque, and P. B. Stoicheff, *J. Chem. Phys.* **89**, 4535 (1988).
- [8] L. A. Curtiss, D. J. Frurip, and M. Blander, *J. Chem. Phys.* **71**, 2703 (1979).
- [9] K. Hinsen, *J. Comp. Chem.* **21**, 79 (2000).
- [10] F. N. Keutsch and R. J. Saykally, *Proc. Natl. Acad. Sci. U. S. A.* **284**, 10533 (2001).
- [11] K. Liu et al., *Nature* **381**, 501 (1996).
- [12] K. Liu, M. G. Brown, and R. J. Saykally, *J. Phys. Chem. A* **101**, 8995 (1997).
- [13] J. K. Gregory and D. C. Clary, *J. Phys. Chem. A* **101**, 6813 (1997).

- [14] M. W. Severson and V. Buch, *J. Chem. Phys.* **111**, 10866 (1999).
- [15] J. B. Paul, C. P. Collier, R. J. Saykally, J. J. Scherer, and A. O'Keefe, *J. Phys. Chem. A* **101**, 5211 (1997).
- [16] K. Nauta and R. E. Miller, *Science* **287**, 293 (2000).
- [17] M. E. Fajardo and S. Tam, *J. Chem. Phys.* **115**, 6807 (2001).
- [18] S. Hirabayashi and K. M. T. Yamada, *Chem. Phys. Lett.* **435**, 74 (2007).
- [19] M. Losada and S. Leutwyler, *J. Chem. Phys.* **117**, 2003 (2002).
- [20] D. J. Wales and M. P. Hogdes, *Chem. Phys. Lett.* **286**, 65 (1998).
- [21] V. L. Tal'roze and K. Lyubimova, *Dokl. Akad. Nauk. SSSR* **86**, 909 (1952).
- [22] E. T. White, J. Tang, and T. Oka, *Science* **284**, 135 (1999).
- [23] O. Asvany et al., *Science* **309**, 1219 (2005).
- [24] D. Marx and M. Parrinello, *Science* **284**, 59 (1999).
- [25] P. R. Schreiner, S. J. Kim, H. F. Schaefer III, and P. von Ragué Schleyer, *J. Chem. Phys.* **99**, 3716 (1993).
- [26] A. L. Kaledin, S. D. Kunikeev, and H. S. Taylor, *J. Phys. Chem. A* **103**, 4995 (2004).
- [27] A. B. McCoy et al., *J. Phys. Chem. A* **108**, 4991 (2004).
- [28] R. Ramirez, T. Lopez-Cuidad, P. Kumar, and D. Marx, *J. Chem. Phys.* **121**, 3973 (2004).
- [29] A. Brown, A. B. McCoy, B. J. Braams, Z. Jin, and J. M. Bowman, *J. Chem. Phys.* **121**, 4105 (2004).

Appendix A

WKB approximation

The material presented here is adapted from Refs. [1, 2].

The one-dimensional time-independent Schrödinger equation

$$\frac{d^2\psi}{dx^2} + \frac{p^2(x)}{\hbar^2}\psi = 0 , \quad (\text{A.1})$$

where the momentum $p(x)$ is classically given by

$$p(x) = \sqrt{2m(E - V(x))} , \quad (\text{A.2})$$

has solutions of the general form

$$\psi(x) = e^{iS(x)/\hbar} . \quad (\text{A.3})$$

Substituting the above expression in Eq. (A.1) yields,

$$-\frac{S'^2}{\hbar^2} + \frac{iS''}{\hbar} + \frac{p^2(x)}{\hbar^2} = 0 , \quad (\text{A.4})$$

which is still a non-linear differential equation and therefore no simpler than the original Schrödinger equation. In the semiclassical limit $\hbar \rightarrow 0$, however, we can expand the function $S(x)$ in terms of \hbar ,

$$S = S_0 + \hbar S_1 + \hbar^2 S_2 + \dots , \quad (\text{A.5})$$

and re-write Eq. (A.4) after grouping like powers of \hbar as

$$[-S_0'^2 + p^2(x)] + \hbar[-2S_0'S_1' + iS_0''] + \hbar^2[-2S_0'S_2' - S_1'^2 + iS_1''] + \dots = 0 . \quad (\text{A.6})$$

Equating all the coefficients of the different powers of \hbar to zero leads to the following equations for the zeroth order term

$$S_0'^2 = p^2(x) , \quad (\text{A.7})$$

and the linear term

$$S_1' + i(S_0''/2S_0') , \quad (\text{A.8})$$

with solutions

$$S_0 = \pm \int p(x)dx , \quad (\text{A.9})$$

and

$$S_1 = \frac{i}{2} \ln|p(x)| , \quad (\text{A.10})$$

respectively. By combining Eq. (A.9) and (A.10) we construct the WKB wave functions as two linearly independent solutions

$$\psi_{WKB} = \frac{1}{\sqrt{|p(x)|}} e^{\pm \frac{i}{\hbar} \int p(x)dx} . \quad (\text{A.11})$$

This result was obtained from the time-independent Schrödinger equation and is therefore an approximation to the stationary state. In order to describe dynamical systems, however, the wave function requires a time dependence, which is achieved by including a time-dependent phase factor. The resulting time-dependent WKB wave function becomes

$$\psi_{WKB} = \frac{1}{\sqrt{|p(x)|}} e^{\pm \frac{i}{\hbar} \int p(x)dx - \frac{i}{\hbar} Et} , \quad (\text{A.12})$$

where E is the conserved energy of the trajectory. Noting that the phase $S(x, t)$ can be re-written as

$$\begin{aligned} S(x, t) &= \int p(x)dx - \int E dt \\ &= \int (p(t)\dot{x}(t) - E) dt \\ &= T - V , \end{aligned} \quad (\text{A.13})$$

leads to the conclusion that the phase is simply the action along the classical trajectory. The WKB wave functions therefore are ‘classical wave functions’ which satisfy

exactly classical equations of motion and approximately the Schrödinger equation Eq. (A.1). The results are valid as long as the condition

$$\left| \frac{d\lambda}{dx} \right| \ll 2\pi \quad (\text{A.14})$$

holds true. $\lambda(x)$ is the de Broglie wavelength given by $2\pi\hbar/p(x)$. The condition is satisfied for potential energy functions that vary smoothly with x and unfortunately breaks down at turning points since the classical momentum is zero.

Bibliography

- [1] J. Z. H. Zhang, *Theory and Application of Quantum Molecular Dynamics* (World Scientific, Singapore, 1999).
- [2] P. R. Holland, *Quantum Theory of Motion* (Cambridge University Press, 1993).

Appendix B

Van Vleck's Propagator

For simplicity, we derive an expression for van Vleck's propagator for a one-dimensional problem and later generalize for the multidimensional case. Note that the derivation presented here is not the actual work of van Vleck, which is unfortunately too complex for me to decipher. An alternative derivation taken from Ref. [1] is offered. Consider the path integral expression (see Sec. 1.5) for the transition amplitude $K(x, y, t)$ in one dimension

$$\begin{aligned} K(x, y, t) &= \langle x | e^{-i\hat{H}t/\hbar} | y \rangle \\ &= \left(\frac{m}{2\pi i \hbar \Delta t} \right)^{N/2} \int dx_1 \dots \int dx_{N-1} e^{\frac{i}{\hbar} S(x, x_1, \dots, x_{N-1}, y, t)}, \end{aligned} \quad (\text{B.1})$$

where

$$\begin{aligned} S(x, y, t) &= \sum_{i=1}^{N-1} S(x_i, x_{i-1}, \Delta t) \\ &= \sum_{i=1}^{N-1} \frac{m}{2\Delta t} |x_i - x_{i-1}|^2 - \Delta t V(x_i), \end{aligned} \quad (\text{B.2})$$

is the classical action evaluated for all paths connecting $x = x_0, x_1, \dots, x_{N-1}, x_N = y$. In the semiclassical limit of $\hbar \rightarrow 0$, the phase in the path integral is highly oscillatory. Consequently, the most significant contribution to the integral comes from classical paths characterised by stationary classical actions S_c , i.e., $\delta S_c(x, y, t) = 0$. Therefore, we apply the Stationary Value Approximation (SPA) which involves expanding $S_c(x, y, t)$ around the stationary phase points to second order. In $N - 1$

dimensions, this corresponds to

$$S_c(x, y, t) = S_c(\mathbf{x}) \simeq S_c(\mathbf{x}_\alpha) + \frac{1}{2}(\mathbf{x} - \mathbf{x}_\alpha)^T \mathbf{S}''(\mathbf{x}_\alpha)(\mathbf{x} - \mathbf{x}_\alpha) , \quad (\text{B.3})$$

where \mathbf{x} is an $N - 1$ dimensional vector with components $x_i (i = 1, 2, \dots, N - 1)$, \mathbf{x}_α is a vector of stationary points and $\mathbf{S}''(\mathbf{x}_\alpha)$ is the second derivative matrix defined as

$$\mathbf{S}''_{ij}(\mathbf{x}_\alpha) = \left. \frac{\partial^2 S_c(\mathbf{x})}{\partial x_i \partial x_j} \right|_{\mathbf{x}=\mathbf{x}_\alpha} . \quad (\text{B.4})$$

Substituting Eq. (B.3) in Eq. (B.1) affords a multidimensional Gaussian integral with the following solution

$$K(x, y, t) \xrightarrow{\hbar \rightarrow 0} \sum_c A_c(x, y, t) e^{-i\frac{\pi}{4}} e^{\frac{i}{\hbar} S_c(x, y, t)} e^{-iM_c \frac{\pi}{2}} , \quad (\text{B.5})$$

where the sum runs over all classical paths. M_c is the number of negative eigenvalues of the matrix of the action, $\mathbf{S}''(\mathbf{x}_\alpha)$ and is called the Maslov index. The amplitude $A_c(x, y, t)$ is defined by

$$\begin{aligned} A_c(x, y, t) &= \left(\frac{m}{2\pi i \hbar \Delta t} \right)^{N/2} \left[\frac{(2\pi \hbar)^{N-1}}{|S''_{N-1}|} \right]^{1/2} \\ &= \left[\frac{1}{2\pi \hbar} \left| \frac{\partial^2 S_c(x, y, t)}{\partial x \partial y} \right| \right]^{1/2} . \end{aligned} \quad (\text{B.6})$$

The final expression for the propagator in the stationary phase for a one-dimensional problem is therefore

$$K(x, y, t) \xrightarrow{SPA} \sum_c \left[\frac{1}{2\pi i \hbar} \left| \frac{\partial^2 S_c(x, y, t)}{\partial x \partial y} \right| \right]^{1/2} e^{\frac{i}{\hbar} S_c(x, y, t)} e^{-iM_c \frac{\pi}{2}} , \quad (\text{B.7})$$

where the phase factor $e^{-i\frac{\pi}{4}}$ has been absorbed in the amplitude for simplicity. Similarly, the generalization of the Van Vleck propagator to a multidimensional system is

$$\begin{aligned} K(\mathbf{x}_i, \mathbf{x}_f, t) &= \langle \mathbf{x}_i | e^{-i\hat{H}t/\hbar} | \mathbf{x}_f \rangle \\ &= \sum_c \left[\frac{1}{(2\pi i \hbar)^F} \left| \frac{\partial^2 S_c(\mathbf{x}_i, \mathbf{x}_f, t)}{\partial \mathbf{x}_i \partial \mathbf{x}_f} \right| \right]^{1/2} e^{\frac{i}{\hbar} S_c(\mathbf{x}_i, \mathbf{x}_f, t)} e^{-iM_c \frac{\pi}{2}} . \end{aligned} \quad (\text{B.8})$$

Bibliography

- [1] J. Z. H. Zhang, *Theory and Application of Quantum Molecular Dynamics* (World Scientific, Singapore, 1999).

Appendix C

Manual

This section illustrates the software development aspect of this thesis and is intended as documentation for future users. Listed in an alphabetical fashion, is a collection of the modules, their constituent classes and member functions, built from the existing MMTK structure and set of computer codes. Original functions and attributes of MMTK are not re-defined here. Relevant documentation can be found at http://dirac.cnrs-orleans.fr/Manuals/MMTK/MMTK_10.html Computer codes were written for the most part in the object oriented *Python* language, supplemented with *C++* for numerical implementations.

MODULE : Analysis

Class: PairDistances

Class calculates the distances between pair of atoms in the universe. By default, the distances for all possible pairs are calculated, unless a *pair_list* specified. In that case, distances are determined only for the specified pairs.

Constructor: `PairDistances(universe, pair_list=None)`

universe

the system which contains the objects whose pair distances are being calculated

pair_list

the list of pairs of atoms for which pair distances are calculated

Methods:

- `getPairDistanceList()`
returns a list of distances for all pairs of atoms in the universe
- `getPairDistancesFromConfiguration(A, D)`:
writes to a file in the directory *D* a list of distances for all pairs of atoms in the universe corresponding to the geometry specified by the array *A*
- `getPairDistancesFromArray(A, D)`
A refers to a array of several configurations/geometries. The functions writes to a file in the directory *D* a list of distances for all pairs of atoms in the universe corresponding to the geometry. A file is created for each configuration.

Class: **TrajectoryAnalysis**

Class extracts data from netCDF (.nc) files into arrays or textfiles.

Constructor: `TrajectoryAnalysis(trajectory, nAtoms, D, **options=None)`

trajectory

MMTK trajectory file object

nAtoms

an integer corresponding to the number of atoms in the universe

D

the directory where the files are to be written

**options

option = 'Array' (default option) - writes arrays for positions, velocities, time,

kinetic energy, potential energy and temperature (in this order).

option = 'Textfile' - creates Textfiles for each of positions, velocities, time, kinetic energy, potential energy and temperature (in this order).

Class: Wavefunction

Class generates the wavefunction described by a Gaussian function centered at the *ref_geometry*.

Constructor: TrajectoryAnalysis(*universe*, *ref_geometry*, *D*)

universe

the system which contains the objects whose pair distances are being calculated

ref_geometry

the geometry about which the wavefunction is centered

D

the directory where the files are to be written

Methods:

- inNormalCoordinates(*a*, *nPoints*, *min*, *max*)
a is the matrix of widths of the Gaussian function and indicates the number of normal modes. The function constructs the wavefunction along a normal coordinate numerically using *nPoints* ranging from *min* to *max*. As many wavefunctions as there are normal modes in *a* are constructed. Each wavefunction is written to an array in the directory *D*
- sampleCoordinates(*a*)
a is the matrix of widths of the Gaussian function. Function builds the wavefunction by a multivariate Gaussian sampling.

Class: Atomic Densities

Class takes a series of geometries or configurations *positions* and bins the positions of each atom

Constructor: AtomicDensities(*universe*, *positions*, *nAtoms*, *number_of_bins*, *xmin*, *dx*)

universe

the system which contains the objects whose pair distances are being calculated

positions

an array object with dimensions (L x N x 3) where L = length of array, N = number of atoms in system (or *nAtoms*), 3 (cartesian coordinates: x,y,z)

nAtoms

an integer corresponding to the number of atoms in the universe

number_of_bins

the number of bins (or intervals)

xmin

starting value for binning

dx

the interval or bin size

Methods:

- getDensity(*atomtype*, option=None, coord1=None, coord2=None)
the function returns the binned density of positions for the atom given by *atomtype* in 2D or 3D (if 2D binning is desired, the 2 binning coordinates need to be specified).

Arguments:

atomtype – a string corresponding to the atom type of the atom for which the density is binned; *atomtype* can refer to the symbol (e.g ‘H’) or name of the atom (e.g., ‘H1’) in the database entry.

option – optional keyword; a string (either ‘3D’ or ‘2D’) specifying the number of dimensions in which binning is carried out. Default is 3D binning of densities.

coord1 – a string (‘x’, ‘y’, or ‘z’); only provide this if 2D binning is required.

coord2 – see above

- `extractPositionsofSelectedAtoms(atomtype)`
function extracts and returns the positions of atoms (corresponding to the symbol specified in *atomtype*) from the positions array. *atomtype* is a string corresponding to the symbol of the atom in the database entry, for which the density is binned.
- `extractPositionsofASpecificAtom(atomtype)`
function extracts and returns the positions of atoms (corresponding to the name specified in *atomtype*) from the positions array. *atomtype* is a string corresponding to the name of the atom in the database entry, for which the density is binned
- `BinneR_3d()`
function performs the 3D-binning of the positions and returns an array (*number_of_bins* × *number_of_bins* × *number_of_bins*)
- `BinneR_2d(coord1, coord2)`
function performs the 2D-binning of the positions and returns an array (*number_of_bins* × *number_of_bins*). For a definition of the arguments, see `getDensity()`

MODULE : **Atomics**

Class: AtomicCollection

The actual distance calculations used in PairDistances() are performed in this class.

Constructor: AtomicCollection(*universe*, *object_list*=None)

universe

the system which contains the objects whose pair distances are being calculated

pair_list

the list of pairs of atoms for which pair distances are calculated

Methods:

- interAtomicPairs(option=None)
returns a list of distances for pair of atoms located on different molecules in the universe. If option='verbose', the list includes details of the atoms with their fullnames.
- intraAtomicPairs(option=None)
returns a list of distances for pair of atoms belonging to the same molecule in the universe. If option='verbose', the list includes details of the atoms with their fullnames.
- intraAtomicPairs(option=None)
returns interAtomicPairs(option) and intraAtomicPairs(option). If option='verbose', the list includes details of the atoms with their fullnames.

Class: AtomicDictionary

Class creates a dictionary with keys given by entries from *list* and *values* given by indices

Constructor: AtomicDictionary(universe, list=None)

universe

the system containing the objects whose pair distances are being calculated

`list=None`

The default option uses `universe.atomList()` [i.e., a list of all atoms in the universe] as its source for creating the dictionary. Of course, any list of atoms can be used.

MODULE : **ConstrainedDynamics**

Class: ConstraintDynamics

Class performs the dynamics of constrained molecules via the integration of constrained equations of motion (handled by the velocity verlet algorithm)

Constructor: `ConstraintDynamics(universe, constraintList, dt, timesteps, filename, skip=1)`

universe

the system for which the dynamics are performed. It must have a starting configuration specified as well as a forcefield that provides the energy, gradients and second-derivatives.

constraintList

a list of pairs of atoms between which the distance is constrained based on the starting geometry

dt

the timestep in MMTK units (ps)

timesteps

the length of the trajectory (number of time steps)

filename

the filename of the trajectory in netCDF format (.nc)

skip=1

the number of time steps between which trajectory data is written. Default value is 1. i.e., all consecutive steps are recorded.

Methods

- `performDynamics()`
performs the dynamics and records trajectory data (configuration, velocities, energy, thermodynamic, time - see MMTK. Trajectory for description)
- `final_configuration`
returns an array corresponding to the geometry of the final step of the trajectory

Class: `ConstrainedWaterDynamics`

Class performs the dynamics of constrained water molecules via the integration of constrained equations of motion (handled by the velocity verlet algorithm)

Constructor: `ConstraintDynamics(universe, dt, timesteps, filename, constraint_option='rigid', skip=1)`

universe

the system for which the dynamics are performed. It must have a starting configuration specified as well as a forcefield that provides the energy, gradients and second-derivatives.

dt

the timestep in MMTK units (ps)

timesteps

the length of the trajectory (number of time steps)

filename

the filename of the trajectory in netCDF format (.nc)

constraint_option='rigid'

an optional keyword specifying the type of constraints to be imposed on the system. Default option is 'rigid'. In this case, constraints are set based on the database configuration entry (equilibrium geometry of individual water molecules). Alternative option is 'distance', where constraints are set based on the starting geometry.

skip=1

the number of time steps between which trajectory data is written. Default value is 1. i.e., all consecutive steps are recorded.

Methods and Attributes

- `performDynamics()`
performs the dynamics for the system and records trajectory data (configuration, velocities, energy, thermodynamic, time - see MMTK. Trajectory for description)
- `final_configuration`
returns an array corresponding to the geometry of the final step of the trajectory

MODULE : Custom Subspace

Class: `InterAtomicPairDistances`

Class constructs displacement vectors corresponding to intermolecular motion only (modelled after `MMTK.RigidMotionSubspace`) for eventual use with a projector.

Constructor: `InterAtomicPairDistances(universe, object_list)`

universe

the system containing the objects for which displacement vectors are determined. It must have a configuration.

object_list

a list of objects present in the universe between which atomic pair distances are determined

Attributes

- **vectors** the normalized displacement vectors built from atomic pair distances corresponding to intermolecular motion

Class: MultiWaterPairDistances

Class constructs displacement vectors corresponding to all possible motion of water molecules.

Constructor: MultiWaterPairDistances(*universe*, pairs='all')

universe

the system containing the water molecules for which displacement vectors are determined. It must have a configuration.

pairs='all'

the default value calculates distances for all the pairs i.e intra- and intermolecular pairs

other valid options are just 'intra' or 'inter', in which cases only the specified type of distances are calculated.

Attributes

- **AtomicPairList** the atomic pair list - can be complete list or specific depending on the input. If 'all' is specified, then the intramolecular pairs list is returned first followed by the intermolecular pairs list.

- **vectors** the displacement vectors corresponding to normalized distances of the elements in the AtomicPairList

Class: SingleWaterPairDistance

Class constructs displacement vectors corresponding to intramolecular motion of a water molecule.

Constructor: SingleWaterPairDistance(*universe*, *atom_list*)

universe

the system containing the water molecule for which displacement vectors are determined. It must have a configuration.

atom_list

the list of atoms for which the displacement vectors are to be determined.

Attributes

- **AtomicPairList** the list of atomic pairs present in the *atom_list*.
- **vectors** the displacement vectors corresponding to the normalized distances for atomic pairs of the AtomicPairList

Class: ClusterPairDistances

Class constructs displacement vectors corresponding to interatomic pair distance on atomic clusters.

Constructor: ClusterPairDistances(*universe*, *atom_list*).

Description and attributes are identical to SingleWaterPairDistance() with the exception that the water molecule is replaced by an atomic cluster

MODULE : HessianAnalysis

Class: HessianAnalyzer

Class performs operations on or related to the force constant matrix.

Constructor: `HessianAnalyzer(universe)`

universe

the system for which the dynamics are performed. It must have a starting configuration specified as well as a forcefield that provides the energy, gradients and second-derivatives.

Methods

- `gradientAndHessian()`
returns arrays corresponding to the gradient ($3N$) and force constant matrix ($3N \times 3N$)
- `hessian()`
returns the symmetric force constant matrix ($3N \times 3N$)
- `forceConstantMatrix()`
returns mass-weighted force constant matrix
- `massWeigher(A)`
performs the mass-weighing on the array *A*
- `massWeighAndSymmetrize(A)`
performs the mass-weighing and symmetrizes the *A*
- `gradient(mass=None)`
returns an array containing the gradient. the result is mass-weighted if a mass vector is specified in the input command.
- `eigenVs(H)`
returns the eigenvalues and eigenvectors of the diagonalised force constant or Hessian matrix *H*. The diagonalisation uses the lapack routine

- `diagonalize(H)`
returns the eigenvalues and eigenvectors of the symmetric force constant or Hessian matrix H . The diagonalisation uses python's diagonaliser.
- `getFrequencies(FCM=None)`
returns the frequencies from the eigenvalues of the force constant matrix FCM . The default calculation is done for the force constant matrix at the current state (configuration and forcefield) of the universe.

MODULE : InitialConditionsFactory

Class: CovarianceMatricesCalculator

Class calculated the covariance matrices for the multivariate Gaussian sampling of initial conditions

Constructor: `CovarianceMatricesCalculator(universe, subspace, option=None, displacement=None, description=None)`

universe

the system for which covariance matrices are calculated. This involves calculation of the projected Hessian (see Projector for details) for constrained system. All eigenvalues of Projected frequency need to be real. So system must be at its equilibrium geometry.

subspace

the subspace in which the projection is carried out. See MMTK.Subspace for details.

`option=None`

defines the position of the wavefunction in the position representation.

if `option = None` (default), the wavefunction is centered at the equilibrium geometry.

if option = 'Displaced', the wavefunction is displaced from the minimum, as specified by displacement.

displacement=None

an array, specifying the displacement of the wavefunction from the minimum. The number of entries in the array and its shape should be identical to the configuration array i.e, consisting of vectors for the displacement of each atom in each Cartesian coordinate. Note: if option = None, displacement should also be None.

description=None

a string describing the type of cluster under investigation: 'dimer' or 'trimer' or 'dimer_atom'

Methods and Attributes

- centerOfWavefunction_position
the center of the wavefunction calculated based on the geometry of the universe and the displacement vector in the position representation
- centerOfWavefunction_momentum
the center of the wavefunction in the momentum representation
- fullGamma
the full mass-weighted matrix ($3N \times 3N$) of the widths of the gaussian wavepackets
- subspaceGamma
the reduced-space mass-weighted matrix ($(3N - c) \times (3N - c)$) of the widths of the gaussian wavepackets, where c = number of constraints
- formCovarianceMatrices()
function returns the mass-weighted covariance matrices for the positions and momenta

- `generateGamma(subspace=None, subspace_option)`
 function returns the mass-weighted gamma matrix (from which the covariances matrices are built). Note: if `subspace=None`: no projection of force constant matrix is performed
subspace_option='projected': full gamma matrix after projection of force constant matrix
subspace_option='subspace': reduced-dimension gamma matrix after projection of force constant matrix

Class: InitialConditionSampler

Class generates initial conditions for dynamics from the multivariate Gaussian sampling using covariances matrices calculated by `CovarianceMatricesCalculator()`. Sampled initial conditions are initially mass-weighted. They are unmassi-weighted prior to writing to the array.

Constructor: `InitialConditionSampler(Emax, nMC, factor, CV, option=None)`

*E*max

the total energy ceiling for bound states. Any sampled phase space point with total energy above *E*max is discarded.

*n*MC

the number of initial conditions required.

*f*actor

a number (floating point/integer). Since some initial conditions are discarded, the actual number of sampled points need to be larger than *n*MC. The actual value is very system-dependent as is determined by trial and error: for some systems, a number as low as 1.2 is good enough; other systems require a value of 3.

CV

class instance for CovarianceMatricesCalculator(). The *universe*, *covariancematrices*, *centerofwavefunction* (in position and momentum) are obtained from it.

option=None

option regarding the treatment of center of mass motion. Default (None) option removes center of mass (com) motion from the initial conditions, i.e., set the com to zero and also removes linear and angular momenta from the sampled positions and momenta. Other option is 'Leave COM motion' and only sets the com to zero, without operating on the linear and angular momenta.

Methods and Attributes

- Positions
an array containing the *nMC* sampled non-massweighted initial positions vectors for each atom.
- Velocities
an array containing the *nMC* sampled non-massweighted initial velocities vectors for each atom.
- energies
an array containing the potential, kinetic and total energies of the *nMC* initial conditions.
- calculateRatio()
returns two numbers: the ratio of initial conditions accepted to the total number of sampled phase space points followed by the total number of sampled phase space points.

MODULE : Projection

Class: MySubspace

Class is essentially a customized version of MMTK.Subspace

Constructor: MySubspace(*universe*, *subspace*)

universe

the system from which the subspace is constructed.

subspace

a set of (displacement) vectors defining the motion in a reduced space from within the universe.

Methods

- setupBasis()

function returns a basis formed from the set of vectors specified in the class instance. the basis is created by orthonormalisation of the displacement vectors via Singular Value Decomposition.

Class: Projector

Class performs the projection of unwanted motions from the force constant matrix and related operations

Constructor: MySubspace(*universe*, *subspace*)

universe

the system from which the subspace is constructed.

subspace

a set of (displacement) vectors defining the motion in a reduced space from within the universe.

Methods and Attributes

- `evalues`
returns the eigenvalues of the projected force constant matrix.
- `eectors`
returns the eigenvalues of the projected force constant matrix.
- `getProjectedHessian()`
returns the symmetric projected full space force constant matrix ($3N \times 3N$)
- `getFrequencies()`
returns the frequencies associated with the projected normal modes. Small non-zero frequencies are rounded off to zero.
- `getFullFrequencies()`
returns the all frequencies associated with the projected normal modes, no round-off.
- `getMassWeightedHessian()`
returns the mass-weighted force constant matrix

MODULE : SchlegelProjection_PDS

Class: ConstrainedProjection

Class contains functions that perform operations related to the projection of constraints and redundancies based on the method of Schlegel and Pulay [1], ayala98. First a subspace is built from all possible pair distances along with a force constant matrix in internal coordinates. The redundancies and constrained motions are then removed through a projection procedure, so as to allow motion between unconstrained pairs of atoms. Constructor: `ConstrainedProjection(universe)`

universe

the system for which the projection is performed.

Methods and Attributes

- `evalues`
eigenvalues of the projected force constant matrix.
- `evecs`
eigenvectors or normal modes of the projected force constant matrix.
- `frequencies()`
returns the frequencies associated with the normal modes of the allowed motions.

MODULE : `SchlegelProjection_RMS`

Class: `ConstrainedProjection`

Class contains functions that perform operations related to the projection of constraints and redundancies based on the method of Schlegel and Pulay [1], ayala98. First a subspace is built from displacement vectors along with a force constant matrix in internal coordinates. The redundancies and constrained motions are then removed through a projection procedure. This subspace differs from the Module `SchlegelProjection_PDS` in the way the subspace is created. In the present module, the displacement vectors are chosen so as to create rigid bodies out of objects in the universe. Constructor: `ConstrainedProjection(universe)`

universe

the system for which the projection is performed.

Methods and Attributes

- `evalues`
eigenvalues of the projected force constant matrix.

- `evector`s
eigenvectors or normal modes of the projected force constant matrix.
- `frequencies()`
returns the frequencies associated with the normal modes of the allowed motions.

MODULE : SemiclassicalDynamics

Class: SemiclassicalDynamics

Class launches classical trajectories using the sampled positions and momenta as starting conditions. Each sampled phase space point gives rise to a trajectory, stored in a trajectory netCDF file (.nc). After the dynamics, the trajectories are scanned for unbound ones (sometimes, a couple escape the PES) from which data is extracted and saved into a file for further manipulation by a *C++* code.

Constructor: `SemiclassicalDynamics(universe, dt, timesteps, constraintList, Emax, D)`

universe

the system for which the dynamics are carried out.

dt

the timestep to be employed during the dynamics.

timesteps

the number of steps in each trajectory.

E_{max}

the maximum value of the kinetic energy for a bound trajectory.

D

the directory where the trajectory files are written.

Methods

- `generateTrajectory(initialPositions, initialVelocities)`
function performs the classical dynamics based on the *initial positions* (an array corresponding to the starting sampled positions) and *initial velocities* (an array corresponding to the starting sampled velocities) and scans the energies to verify that the trajectories are bound
- `extractData(subspaceType, objectList, B_0, filename)`
function saves dynamical data to a textfile named *filename* in the directory *D* for future analysis by a c-code. Dynamical data is saved in the following order: configuration, momenta, action, force constant matrix (unprojected), bases (time-independent basis and time-dependent bases)
subspaceType = RigidMotionSubspace or PairDistanceSubspace; any subspace in MMTK is valid.
objectList = list of objects (atoms or molecules) in the universe to be included in the subspace
B_0 = time-independent basis (basis generated at the equilibrium geometry)

MODULE : Water_SemiclassicalDynamics

Class: Water_SemiclassicalDynamics

Class launches classical trajectories using the sampled positions and momenta as starting conditions. Each sampled phase space point gives rise to a trajectory, stored in a trajectory netCDF file (.nc). After the dynamics, the trajectories are scanned for unbound ones (sometimes, a couple escape the PES) from which data is extracted and saved into a file for further manipulation by a C++ code.

Constructor: `Water_SemiclassicalDynamics(universe, dt, timesteps, constraintList, Emax, D)`

universe

the system for which the dynamics are carried out.

dt

the timestep to be employed during the dynamics.

timesteps

the number of steps in each trajectory.

E_{max}

the maximum value of the kinetic energy for a bound trajectory.

D

the directory where the trajectory files are written.

Methods

- `generateTrajectory(initialPositions, initialVelocities)`
function performs the classical dynamics based on the *initial positions* (an array corresponding to the starting sampled positions) and *initial velocities* (an array corresponding to the starting sampled velocities) and scans the energies to verify that the trajectories are bound
- `extractData(filename, nInternal)`
function saves dynamical data to a textfile named *filename* in the directory *D* for future analysis by a c-code. Dynamical data is written in the following order: configuration, momenta, action, eigenvalues of the projected force constant matrix)
nInternal = the total number of degrees of freedom (including redundancy).

Bibliography

- [1] P. Pulay and G. Fogarasi, J. Chem. Phys. **96**, 2856 (1992).